

Metabolites and Proteins of
***Pseudomonas aeruginosa* Biofilms**

BY

YENI PAMELA YUNG
B.A., University of Illinois at Chicago, 2009
M.S., University of Illinois at Chicago, 2016

THESIS

Submitted as partial fulfillment of the requirements
for the degree of Doctor of Philosophy in Chemistry
in the Graduate College of the
University of Illinois at Chicago, 2018

Chicago, Illinois

Defense Committee:

Luke Hanley, Chair and Advisor
Scott A. Shippy, Department of Chemistry
Stephanie M. Cologna, Department of Chemistry
Laura M. Sanchez, Department of Medicinal Chemistry and Pharmacognosy
Yang Cui, PDF Solutions

DEDICATION

This thesis is dedicated to my family, friends, and colleagues.

ACKNOWLEDGEMENTS

First and foremost, I would like to extend my deepest gratitude to my research advisor, Dr. Luke Hanley. His support and guidance help shape me into the analytical researcher I am today. Given the opportunity to join his research group for my PhD studies, I am very fortunate to have learned as much as I can from him. I thank all my colleagues in the Hanley group, past and present, especially Dr. Yang Cui, Dr. Igor V. Veryovkin, and Dr. Igor Bolotin for all their technical expertise as much of my aspirations and creativity stemmed from them.

I thank Dr. Scott A. Shippy, Dr. Stephanie M. Cologna, Dr. Laura M. Sanchez, for being on my committee and teaching me various aspects of analytical chemistry with mass spectrometry. The knowledge I gained from their courses and trainings have been invaluable and have broaden my horizons. I thank my collaborators Dr. Ross P. Carlson, Dr. Ashley Beck, and S. Lee McGill at the Montana State University Center for Biofilm Engineering, Dr. Anu Vaikkinen and Dr. Tiina J. Kauppila at the University of Helsinki, and Dr. Hui Chen at the UIC Research Resources Center. I thank the machine shop, especially Kevin Lynch, Richard Frueh, and Dave Kuntzelman for all their machining support which tremendously helped me in with my instrumental developments.

Last but not least, I am most thankful for my family, fiancé, and friends for their love, patience, and support. They are my strength, foundation, and the reason why I stay motivated, strive to do better, and aim high.

YPY

CONTRIBUTION OF AUTHORS

Chapter 1 is an introduction to my thesis, of which I was the primary author.

Chapter 2 is a review of laser ablation mass spectrometry (MS) applications, which is to be submitted as a book chapter. I was the primary author and Dr. Luke Hanley was my adviser and contributed to the writing of this book chapter.

Chapter 3 represents unpublished work, for which I was the primary author. I carried out sample preparations and analyses.

Chapter 4 represents a publish manuscript [Yeni P. Yung, Raveendra Wickramasinghe, Anu Vaikkinen, Tiina J. Kauppila, Igor V. Veryovkin, and Luke Hanley. Solid Sampling with a Diode Laser for Portable Ambient Mass Spectrometry. *Analytical Chemistry* (2016) 89 (14), 7297–7301. DOI: 10.1021/acs.analchem.7b01745], for which I was the primary author and major driver of the research. Raveendra Wickramasinghe and I both carried out the analyses. Dr. Igor V. Veryovkin contributed to the implementation of a wire grid in the apparatus. Dr. Anu Vaikkinen, Dr. Tiina J. Kauppila, and Dr. Luke Hanley were mentors and contributed to the writing of the manuscript.

Chapter 5 represents an unpublished experiment, for which I was the primary author and major driver of the research. I collected and analyzed the proteomics data. S. Lee McGill collected and analyzed the metabolomics data. Dr. Stephanie M. Cologna, Dr. Hui Chen, Dr. Ross P. Carlson, and Dr. Luke Hanley were mentors and contributed to the writing.

Chapter 6 represents research to be submitted later, for which I was the primary author and major driver of the research. I collected and analyzed the proteomics data. S. Lee McGill collected and analyzed the metabolomics data. Dr. Stephanie M. Cologna, Dr. Hui Chen, Dr. Ross P. Carlson, and Dr. Luke Hanley were mentors and contributed to the writing.

Chapter 7 represents my conclusion of the research presented in this thesis.

TABLE OF CONTENTS

| | |
|--|----|
| 1. INTRODUCTION | 1 |
| 1.1 Biofilms Background..... | 1 |
| 1.2 Physiology: Stages of Biofilm Formation..... | 2 |
| 1.3 Extracellular Polymeric Substance (EPS)..... | 4 |
| 1.4 Quorum Sensing (QS)..... | 4 |
| 1.5 Antibiotic Resistance | 5 |
| 1.6 Strategies for Combating or Preventing Bacterial Biofilms | 6 |
| 1.7 Methods for Culturing Biofilms for Laboratory | 7 |
| 1.8 Characterization of Biofilm-Forming Bacteria with Mass Spectrometry (MS) | 7 |
| 1.9 Thesis Overview | 10 |
| 2. APPLICATIONS OF LASER ABLATION MS | 13 |
| 2.1 Nature of Samples and Information to be Gained from Laser Ablation Mass Spectra | 13 |
| 2.2 Laser Ablation for Elemental Analysis..... | 14 |
| 2.3 Non-Imaging UV Matrix Assisted Laser Desorption Ionization MS (UV-MALDI-MS) for Molecular Analysis | 16 |
| 2.4 UV-MALDI-MS Imaging for Molecular Analyses | 18 |
| 2.5 UV-MALDI-MS for <i>Pseudomonas aeruginosa</i> , With and Without Imaging | 21 |
| 2.6 Alternatives to UV-MALDI-MS..... | 23 |
| 2.7 Methods that Utilize Postionization of Desorbed Neutrals..... | 24 |
| 2.7.1 Laser Desorption Photoionization Mass Spectrometry (LDPI-MS) – VUV Single Photon Ionization (SPI) of Laser Desorbed Neutrals in Vacuum | 24 |
| 2.7.2 Laser Ablation Atmospheric Pressure Photoionization Mass Spectrometry (LAAPPI-MS) – Atmospheric Pressure Ionization Initiated by VUV Single Photon Ionization..... | 25 |
| 2.7.3 Laser Ablation Electrospray Ionization Mass Spectrometry (LAESI-MS) and Laser Electrospray Mass Spectrometry (LESI-MS) | 26 |
| 2.8 Laser Ablation Sampling | 28 |
| 3. MALDI-MS OF BIOFILMS | 30 |
| 3.1 Introduction..... | 30 |
| 3.2 Experimental Details..... | 31 |

TABLE OF CONTENTS

| | |
|--|----|
| 3.2.1 Instrumentation..... | 31 |
| 3.2.2 Sample Preparation | 33 |
| 3.3 Results and Discussion | 35 |
| 3.3.1 Non-Imaging UV-AP-MALDI-MS on a Quadrupole Ion Trap (QIT) Instrument . | 35 |
| 3.3.2 Non-Imaging IR-AP-MALDI-MS on a QIT Instrument..... | 36 |
| 3.3.3 Non-Imaging UV-AP-MALDI-MS on an Fourier Transform Ion Cyclotron Resonance (FTICR) Instrument | 37 |
| 3.3.4 Imaging Vacuum UV-MALDI-MS on a Time-of-Flight (TOF) Instrument | 38 |
| 3.4 Conclusion | 41 |
| 4. SOLID SAMPLING WITH A DIODE LASER FOR PORTABLE AMBIENT MASS SPECTROMETRY | 42 |
| 4.1 Introduction..... | 42 |
| 4.2 Experimental Details..... | 44 |
| 4.2.1 Ion Source and Ambient Mass Spectrometry..... | 44 |
| 4.2.2 Chemicals, Samples, and Replicates | 47 |
| 4.3 Results and Discussion | 48 |
| 4.4 Conclusion | 57 |
| 5. USING PROTEOMICS TO ILLUMINATE METABOLIC PROCESSES IN BACTERIAL COMMUNITIES | 59 |
| 5.1 Introduction..... | 59 |
| 5.2 Experimental Details..... | 61 |
| 5.2.1 Bacterial Strains and Culturing Conditions..... | 61 |
| 5.2.2 Exogenous Metabolomics | 62 |
| 5.2.3 Sample Preparation for Proteomics..... | 62 |
| 5.2.4 Liquid Chromatography Tandem Mass Spectrometry (LC-MS/MS) | 63 |
| 5.3 Results..... | 65 |
| 5.3.1 LldD (L-Lactate Dehydrogenase) Protein Identification and Quantification | 65 |
| 5.3.2 Overall Protein Identifications and Differential Expressions..... | 68 |
| 5.3.3 Glucose and Lactate Metabolism vs. LldD Differential Expression..... | 73 |
| 5.4 Discussion | 75 |

TABLE OF CONTENTS

| | |
|--|-----|
| 5.4.1 Lactate, Glucose, and Acetate Metabolisms | 75 |
| 5.4.2 Determination of Protein Associations and Metabolic Pathways | 76 |
| 5.5 Conclusion | 79 |
| 6. DELINEATING <i>PSEUDOMONAS AERUGINOSA</i> METABOLISM IN PLANKTONIC AND BIOFILM CULTURES THROUGH MULTI-OMICS..... | 81 |
| 6.1 Introduction..... | 81 |
| 6.2 Experimental Details..... | 82 |
| 6.2.1 Bacterial Strains and Growth Conditions..... | 82 |
| 6.2.2 Exogenous Metabolomics | 82 |
| 6.2.3 Sample Preparation for Proteomics..... | 82 |
| 6.2.4 LC-MS/MS..... | 83 |
| 6.3 Results..... | 83 |
| 6.3.1 Metabolomics | 83 |
| 6.3.2 Proteomics | 85 |
| 6.4 Discussion | 89 |
| 6.4.1 Protein Associations | 89 |
| 6.4.2 Carbon Catabolite Repression | 90 |
| 6.5 Conclusion | 95 |
| 7. CONCLUSION..... | 96 |
| CITED LITERATURE | 100 |
| APPENDIX..... | 121 |
| VITA..... | 122 |

LIST OF FIGURES

| | |
|---|----|
| Figure 1. Biofilm heterogeneity – phenotypic variation of cells in response to oxygen, nutrient, pH and quorum sensing “QS” gradient. Image is adapted from Ref. [3]. | 2 |
| Figure 2. Stages of biofilm formation on a surface – (1) adhesion, (2) colonization, (3) development, (4), maturation, (5) dispersion. Image is adapted from Ref. [4]. | 3 |
| Figure 3. Basic components of a mass spectrometer. Samples are volatilized and ionized in the ion source. The generated ions are separated by the mass analyzer based on its m/z before reaching the detector. The resulting mass spectrum, “MS,” shows the ion abundance at a particular m/z from the sample. The selected ion is fragmented after dissociation, and the pattern is revealed in a tandem mass spectrum, “MS/MS.” | 9 |
| Figure 4. Schematic configuration of laser ablation inductively coupled plasma mass spectrometry (LA-ICP-MS). Laser ablated material from a sample is transferred to an ICP source by carrier gas then to a MS. Image is redrawn based upon figure from Ref. [35]. | 15 |
| Figure 5. Matrix assisted laser desorption ionization mass spectrometry (MALDI-MS) imaging schematic workflow. Steps show the matrix application on a tissue slice in which a laser irradiates across the sample plate. The ion intensities of the m/z at each particular x, y -coordinate are plotted in a false-color image. Image is redrawn based upon figure from Ref. [53]. | 19 |
| Figure 6. Schematic of laser desorption photoionization mass spectrometry (LDPI-MS). A laser (in red) is focused onto the sample plate for sample desorption and an intersecting vacuum ultraviolet (VUV) beam (in purple) is used for postionization of ablated neutral plume. Image is redrawn based on figure from Ref. [22]. | 25 |
| Figure 7. Schematic of laser ablation with electrospray ionization (ESI) mass spectrometry. A laser is used for ablation in which neutrals are postionized by ESI. | 27 |
| Figure 8. Schematic of laser ablation sample transfer (LAST). Mid-infrared (IR) laser is used to generate an ablation plume which is captured into a solvent droplet suspending from a syringe. | 29 |

LIST OF FIGURES

| | |
|---|----|
| Figure 9. Atmospheric pressure matrix assisted laser desorption ionization (AP-MALDI) setup on a field-deployable quadrupole ion trap (QIT) mass spectrometer. Bottom: side view of entire AP-MALDI setup. Top: Optical components for (a) IR and (b) UV attenuation. IR attenuation consist of (1) beamsplitter, (2) neutral density filter, (3) focusing lens, and (4) germanium oxide fiber patch, which all transmit mid-IR. UV attenuation consist of (1) neutral density filter, (2) half-wave plate, (3) polarizer, (4) beamsplitter, (5) UV-enhanced Al mirror, (6) focusing lens, and (7) fiber patch, which all transmit UV. | 32 |
| Figure 10. Components for interfacing AP-MALDI source onto a Fourier transform ion cyclotron resonance (FTICR) mass spectrometer. (a) Fiber-coupling between the 355 nm output of the Nd:YAG laser and the AP-MALDI source. (b) Laser enclosure and fiber collimator..... | 33 |
| Figure 11. Images of blotted fixed biofilms and results. (a) Thawed blotted biofilms on MALDI plate. (b) Completely dried biofilms after matrix application..... | 35 |
| Figure 12. Images of agar embedded biofilms. (a) Blotted biofilms embedded in agar - top two biofilms were not treated with trypsin and bottom two are treated with trypsin. Letters indicate angiotensin II (A), trypsin (T), and <i>Clostridium Staphylococcus Pseudomonas</i> (CSP) medium (C) spotted on agar prior to matrix application. (b) Semi-dried biofilm following matrix application. | 35 |
| Figure 13. Mass spectrum of peptides – bradykinin (m/z 757.60), angiotensin II (m/z 1046.92), and P14R (m/z 1533.92)..... | 36 |
| Figure 14. Fiber attachment piece on the AP-MALDI source. Left: Adjustable fiber attachment tube removed from the MALDI source. Right: Fiber attachment piece relative to the AP-MALDI setup. | 37 |
| Figure 15. Mass spectra of (a) lysozyme and (b) albumin tryptic digests. Peaks corresponding to fragments from trypsin digestion are circled in red. | 38 |
| Figure 16. Mass spectra and images of biofilms. (a) Fixed <i>P. aeruginosa</i> mass spectrum with heat intensity of m/z 1424. (b) Mass spectrum and image of m/z 1046 for angiotensin II as a standard check. (c) Unfixed <i>P. aeruginosa</i> mass spectrum and image of m/z 655. | 40 |
| Figure 17. A schematic diagram of the laser diode thermal desorption atmospheric pressure photoionization (LDTD-APPI) source with a battery-powered, portable, pseudo-continuous wave (CW) near-IR at 940nm diode laser. | 45 |
| Figure 18. A schematic diagram of the laser ablation atmospheric pressure photoionization (LAAPPI) source with a fiber coupled laboratory mid-IR laser at 2940 nm. | 46 |

LIST OF FIGURES

- Figure 19. Mass spectra of the 4-amino-5-chloro-2-methoxybenzoic acid (MACA) standard (inset shows chemical structure) analyzed by (from top to bottom) 2940 nm laser ablation atmospheric pressure photoionization (LAAPPI), LDTD-APPI, 2940 nm laser ablation (without VUV lamp), and 940 nm LDTD (without VUV)..... 49
- Figure 20. Representative analyses of sage leaves by (top) LAAPPI and (middle) LDTD-APPI with anisole dopant. Anisole dopant background in APPI (bottom). The letters “(a)” to “(e)” annotate peaks observed by both LAAPPI and LDTD-APPI for whom with tentative assignments were possible based on phytochemicals previous detected by LAAPPI (see Table 1) [89, 134]. The arrows indicate other peaks observed in the LDTD-APPI mass spectrum that are labelled in the LAAPPI mass spectrum. * indicates background peaks. 51
- Figure 21. Representative analyses of *P. aeruginosa* membrane grown biofilms by (top) LAAPPI and (middle) LDTD-APPI with toluene. Toluene dopant background in APPI (bottom). The peaks annotated with “(a)” to “(g)” annotated in the figure correspond to peaks observed in both LAAPPI and LDTD-APPI that have been tentatively assigned to known metabolites reported in literature (see Table II) [25, 70, 113, 135, 136]. The arrows indicate other peaks observed in the LDTD-APPI mass spectrum that are labelled in the LAAPPI mass spectrum. * indicates background peaks. 55
- Figure 22. Mass spectra used to identify L-lactate dehydrogenase (LldD). (a) Full scan mass spectrum at a specific elution time from liquid chromatography (LC), with inset showing expanded region around with m/z 600.83 along with its isotope peaks (marked by stars). (b) Schematic of peptide sequence of NVEDLSAIALR and standard notation for its backbone fragmentation by tandem MS. (c) Tandem mass spectrum of m/z 600.38 labelled with a- and y- fragment ions that identifies it as NVEDLSAIALR, a peptide sequence from LldD enzyme..... 67
- Figure 23. Scatter plots of significant protein expression differentials, $\log_2(x_{LCSP}/x_{CSP})$, where x = peptide ion intensities from LC-MS/MS data at (a) 4 h, (b) 7 h, (c) 11 h, and (d) 21 h for LCSP vs. CSP media. Proteins deemed statistically significant (p -values < 0.05) are highlighted above the horizontal black line and non-significant proteins below the black line. Protein expression differentials, with at least ~10% sequence coverage, highlighted in blue (less than -1.5) were downregulated and proteins highlighted in red (greater than 1.5) were upregulated. 70

LIST OF FIGURES

- Figure 24. Millimolar concentrations of extracellular glucose and lactate taken from growth media (supernatant) at time (a) 0 and (b) 11 h. (c) Protein expression at 11 h of LldD based on $\log_2(x)$ values of peptide abundances from LldD..... 74
- Figure 25. Schematic of the abbreviated metabolic pathways [178] of small molecule (green) metabolism en route to pyruvate, lactate and acetate. Black arrows with associated proteins (blue) indicate reactions involving single reaction (solid) or multiple reactions (dotted). Yellow stars indicate key proteins that showed significant expression differentials at 7 and 11 h (refer to Table III and text for protein names). Red dotted lines represent STRING protein-protein interactions, with thicker lines indicating more associations. Additional metabolites noted are G6P, 6-PGDL, Gln-6P, and 13-DPG (see text)..... 78
- Figure 26. Metabolite profiling of (i) lactate & (ii) glucose in (a) planktonic and (b) biofilm *P. aeruginosa* cultures grown in CSP and lactate-supplemented CSP media (LCSP) for 0 h and 11 h. 84
- Figure 27. Protein expression in LCSP vs. CSP for planktonic and biofilm *P. aeruginosa* growth at 11 h. Scatter plots of \log_2 fold-change [$\log_2(x_{\text{LCSP}}/x_{\text{CSP}})$] vs $-\log_{10}(p\text{-value})$. Statistically significant proteins ($p\text{-value} < 0.05$) are highlighted above horizontal black line. Significant down- or up-regulation with greater than 1.5-fold change and at least ~10% sequence coverage are annotated in the gray regions. 86
- Figure 28. Schematic of glucose and lactate metabolisms in (a) planktonic and (b) biofilm *P. aeruginosa* cultures. Dashed lines indicate protein-protein associations, where thickness correlates to stronger associations. Upregulated and downregulated proteins are represented by red upward facing arrows and blue downward facing arrows, respectively. (a) Planktonic culture: lactate conversion to pyruvate by LldD is upregulated. Downregulation is observed for proteins, OprB, Glk, Zwf, Pgl, Gap, involved in glucose conversion (see text or Table VI for full protein names). (b) Biofilms: LldD is similarly upregulated. Upregulation is observed for proteins within the citric acid (TCA) cycle: FumC1, in fumarate conversion to S-malate, and Mqo1, in S-malate conversion to oxaloacetate. 94

LIST OF TABLES

| | |
|--|----|
| Table I. Peaks observed in LAAPPI- and LDTD-APPI-MS spectra of sage leaves with anisole as the dopant. *The letters “(a)” to “(e)” annotate the same peaks so noted in Figure 20 while italicized peaks in LDTD-APPI are those that also appeared with toluene dopant. | 53 |
| Table II. Peaks observed in LAAPPI and LDTD-APPI spectra of <i>P. aeruginosa</i> biofilms with toluene as the dopant *The letters “(a)” to “(g)” annotate the same peaks so noted in Figure 21..... | 56 |
| Table III. List of up- and downregulated proteins, with its Kyoto Encyclopedia of Genes and Genome identification (KEGG ID), protein name, unique peptides, sequence coverage percentage, molecular weight (kDa), and $\log_2(X_{LCSP}/X_{CSP})$ differential value (LCSP vs CSP culture media) observed at 4, 7, 11, and 21 h for planktonic <i>P. aeruginosa</i> cultures. *indicates protein homology | 71 |
| Table IV. Statistically significant proteins and KEGG IDs with non-significant differential values (LCSP vs CSP) at 4 (blue region), 7 (red region), 11 (yellow region), and 21 h (green region). *indicates protein homology..... | 72 |
| Table V. KEGG metabolic pathway functional annotation of proteins at 7 and 11 h planktonic <i>P. aeruginosa</i> cultures. FDR are false discovery rates with protein networks listed in the KEGG pathways..... | 79 |
| Table VI. List of up- and downregulated proteins, with its KEGG ID, protein name, unique peptides, sequence coverage percentage, molecular weight (kDa), and $\log_2(X_{LCSP}/X_{CSP})$ differential value (LCSP vs CSP culture media) observed from planktonic and biofilm <i>P. aeruginosa</i> cultures. *indicates protein homology..... | 87 |
| Table VII. Statistically significant proteins and KEGG IDs with non-significant differential values (LCSP vs CSP) in planktonic and biofilm <i>P. aeruginosa</i> cultures. *indicates protein homology | 88 |
| Table VIII. KEGG metabolic pathway functional annotation on enzymatic proteins from planktonic and biofilm <i>P. aeruginosa</i> cultures. FDR are false discovery rates with protein networks listed in the KEGG pathways. | 90 |

LIST OF ABBREVIATIONS

| | |
|----------|---|
| 13-DPG | phosphoglyceroyl-P |
| 1-HP | 1-hydroxyphenazine |
| 1-MP | 1-methoxyphenazine |
| 6-PGDL | 6-phosphogluconolactone |
| AcsA1 | acetyl-CoA synthetase 1 |
| AP-MALDI | atmospheric pressure matrix assisted laser desorption ionization |
| AtoB | acetyl-CoA acetyltransferase |
| ATP | adenosine triphosphate |
| AtpA | ATP synthase subunit alpha |
| BkdB | lipoamide acyltransferase component of branched-chain alpha-keto acid dehydrogenase complex |
| c-di-GMP | 3,5-cyclic diguanylic acid |
| CHCA | α -cyano-4-hydroxy cinnamic acid |
| CoA | coenzyme A |
| CSP | <i>Clostridium Staphylococcus Pseudomonas</i> |
| CW | continuous wave |
| DAPPI | desorption atmospheric pressure photoionization |
| DESI | desorption electrospray ionization |
| DHB | 2,5-dihydroxy benzoic acid |
| DNA | deoxyribonucleic acid |
| EPS | extracellular polymeric substance |
| ESI | electrospray ionization |
| FDR | false discovery rate |
| FolE2 | GTP cyclohydrolase |
| fs | femtosecond |
| FTICR | Fourier transform ion cyclotron resonance |
| FumC1 | fumarate hydratase |
| G6P | glucose-6P |
| Gap | glyceraldehyde 3-phosphate dehydrogenase |
| GC-MS | gas chromatograph-mass spectrometry |

LIST OF ABBREVIATIONS

| | |
|-----------|--|
| Glk | glucokinase |
| Gln-6P | gluconate-6P |
| GlnA | glutamine synthetase |
| GTP | guanosine-5'-triphosphate |
| HAQs | hydroxy-alkyl-quinolones |
| Hfq | RNA-binding protein in <i>P. aeruginosa</i> |
| HHQ | 4-hydroxy-2-heptylquinoline |
| HisA | 1-(5-phosphoribosyl)-5-[(5-phosphoribosylamino) methylideneamino] imidazole-4-carboxamide isomerase |
| Hpd | 4-hydroxyphenylpyruvate dioxygenase |
| HSL | homoserine lactones |
| HupA | DNA-binding protein HU-alpha |
| HutH | histidine ammonia-lyase |
| HutI | imidazolonepropionase |
| HutU | urocanate hydratase |
| ID | identification |
| IE | ionization energy |
| IR | infrared |
| KEGG | Kyoto Encyclopedia of Genes and Genome |
| LA | laser ablation |
| LAAPPI | laser ablation atmospheric pressure photoionization |
| LAESI | laser ablation electrospray ionization |
| LA-ICP-MS | laser ablation inductively coupled plasma mass spectrometry |
| LAST | laser ablation sample transfer |
| LC | liquid chromatography |
| LD | laser desorption |
| LD-ESI | laser desorption-electrospray ionization |
| LDI | laser desorption ionization |
| LDLI | laser desorption lamp ionization |
| LDPI | laser desorption photoionization |

LIST OF ABBREVIATIONS

| | |
|---------|---|
| LDTD | laser diode thermal desorption |
| LEMS | laser electrospray mass spectrometry |
| LldD | L-lactate dehydrogenase |
| m/z | mass-to-charge |
| MACA | 4-amino-5-chloro-2-methoxybenzoic acid |
| MaiA | maleylacetoacetate isomerase |
| MALDESI | matrix-assisted laser desorption electrospray ionization |
| MALDI | matrix-assisted laser desorption ionization |
| MmsA | methylmalonate-semialdehyde dehydrogenase [acylating] |
| MmsB | 3-hydroxyisobutyrate dehydrogenase |
| Mqo1 | probable malate:quinone oxidoreductase 1 |
| MS | mass spectrometry |
| MS/MS | tandem mass spectrum |
| NQNO | nonylquinolone-N-oxide |
| ns | nanosecond |
| OPO | optical parametric oscillator |
| OprB | porin B |
| PA4667 | TPR repeat-containing protein |
| PA5217 | probable binding protein component of ABC iron transporter PA5217 |
| PEG | polyethylene glycol |
| Pgl | 6-phosphogluconolactonase |
| PQS | <i>Pseudomonas</i> quinolone signal |
| PvdA | L-ornithine N(5)-monooxygenase |
| PYO | pyocyanin |
| QIT | quadrupole ion trap |
| QS | quorum sensing |
| RNA | ribonucleic acid |
| RpoZ | DNA-directed RNA polymerase subunit omega |
| SIMS | secondary ion MS |
| SodA | superoxide dismutase [Mn] |

LIST OF ABBREVIATIONS

| | |
|--------|--|
| SpeE1 | polyamine aminopropyltransferase 1 |
| SPI | single photon ionization |
| STRING | Search Tool for Retrieval of Interacting Genes |
| TCS | two-component system |
| TOF | time-of-flight |
| UV | ultraviolet |
| UvrB | UvrABC system protein B |
| VUV | vacuum UV |
| Zwf | glucose-6-phosphate 1-dehydrogenase |

SUMMARY

This thesis develops and applies mass spectrometry (MS) methods that enabled the study of metabolites and proteins in and on bacterial biofilms produced by a *Pseudomonas aeruginosa* chronic wound isolate. To gain an understanding of complex biological systems, two major strategies – atmospheric pressure (AP) ion sources and a bottom-up proteomics MS pipeline – were developed for this study.

Various types of AP laser-based MS methods are available and applicable to biological studies. This thesis first focuses on the development of two separate types of AP ion sources utilizing a laser: (1) for direct ionization and (2) with the addition of postionization. In a scheme for direct ionization, a laser was fiber-coupled to an AP-MALDI (AP-matrix assisted laser desorption ionization) ion source, which can be directly interfaced to various commercial mass spectrometers. Initial testing of peptide standards showed good signal-to-noise ratio from a high-resolution mass spectrometer indicating functionality of the laser configuration. However, before this method could be applied to biofilms, the high-resolution MS instrument was permanently decommissioned. Additionally, biofilm imaging was attempted on a high resolution MALDI time-of-flight instrument, however sample preparation for protein detection from intact thick *P. aeruginosa* biofilms was unsuccessful and the detected species were not determined as the instrument had no tandem MS capability.

The next scheme involved the development of laser diode thermal desorption AP photoionization (LDTD-APPI) with a portable handheld near-infrared (IR) laser which was compared to an established laser ablation APPI (LAAPPI) with a laboratory mid-IR laser. In addition, the use of the portable handheld near-IR laser in LDTD-APPI was investigated for field

SUMMARY

sampling applications of microbial communities. Both configurations operated under different ablation mechanisms but were subjected to the same postionization strategy. Proof-of-concept was first performed on a small molecule standard and the native plant, *Salvia officinalis*, and then applied to biofilms for metabolite analyses. Results between the two methods yielded yet distinct detection of metabolites from plant and biofilm samples. Furthermore, the potential of using a lower cost portable laser for biological sampling of *P. aeruginosa* biofilms was demonstrated.

The second half of this thesis focuses on establishing a bottom-up proteomics pipeline intended to investigate changes in cellular metabolism affected by the addition of a carbon nutrient, lactate. This pipeline consisted of developing sample preparation and data analyses for bottom-up analyses. This proteomic workflow was first analyzed on *P. aeruginosa* planktonic cultures at various growth time points and cross-validated with metabolomic data provided by collaborators at Montana State University. Proteomic results on the planktonic culture correlated well with metabolomics. This established pipeline was then applied to *P. aeruginosa* biofilm cultures in which distinct changes in metabolism of biofilms were observed compared to the metabolism of planktonic cultures were observed.

To summarize, the configuration of the LA- and LDTD-APPI and the method development of a bottom-up proteomic workflow have been established for *P. aeruginosa* biofilm studies. These methods can be applied to metabolomic and proteomic studies of chronic wound biofilms.

1. INTRODUCTION

1.1 Biofilms Background

Biofilms are made up of microorganisms held together by a self-secreted extracellular polymeric substance (EPS). Biofilms have been putatively identified as forming ~ 3.3 billion years ago, but only within the last 30 years has research really begun examining these bacterial structures [1, 2]. Biofilms are nearly omnipresent in nature and can be found on lake beds, soil in the environment, the intestinal lining, dental plaque within the human body, contaminants on medical implants, and food processors [1, 3]. Their roles are complicated, in some cases, biofilms can be beneficial for environmental remediation in ground water decontamination or pathogenic for a human host where they can contribute to prolonged infections.

Biofilms possess structural and physiological heterogeneity [4]. They are typically made up of several different coexisting microorganisms that act as a functional entity with responsive and adaptive characteristics [2, 5, 6]. Residing microorganisms can cohabitate various spatial arrangements (i.e., layers, mix of co-aggregates, or as separate individual colonies) [6]. Spatial arrangements depend on various factors such as the synergy between all resident bacteria (competitive, mutual, or commensal), availability of oxygen and nutrients (sugars and organic acids), and the presence of any environmental perturbations (shear stress, antimicrobials, and dehydration) [2, 5, 6]. Cellular differentiation also exists where cells can alter gene expression in response to oxygen or nutrient gradients within the biofilm resulting in phenotypic variations (Figure 1) [3, 5]. Therefore, one goal of studying biofilms is to understand their dynamic mode of operation, specifically their inherently resistant and pervasive nature. The ability to understand and

predict biofilm responses to antimicrobials will contribute to the broader impact in devising effective treatment strategies, especially since billions of dollars are spent per year treating biofilm-related infections [7].

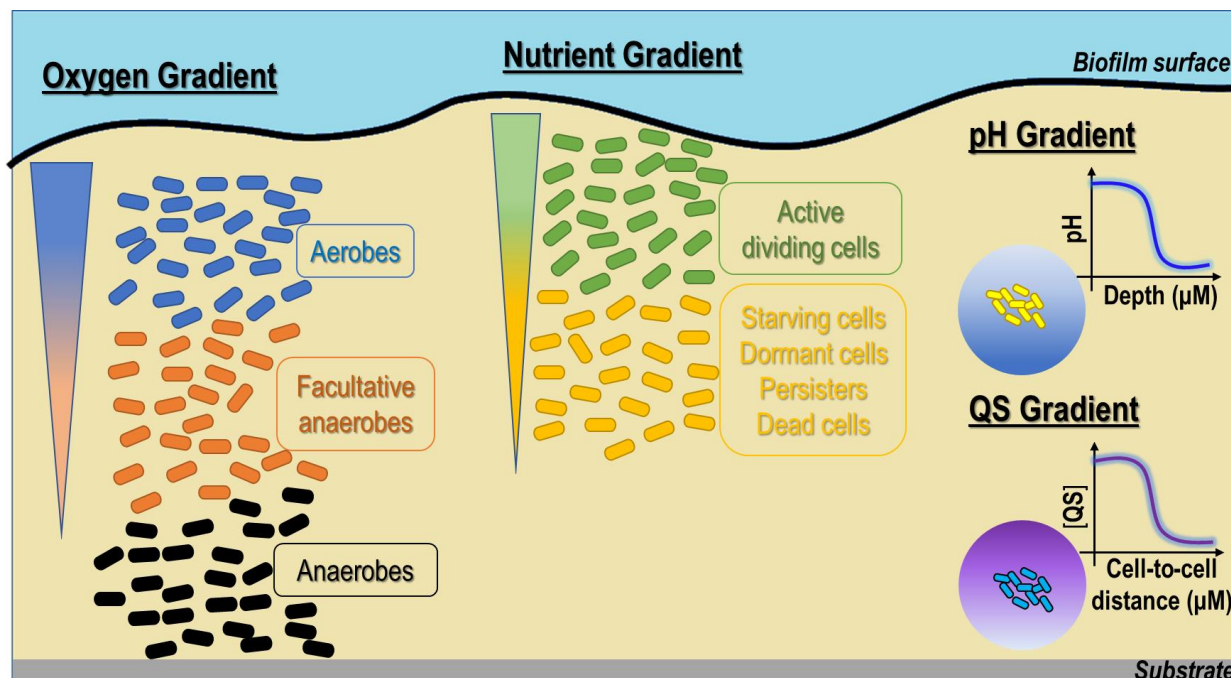


Figure 1. Biofilm heterogeneity – phenotypic variation of cells in response to oxygen, nutrient, pH and quorum sensing “QS” gradient. Image is adapted from Ref. [3].

1.2 Physiology: Stages of Biofilm Formation

The physiology of biofilm formation has been described in five stages [4, 8], as depicted in Figure 2. , (1) individual bacterial cells initially adhere to a surface, (2) cells begin the process of biofilm formation by secreting the EPS to adhere to the surface, (3) the structure of biofilm begins to develop as cells grow and divide, (4) upon biofilm maturation, channels form for water, nutrient, and chemical exchange. Cells alter their physiology based on their spatial location,

nutrients available, and environmental conditions. (5) Upon maturation, cells may disperse away from the biofilm or revert to its planktonic physiology, and spread to other surfaces where the cycle of biofilm formation is repeated.

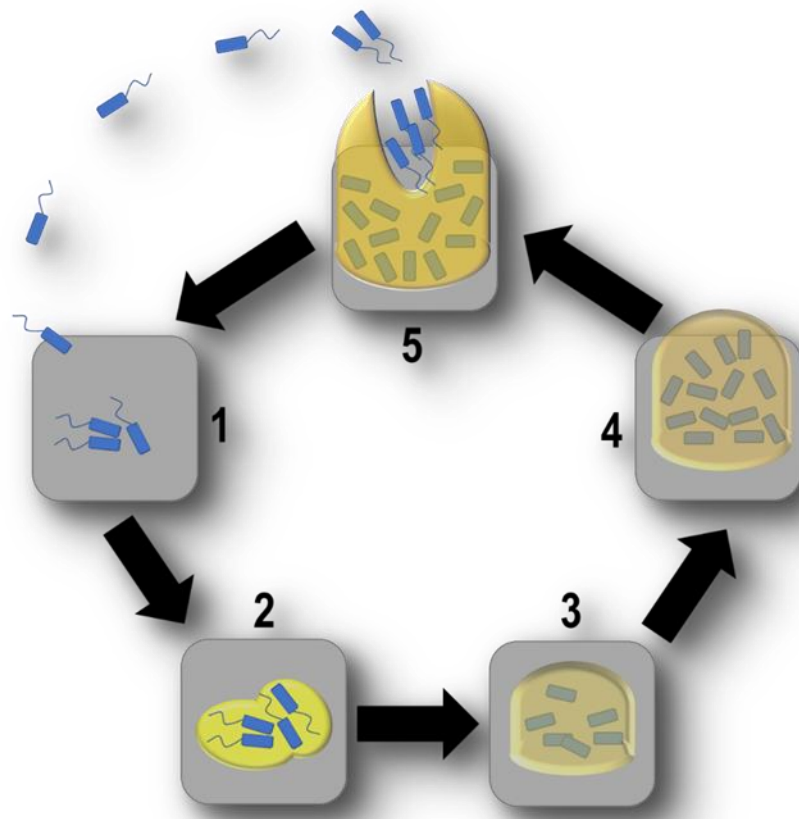


Figure 2. Stages of biofilm formation on a surface – (1) adhesion, (2) colonization, (3) development, (4), maturation, (5) dispersion. Image is adapted from Ref. [4].

1.3 Extracellular Polymeric Substance (EPS)

The EPS is a sticky and slimy substance that provides the three-dimensional architectural support for all encapsulated bacterial cells and keeps biofilms attached to a surface such as a host body. The EPS accounts for approximately 90% of the biofilm biomass and is made up of polysaccharides, proteins, lipids, RNA, and DNA [8]. The EPS contains enzymes secreted from cells which can be used to further generate or degrade the EPS, dependent on cellular response to changing environments [3]. The sorptive properties of the EPS allow for nutrient and resource uptakes from the environment. Most importantly, the EPS is an active barrier for bacteria against desiccation and antimicrobials, at least partially imparting to biofilms their resistant and pervasive nature [8].

1.4 Quorum Sensing (QS)

Cells embedded within the EPS are held in close proximity, unlike free floating (planktonic) cells. This close physical proximity enables cells to communicate with one another through a chemical signaling process known as quorum sensing (QS) [3]. QS involves the extracellular release of small molecule autoinducers, (i.e., acyl homoserine lactones (AHL) and quinolones) where the concentration level of autoinducers is a function of cell density. QS can induce a coordinated gene expression in response to changes in physiological conditions [3, 6, 9]. QS plays a role in intra- and inter-species communications, biofilm development, and can influence the spatial organizations within mixed species biofilms [6].

1.5 **Antibiotic Resistance**

The role of biofilms in infectious disease and on biomedical devices has been of growing concern, especially since treatments and prevention strategies all depend on physiological and metabolic conditions of the cells – whether cells are in their exponential growth or stationary phase during a given stage of biofilm formation [1, 8]. Moreover, cells in biofilms possess both an inheritable genotype and transient phenotype resistance. In phenotype resistance, defined as occurring without any genetic modification, persisters are dormant non-dividing cells indifferent to antibiotic treatments whereas actively dividing cells are more susceptible to antibiotics [10]. Persisters can resume growth following the removal of antibiotics and the resulting population will have the same antibiotic sensitivity as the original population [11]. Further complicating the treatment process, oxygen and nutrient gradients within the biofilm influence differential cellular metabolic states.

In response to antibiotic treatments, biofilms have putative defense mechanisms which prevent antibiotics from penetrating within the cell. The EPS limits the diffusion of antibiotics and inactivates antibiotics at low pH and high-metal concentration, thereby impairing the overall treatment [8]. Other mechanisms to keep antibiotics from entering the cell include binding to the antibiotics at the cell surface (i.e., by forming outer membrane vesicles or modifying lipopolysaccharides in the cell outer membrane) and limiting the number of transporters (i.e., membrane transport proteins and porin channel proteins) through which antibiotics can gain entrance [10]. In the event that antibiotics penetrate the cells, increasing expression of efflux pumps (cytosolic transport proteins) can transport antibiotics out of the cytosol [10]. The search is ongoing for products to make antibiotics more permeable or for enzymes to inhibit the expression of efflux pumps [10].

1.6 Strategies for Combating or Preventing Bacterial Biofilms

There are multiple strategies aimed to inhibit, disrupt, or disassemble biofilms in addition to the use of antibiotics. The two-component system (TCS) is a regulatory system composed of a kinase sensor domain that detects the environmental stimuli and a response regulatory domain which activates the appropriate physiological gene expression response (i.e., switching between motile or sessile stages of biofilm development) upon phosphorylation by the sensor kinase [12, 13]. The TCS influences expression of extracellular appendages (i.e., type IV pili or curli fibers) allowing bacteria to move on or attach onto surfaces [8, 13]. Strategies to prevent attachment of the cell to surfaces include interfering with the TCS signal transduction of bacteria to inhibit biofilm initiation or the use of anti-adhesion agents (i.e., pilicides or curlicides) that inhibit the assembly of type IV pili and curli fibers [8].

Strategies to disrupt the formation or eradicate biofilms include the use of antibiofilm polysaccharides, degradative enzymes, chelating agents, antimicrobial peptides, silver nanoparticles, and phage treatment [8]. Since low levels of c-di-GMP (3,5-cyclic diguanylic acid) have been implicated in promoting cell motility, protein engineering to improve protein binding affinities to sequester c-di-GMP has been considered for biofilm dispersal [8]. Surface modifications [14, 15] have also been examined to reduce biofilm formation, such as the use of small diameter nanoscale pores on anodic alumina surfaces to reduce biofilm formation [16].

1.7 Methods for Culturing Biofilms for Laboratory

The complexity of biofilms in terms of their cellular and communal dynamics are not fully understood. It is perhaps not surprising that while there are strategies for combating biofilms, they are generally not universally applicable to all biofilms. For understanding and modelling biofilm dynamics, *in vitro* studies are done by culturing biofilms in conditions that mimic their natural state [17]. Culturing methods can differ in how nutrients are introduced and if shear stress is involved [17]. The most basic method for static biofilm growth is on nutrient agar plates [18], where the cell culture is either inoculated directly on nutrient agar plates or inoculated onto a polycarbonate membrane which is placed above the nutrient agar. Other methods use drip-flow reactors, rotary biofilm reactors, or flow chambers, in which nutrients can be recycled or replenished and shear stress conditions can be introduced [17].

1.8 Characterization of Biofilm-Forming Bacteria with Mass Spectrometry (MS)

Numerous microscopy- and spectroscopy-based strategies have been employed to study biofilm heterogeneity in terms of their chemical and physical makeup [19]. Mass spectrometry (MS) is an alternative strategy which offers complementary molecular information to microscopy and spectroscopy. MS analysis can be used to determine the molecular mass and the structure of a molecule based on the mass-to-charge (m/z) ratio from the mass spectrum and fragmentation pattern of the ion from the tandem mass spectrum (MS/MS), respectively (Figure 3). Additionally, molecular spatial distribution of the sample can be visualized through MS imaging experiments [20]. The ion source, mass analyzer, and detector are the basic components that make up the mass spectrometer (examples of different types of these components are listed in Figure 3). With current

technological advancements for mass analyzers and detectors, MS characterization of biomolecules is being performed at increasing data acquisition speed, higher mass resolving power and mass accuracy [21].

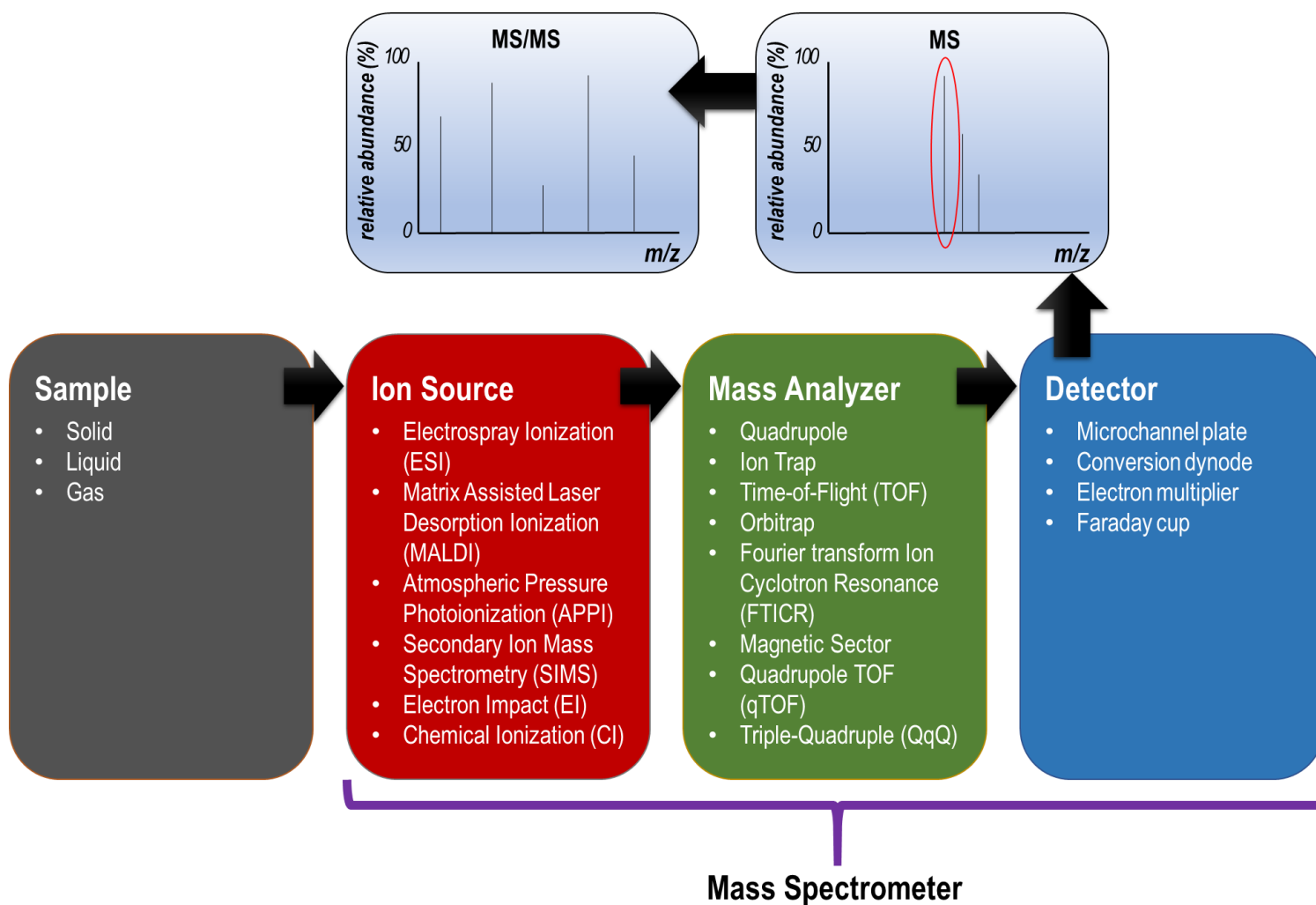


Figure 3. Basic components of a mass spectrometer. Samples are volatilized and ionized in the ion source. The generated ions are separated by the mass analyzer based on its m/z before reaching the detector. The resulting mass spectrum, “MS,” shows the ion abundance at a particular m/z from the sample. The selected ion is fragmented after dissociation, and the pattern is revealed in a tandem mass spectrum, “MS/MS.”

The function of a mass spectrometer's ion source is to transfer molecules from the condensed state and ionize them for mass analysis. Ion sources come in various forms and can be categorized in terms such as vacuum vs. ambient and hard vs. soft ionization [22]. The deciding factors for choosing an ion source depend on the chemical and physical properties of the sample and whether the analysis is targeted or untargeted. Electrospray ionization (ESI) and laser desorption-based ion sources are some of the most commonly used methods for planktonic or biofilm bacteria studies [22].

ESI is typically used in conjunction with liquid chromatography (LC), where the LC effluent containing the analyte goes through a conductive capillary (at high voltage potential) and is nebulized resulting in the generation of charged droplets. Gas phase ions are formed either when all the solvents are evaporated through Coulombic fission or the analyte ion ejects itself from the droplet through Coulombic repulsion [23]. In laser desorption-based ion sources, analyte ions from native samples are created either by direct laser desorption ionization with the addition of matrix (referred to as matrix-assisted laser desorption ionization, MALDI), or other strategies [22]. MS-based methods do allow for protein (proteomics) and small molecule (metabolomics) analyses of bacterial samples [24-29].

1.9 Thesis Overview

The primary research objective of this thesis is to develop atmospheric pressure (AP) laser-based ionization sources and traditional bottom-up proteomics MS methods to study small molecule metabolites and proteins of planktonic and intact biofilm from *Pseudomonas aeruginosa* cultures.

Chapter 2 reviews laser ablation (LA) MS applications for elemental and molecular analyses. The nature of samples and information to be gained from LA-based mass spectra are discussed briefly. Elemental analyses using laser ablation methods and molecular analyses using MALDI-MS (non-imaging and imaging) and alternatives are discussed. In addition, postionization methods for laser desorbed neutrals (elemental and molecular) and laser ablation for sampling are covered.

Chapter 3 focuses on the development of an AP-MALDI source. The source configuration of the laser fiber-coupled onto the AP-MALDI source and its interfacing to two MS instruments, a quadrupole ion trap and a Fourier transform ion cyclotron resonance, are discussed. In addition, this chapter also covers biofilm imaging attempts with a high-resolution vacuum MALDI time-of-flight MS.

Chapter 4 describes the development of two AP photoionization (APPI)-based MS methods – laser ablation (LAAPPI) and laser diode thermal desorption (LDTD-APPI). Source configurations, results on *P. aeruginosa* biofilms, and the potential of this portable diode laser for MS applications are discussed.

Chapter 5 describes bottom-up proteomics sample processing and data analyses for metabolic studies with bacterial samples. This protocol is demonstrated on *P. aeruginosa* planktonic cultures grown between two nutrient media – amino acid rich (CSP) and lactate-supplemented CSP (LCSP) media – across four time points.

Chapter 6 describes the aforementioned proteomics method applied to biofilms at a timepoint corresponding to the planktonic culture depletion of the lactate as a comparison. Differences in metabolism between *P. aeruginosa* planktonic and biofilm cultures are investigated.

Chapter 7 describes the concluding remarks and future directions for MS biofilm analysis. This will touch upon the implementation of laser ablation sample transfer (LAST), an offline sampling technique for a spatially resolved analysis of proteins for MS analyses.

2. APPLICATIONS OF LASER ABLATION MS

2.1 Nature of Samples and Information to be Gained from Laser Ablation Mass Spectra

Laser ablation (LA) or laser desorption (LD) has been applied to the mass spectrometric analyses across a wide variety of sample types [30, 31]. These applications can be classified based upon whether the desired information from MS is of atomic or molecular composition [30]. Molecular analyses by LA-MS can be further broken down into specific compound classes or chemical characteristics of those classes that can include polarity, volatility/thermolability, molecular weight, and/or extent of cross-linking (if a polymer). Samples can additionally be characterized physically based upon whether they are liquids, gels, solids, films, or powders as well as whether they are pure, in their “native” state (such as an intact semiconductor device or a piece of biological tissue), or extracted from the native state [31].

The specific type of LA-based MS analysis is an important consideration for any general studies. Some methods and samples allow ions to be formed directly by LA, in a process generally referred to laser desorption ionization (LDI) [22]. Other methods and samples require photoionization, electrospray ionization, or another type of postionization to form ions from gaseous neutrals generated by LA [22]. Finally, analyses can be categorized as either simple MS analysis of a homogeneous sample or MS imaging of a spatially heterogeneous sample [20, 22, 32, 33]. Depth profiling is a subset of the latter [20, 22]. Limitations in these analyses can occur based on the type of mass analyzer and its mass range, mass accuracy, mass resolution and/or tandem MS capabilities.

2.2 Laser Ablation for Elemental Analysis

Laser ablation inductively coupled plasma mass spectrometry (LA-ICP-MS) is a highly sensitive method with a linear dynamic range covering up to twelve orders of magnitude and is widely used for elemental and isotopic quantitative analyses of intact samples of metals, semiconductors, and biological tissues [30, 34-36]. Fields as diverse as chemistry, biology, medicine, geology, and material science utilize LA-ICP-MS for quantification, spatial imaging/mapping, and depth profiling of elements in solids [30, 34-36]. Nanosecond (ns) pulse length lasers emitting mid to far ultraviolet (UV) radiation and femtosecond (fs) pulse length lasers emitting near infrared (IR) to UV can be easily focused onto a small, targeted volume of a solid for subsequent volatilization and ionization by ICP [34] (refer to Figure 4 for schematic). For example, the distribution and concentrations of trace transition metals within human and rat biological tissues have been determined through spatial imaging by ns-LA-ICP-MS [35]. Depth profiling with fs-LA-ICP-MS can be performed on metal layers that are <50 nm thick [34].

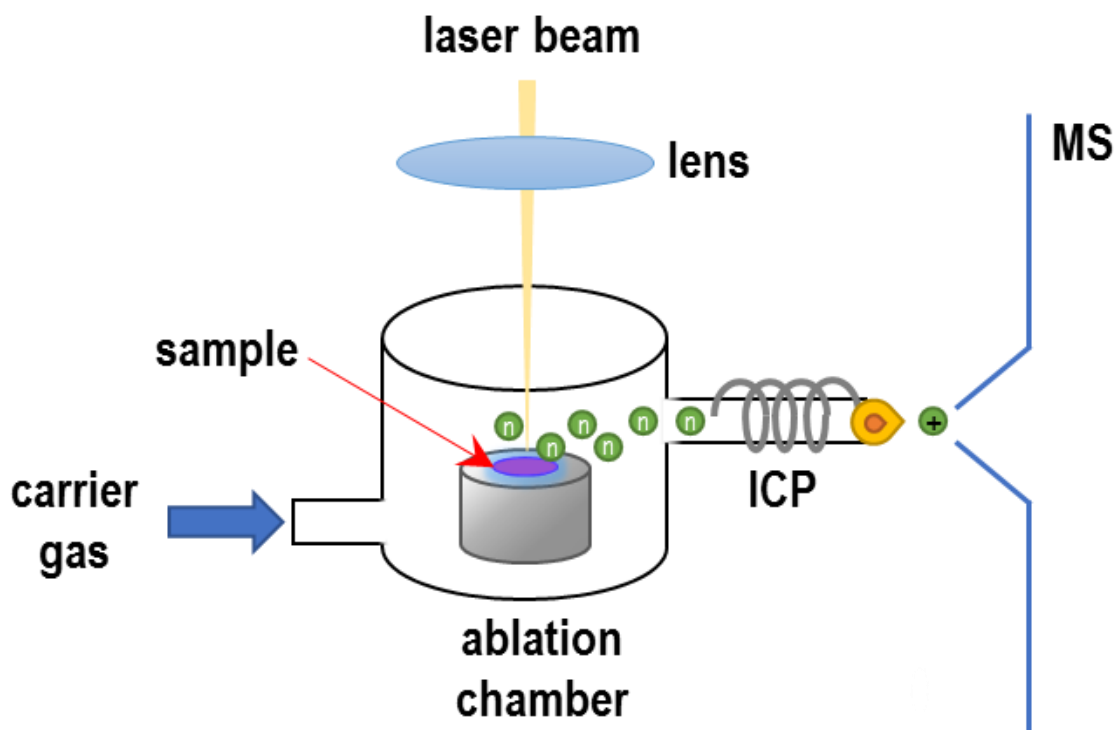


Figure 4. Schematic configuration of laser ablation inductively coupled plasma mass spectrometry (LA-ICP-MS). Laser ablated material from a sample is transferred to an ICP source by carrier gas then to a MS. Image is redrawn based upon figure from Ref. [35].

Nanosecond lasers have been somewhat limited in their use for direct, MS-based elemental analysis (i.e., without ICP) of solids. However, ~ 800 nm, <100 fs lasers have been shown to be effective for direct laser desorption ionization (fs-LDI), without ICP, by reducing matrix effects and improving quantification [37-39]. The fluctuation in sensitivity for different elements detected by fs-LDI-MS limits applications of the method compared to LA-ICP-MS [38, 39]. Nevertheless, fs-LDI-MS has been used for intracellular elemental analysis on single-cell paramecium to obtain pg/cell elemental contents, with ready quantification of nonmetals (i.e., P, S, and Cl) that were difficult to analyze by ICP-MS [40]. Depth resolution of 6 nm and spatial resolution ~ 5 μ m has been achieved for 800 nm fs-LDI-MS and roughly confirmed the elemental composition of

stainless steel and Al 5182 alloy standard [37]. Others have used fs-LDI-MS to probe galvanostatic Cu electrodeposited onto a Cu-seeded Si wafer to determine the major and trace compositions of a ~20 nm layer of contaminants [41].

The question arises whether fs-LDI-MS might be improved to the point that it could replace LA-ICP-MS. While fs-LDI is experimentally simpler, it seems unlikely to generally surpass the sensitivity and wide dynamic range of variants of LA-ICP-MS. Combining LA-ICP-MS with complementary methods such as secondary ion MS (SIMS), other ICP-MS based methods, and matrix assisted laser desorption ionization (MALDI-) MS imaging (see below) provides additional information from biological samples [35].

2.3 Non-Imaging UV Matrix Assisted Laser Desorption Ionization MS (UV-MALDI-MS) for Molecular Analysis

The most popular LA-based MS method for molecular analysis is UV-MALDI also known as MALDI [42]. The versatility of UV-MALDI-MS stems from its ability to analyze a broad range of compound classes (i.e., small metabolites, lipids, proteins, and inorganic materials), making the method an indispensable tool for the mass spectrometry community [20, 32, 42]. UV-MALDI-MS has been utilized for direct profiling lipids, sugars, and proteins such as diacylglycerols, oligosaccharides, and proteoforms, making it useful to identify disease biomarkers for diagnoses in biomedical and clinical studies [43, 44]. UV-MALDI-MS analyses have been used to characterize polymers for the mass repeat units, polymer chain lengths, terminal end units, and impurities [45]. UV-MALDI-MS has also been extended to the analysis of organic photovoltaics and electronics, for example, to characterize the polymerization extent of poly(3,4-ethyl-

enedioxythiophene), a conductive polymer prepared photoelectrochemically on solid-state dye solar cells [46].

UV-MALDI-MS is most commonly performed with 337 – 355 nm, ns laser pulses with samples under vacuum. AP-MALDI is a variant where samples are held at atmospheric pressure [47]. One advantage of AP-MALDI is the samples do not need to be dried prior to analysis, unlike the case with vacuum-based MALDI. However, vacuum MALDI is beneficial for cases which require greater sensitivity [47-49].

Sample preparation is crucial for MALDI and is often very sample specific. The matrix impacts the type of molecules to be ionized and must absorb the laser photon. Sample preparation typically requires homogenous co-crystallization of the analyte with the MALDI matrix [42]. There are various in-house or commercially available MALDI matrices. The two most common UV-MALDI matrices used for small molecules or protein digests are α -cyano-4-hydroxy cinnamic acid (CHCA) and for larger peptides or intact proteins, 2,5-dihydroxy benzoic acid (DHB) [42]. Matrices can be applied by spraying or variations of dried-droplet methods [50, 51]. Laser energy and spot size must be optimized for sample desorption and ionization with minimal molecular fragmentation to obtain reproducible, high quality mass spectra [42]. MALDI-mass spectra typically consist mostly of singly-charged ions (protonated/deprotonated molecules and salt/metal adducts), although multiply-charged species have been observed with larger molecular weight species [42].

2.4 UV-MALDI-MS Imaging for Molecular Analyses

A label-free imaging technique that is complementary to traditional optical imaging methods is two- or three-dimensional (2D/3D) imaging with UV-MALDI-MS referred to as MALDI-MS imaging [20, 32, 52]. Moreover, MALDI-MS imaging allows for molecular specificity which can be selected based on user preferences, enhancing the attractiveness of this technique [20, 32]. The most common modality in MALDI-MS imaging is microprobe mode, where a focused laser rasters across a sample surface while mass spectra are simultaneously collected at each location [52-54]. Heat maps in 2D are generated based on ion intensities which allows for visualizing the distribution of the ions at a particular m/z . A schematic of MALDI imaging is depicted in Figure 5. Individual 2D slices are pieced together generating a 3D image of the sample (i.e., tissue, organ, or inorganic material) [52, 53].

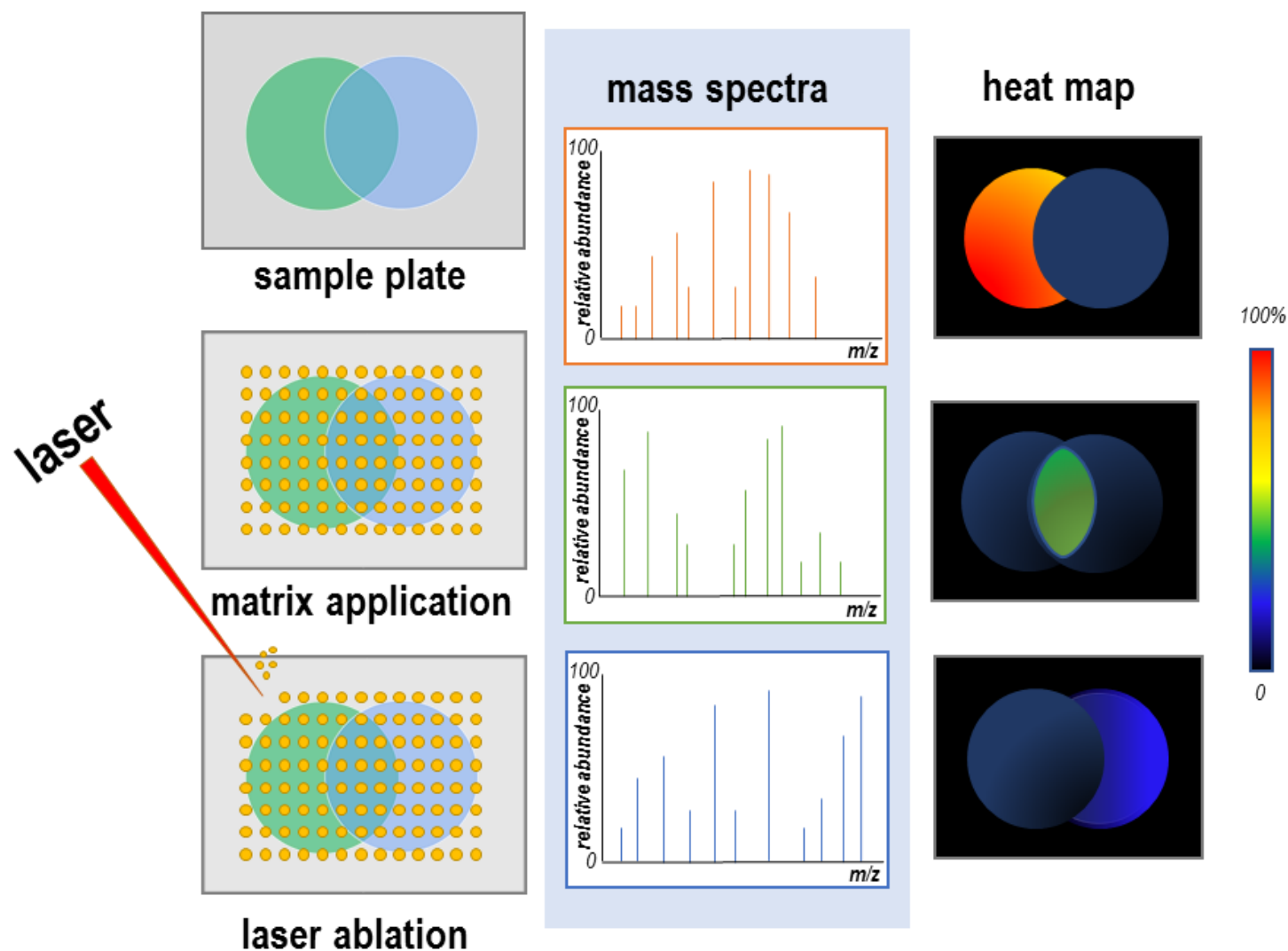


Figure 5. Matrix assisted laser desorption ionization mass spectrometry (MALDI-MS) imaging schematic workflow. Steps show the matrix application on a tissue slice in which a laser irradiates across the sample plate. The ion intensities of the m/z at each particular x , y -coordinate are plotted in a false-color image. Image is redrawn based upon figure from Ref. [53].

The push for higher spatial resolution with MALDI-MS imaging is currently underway by improving methodology and instrumentation. Sampling time and spatial resolution have improved greatly with higher laser repetition rates and optics with micron-size focusing. Current commercial mass spectrometers have high spatial resolution in which the quality of a MALDI image at 15 μm spatial resolution can be comparable to H&E staining in optical microscopy on a mouse brain tissue [55]. Customized or modified instruments have resolution approaching 1 μm [55]. For example, the Caprioli group modified the MALDI source of a commercial mass spectrometer to a transmission geometry configuration which improved spatial resolution to 1 μm that was subsequently used for imaging the axon fiber, molecular layer, Purkinje layer, granule cell layer, and cerebellar medulla of the mouse cerebellum as well as small proteins within pancreas islet cells [56, 57].

MALDI-MS imaging has been used for drug discovery where the efficacy between the drug and the target depends on the delivery method, concentration, and biochemical interactions [33, 52]. Distribution of the drug and its metabolites in untreated and treated tissues/organs has been used to image endogenous and exogenous compounds of samples at near cellular spatial resolution, providing information relevant to drug metabolism and pharmacokinetics as well as absorption, distribution, metabolism, and excretion (ADME) studies [33]. For example, the Hummon group has mapped the changes in protein distribution on 3D cell cultures of colon cancer spheroids and ADME studies of the chemotherapeutic drug, irinotecan, and its metabolites [52, 58].

Time-of-flight (TOF) mass analyzers are more commonly used in protein and metabolite MALDI-MS imaging of biological samples, but resolving power and mass accuracy (20-100 ppm) of a TOF is often insufficient for untargeted identification [59, 60]. MALDI-MS imaging has been

advanced through the use of high resolution mass analyzers such as Fourier transform ion cyclotron resonance (FTICR), Orbitrap, or a quadrupole TOF to generate more highly-resolved peaks and greater mass accuracy [20, 32, 54]. A comprehensive study demonstrated enhanced metabolite identifications in MALDI-MS imaging on formalin-fixed and paraffin-embedded tissue specimen with FTICR in comparison to a much lower resolving power TOF [60]. In a top-down proteomics experiment, proteoforms of the antimicrobial protein subunit, calprotectin, were identified at a mass accuracy <5 ppm on a mouse kidney tissue infected with *Staphylococcus aureus* using an FTICR mass analyzer [59]. However, a tradeoff is a relatively slower acquisition time with Fourier transform-based mass analyzers when compared to TOF mass analyzers [32].

2.5 UV-MALDI-MS for *Pseudomonas aeruginosa*, With and Without Imaging

MALDI-MS can be performed in standard mode for non-imaging analyses or in microprobe mode for imaging mode, as described above. The difference between standard and imaging mode is illustrated here by consideration of their application to microbial cultures with a particular focus on *P. aeruginosa*, as the latter has been widely studied by MALDI-MS. These bacterial examples are also used to demonstrate that MALDI sample preparation varies with target analyte, sample state, and whether experiments are run in standard or imaging mode.

MALDI-MS in standard mode has become a commonplace for the identification of microorganisms [61-64], when the goal here is identification of species and strain of an unknown microbial specimen. Microbial identification with UV-MALDI-MS, as it is most commonly practiced is a subset of proteomics, often performed with specific databases and specialized bioinformatics. Microbial identification is based on ribosomal or other highly abundant proteins.

In one identification strategy, proteins are extracted from microbial samples, then the extracts are spotted onto a MALDI target along with CHCA matrix [65]. Microorganisms such as *Pseudomonas spp.* have been identified in both saliva (planktonic bacteria) and oral biofilms (sessile bacteria) of chronic kidney disease and periodontitis patients [65]. Both TOF and high mass resolution MS instruments have been used to differentiate strains of *P. aeruginosa* clinical isolates [66]. New bioinformatic data processing workflows have been applied to identify extra- and intra-cellular proteins that may be involved in *P. aeruginosa* biofilm formation [67].

MALDI-MS has also been extensively applied to the imaging of intact microbial biofilms, where sample preparation often depends up the target analytes (i.e., proteins vs. metabolites) and the growth conditions of the culture. Matrix deposition on intact biofilms, either grown in liquid nutrient or directly in nutrient agar, are most often done by spray coating liquid matrix or sieving dry matrix powder [50, 68].

MALDI-MS imaging of metabolites in *P. aeruginosa* biofilms grown and analyzed in agar with matrix added by sieving was used to visualize the metabolite response of *P. aeruginosa* in the presence of the antibiotic azithromycin [69]. This strategy was also used to probe the exchange of phenazine metabolites between *P. aeruginosa* and *Aspergillus fumigatus* cocultures [25]. Direct analysis on air-dried *P. aeruginosa* biofilms initially cultivated in liquid nutrient were used to visualize secondary metabolite differences between the wild-type and quorum sensing mutant in MALDI-guided secondary ion MS imaging [70]. Additionally, MALDI-MS for identification and quantitation on *P. aeruginosa* quorum sensing molecules, N-acyl homoserine lactones, has been achieved using synthesized isotope- labeled internal standards [71] or using Girard's reagent T derivatization for accurate quantification [72].

MALDI-MS imaging of proteins in microbial biofilms has also been demonstrated, both by bottom-up and top-down strategies. In bottom-up proteomics, the protease, typically trypsin, is sprayed or spotted directly on the sample. The resulting tryptic digests are then imaged and subsequently identified in MALDI-MS/MS. An early example extending the feasibility of MALDI-MS imaging to bacterial biofilms were on intact *Enterococcus faecalis* and *Escherichia coli* biofilms grown directly on stainless steel and imaged in both top-down and bottom-up proteomics approaches [27]. MALDI-MS biofilm imaging was able to show that regions enriched with host protein, calprotectin, promote *P. aeruginosa* co-colonization with *Staphylococcus aureus* in murine lung [73].

2.6 Alternatives to UV-MALDI-MS

LDI is a matrix-free alternative to UV-MALDI, where little to no sample preparation is needed thereby reducing any matrix suppression and interferences that may occur with MALDI matrix co-crystallization. The resulting mass spectrum is simpler, especially for analyses of low molecular weight molecules (<500 Da). However, LDI only generates useful ion signals for a limited set of samples. Samples containing aromatic groups that absorb the UV laser wavelength can sometimes be ionized, such as the case for the analysis of hydrophobic natural organic matter [74]. LDI was also able to chemotype metabolite (<500 Da) differences between diatoms *Coscinodiscus granii* and *Thalassiosira pseudonana*, which possess biomineralized nanostructures that presumably induce ionization (see below) [75]. Furthermore, by spotting a polyethylene glycol (PEG)600 solution onto a dried diatom suspension solution, the Pohnert group was able to detect the PEG600 polymer which cannot be detected in UV-MALDI [75]. Similarly, a *Drosophila*

melanogaster insect wing with surface hydrophobicity and high optical absorbance was used in LDI in detection of free fatty acids and lipids in mouse liver extract and fingerprint analyses, which are typically low in abundance for MALDI [76]. In addition, nanostructures have also been widely used in LDI for enhancement of desorption/ablation and ionization [77].

2.7 Methods that Utilize Postionization of Desorbed Neutrals

2.7.1 Laser Desorption Photoionization Mass Spectrometry (LDPI-MS) – VUV Single Photon Ionization (SPI) of Laser Desorbed Neutrals in Vacuum

Postionization strategies can enhance signal by ionizing the neutrals generated from laser desorption or ablation [22]. One method of postionization uses vacuum UV (VUV) radiation for single photon ionization (SPI) on laser desorbed neutrals in vacuum (LDPI) [78]. A LDPI schematic is depicted in Figure 6: it is a selective and soft ionization method for molecules that possess ionization energy (IE) less than the VUV photon energy (typically 7.5-11.8 eV for lamp or laser sources), as most background gases with higher IEs are not ionized [78]. LDPI has been used to analyze pharmaceutical drug compounds [79], characterize asphaltenes in complex petroleum mixtures [80], and differentiate metabolites between mixed and pure microbial cultures in a biofilm [81]. LDPI has also been used in MS imaging of bacterial biofilms [82, 83] and depth profiling of biological and electronic materials [84, 85].

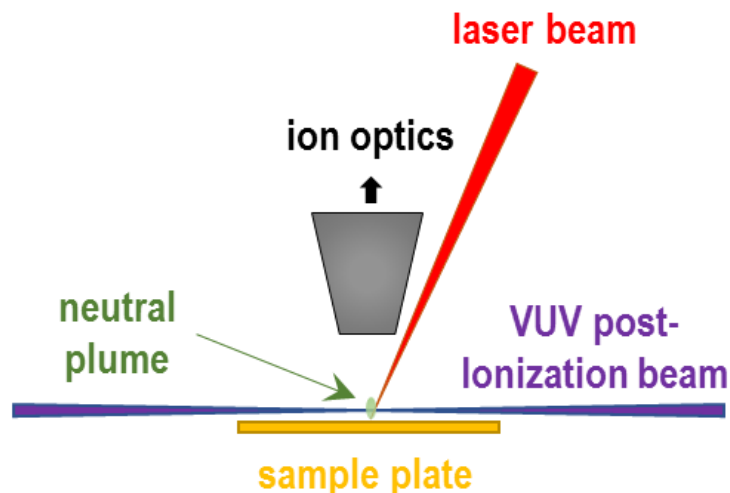


Figure 6. Schematic of laser desorption photoionization mass spectrometry (LDPI-MS). A laser (in red) is focused onto the sample plate for sample desorption and an intersecting vacuum ultraviolet (VUV) beam (in purple) is used for postionization of ablated neutral plume. Image is redrawn based on figure from Ref. [22].

2.7.2 Laser Ablation Atmospheric Pressure Photoionization Mass Spectrometry

(LAAPPI-MS) – Atmospheric Pressure Ionization Initiated by VUV Single Photon

Ionization

Laser ablation atmospheric pressure photoionization (LAAPPI) follows the same principle as LDPI except the source is at atmospheric pressure and a hot solvent vapor jet (dopant) intercepting the ablated neutral plume is used to further improve ionization efficiency [86]. The dopant promotes molecular ionization through protonation/deprotonation and/or charge exchange since it has lower IE that is easily ionized by VUV radiation [87]. The use of a mid-IR laser for ablation in LAAPPI is advantageous for samples with high water content that are therefore highly absorptive at 2940 nm, inducing an explosive event resulting in the ejection of molecules [88]. Applications of LAAPPI have been used to study nonpolar compounds (i.e., cholesterol in rat brain tissue and flavones in *Citrus aurantium* leaves) [88]. LAAPPI is used to detect metabolites in *P.*

aeruginosa biofilms in Chapter 4. Phytochemicals (i.e., terpenes and terpenoids) in *Salvia officinalis*, which are typically studied with gas chromatograph-mass spectrometry (GC-MS), have also been imaged with LAAPPI [89]. Laser desorption lamp ionization (LDLI) is a LAAPPI variant that employs a 1064 nm IR laser operated in high energy mode for desorption and VUV xenon gas discharge lamp for ionization for the detection of inorganic compounds (i.e. copper and zinc in brass samples) [90].

2.7.3 Laser Ablation Electrospray Ionization Mass Spectrometry (LAESI-MS) and Laser Electrospray Mass Spectrometry (LESI-MS)

Lasers have also been alternatively coupled to electrospray for postionization [31]. A general schematic is depicted in Figure 7. Variants include laser electrospray mass spectrometry (LEMS), electrospray-assisted laser desorption/ionization (ELDI), laser desorption-electrospray ionization (LD-ESI), matrix-assisted laser desorption electrospray ionization (MALDESI), and laser ablation electrospray ionization (LAESI) [31]. These variants are similar in that they all use laser desorption followed by subsequent electrospray postionization, but generally differ by the use of ns- or fs-lasers, the presence or absence of a matrix, and/or other experimental parameters [31, 91, 92]. LEMS and IR-ELDI differ by the use of fs-IR lasers and ns-IR lasers, respectively, and neither requires a matrix [31]. While ELDI and LD-ESI both use ns-UV lasers, the distinction with the latter is the spatial separation between the ablation and electrospray ionization events [92]. Although ELDI does not require a matrix, organic matrices have been found to improve desorption in ELDI, which is like MALDESI in that it uses a matrix [31]. IR-MALDESI and LAESI both utilizes ns-IR lasers and are fundamentally equivalent when endogenous water is present [93].

LEMS has been argued to be a softer ionization method where the condensed phase folding of the lysozyme protein arguably remained intact for LEMS, compared with traditional ESI which denatures the protein even without the use of lasers [31]. Samples situated away from the MS are ablated and transferred to ESI for postionization in LD-ESI for rapid metabolite prescreening, used with MALDI imaging to determine spatial distribution, and HPLC/ESI-MS to confirm metabolite identification in a comprehensive analysis of grapes [92]. IR-MALDESI with the use of ice as the matrix has been used for imaging analyses of trace single textile fibers taken from adhesive tapes [94], cholesterol in cervical tissues [95], and quantitative imaging of an antiretroviral drug in cervical tissue [96]. LAESI has been used to study antibiotic susceptibility in bacterial colonies where changes in metabolites and lipids were observed in the zone of inhibition between *E. coli* and *B. subtilis* [97].

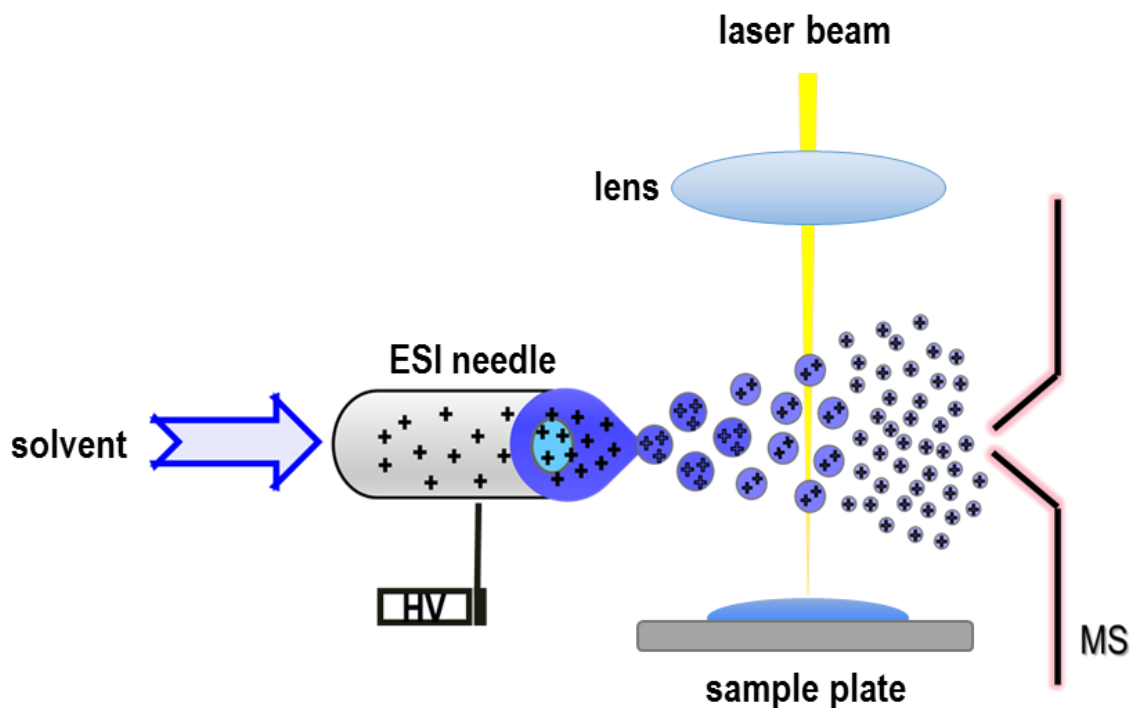


Figure 7. Schematic of laser ablation with electrospray ionization (ESI) mass spectrometry. A laser is used for ablation in which neutrals are postionized by ESI.

2.8 Laser Ablation Sampling

Laser ablation for sample transfer can be used for various offline MS analyses [98-101]. A schematic of laser ablation for sample transfer (LAST) is depicted in Figure 8. Utilizing LAST and nanostructure-assisted LDI, a solvent droplet used to capture ablated material from a bacterial culture was analyzed in nanostructure-assisted LDI, where higher contents of phosphatidylethanolamine were found in *E. coli* and phosphatidylglycerol in *Bacillus cereus*, demonstrating the potential for lipid biomarker discovery with minimal sample preparation [102]. Mid-IR laser ablation with solvent capture by aspiration have been used for MS imaging of plant pigments from *Alstroemeria spp.* flower petal and upper part of the radish taproot without additional sample preparation [103]. Sample transfer via atomic force microscope (AFM) tip-enhanced UV laser ablation has also been used to capture materials onto a silver wire suspended above the tip for LDI analysis on small molecules (i.e., anthracene and rhodamine 6G) and MALDI analysis on larger biomolecules (i.e., angiotensin, insulin, and cytochrome c) [104]. Some challenges in sample transfer are focusing the small laser beam onto the region of interest, transporting the ions and neutrals to the ion source, and being able to ionize molecules efficiently without causing fragmentation. However, the added advantage of sample transfer is with the ability to perform additional analyses such as NMR or fluorescence assays.

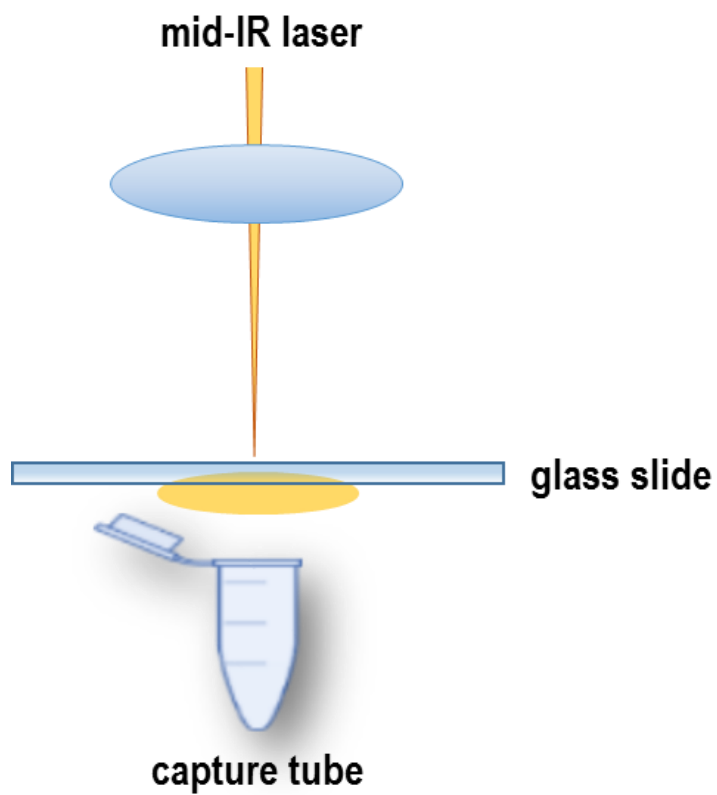


Figure 8. Schematic of laser ablation sample transfer (LAST). Mid-infrared (IR) laser is used to generate an ablation plume which is captured into a solvent droplet suspending from a syringe.

3. MALDI-MS OF BIOFILMS

3.1 Introduction

Non-imaging and imaging MALDI-MS have been central to various metabolomics and proteomics studies of biofilms [20, 25, 27, 105-107]. Traditionally, most ionization takes place under high vacuum conditions; an alternative is AP ionization [108, 109]. AP ion sources are advantageous because samples do not need to be desiccated and sample interchange between analyses can be done in relatively short order [108, 109]. AP ion sources are amenable for bioanalyses, environmental studies, amongst various others [108, 109]. An example is AP-MALDI which is an alternative to traditional vacuum-based MALDI that can be easily implemented to various mass spectrometers for analyses.

This chapter describes the interface of an AP-MALDI source that can be readily coupled to the majority of mass spectrometers that use AP-interfaces [47], and in this case, to two mass spectrometers - a low-resolution quadrupole ion trap (QIT) and a high-resolution Fourier transform ion cyclotron resonance (FTICR). The AP-MALDI configuration was developed for both metabolomic and proteomic studies of bacterial biofilms. In addition, imaging biofilms on a high-resolution vacuum MALDI time-of-flight (TOF) mass spectrometer was attempted by adapting the sample preparation from the Dorrestein group with a sieve for matrix application to biofilms [68].

3.2 Experimental Details

3.2.1 Instrumentation

The AP-MALDI source (AP-MALDI, MassTech, Baltimore, MD) consisted of a motorized stage with power supply to apply an electrical potential to a movable sample plate. Two separate laser systems were used to deliver the laser beam into the fiber optic input attached to the AP-MALDI source by which the laser was delivered onto the sample plate for laser desorption/ionization.

The first configuration consisted of an optical parametric oscillator (OPO) pumped by a Nd:YAG laser (Opolette 2940, Oportek, Carlsbad, CA), attenuation optics, fiber patch, and the AP-MALDI source which was mounted directly on the QIT mass spectrometer (MT Explorer 50, MassTech, Baltimore, MD). The Nd:YAG pumped OPO laser outputs two wavelengths, one in the mid-IR at 2940 nm and the other in the UV at 355 nm, necessitating two separate sets of optical components to transmit each wavelength. An energy meter was used to monitor the input laser energy to the fiber. The entire configuration is shown in Figure 9. The optical components for UV attenuation consisted of (1) neutral density filter, (2) half-wave plate, (3) polarizer, (4) beamsplitter, (5) UV-enhanced Al mirror, (6) focusing lens, and (7) 300 μm core fiber patch with 0.12 numerical aperture (N/A), which all transmit UV. The optical components for IR attenuation consisted of (1) beamsplitter, (2) neutral density filter, (3) focusing lens, and (4) 450 μm core germanium oxide with 0.3 N/A fiber patch, which all transmits IR. This system was interfaced to a field-deployable QIT mass spectrometer [110].

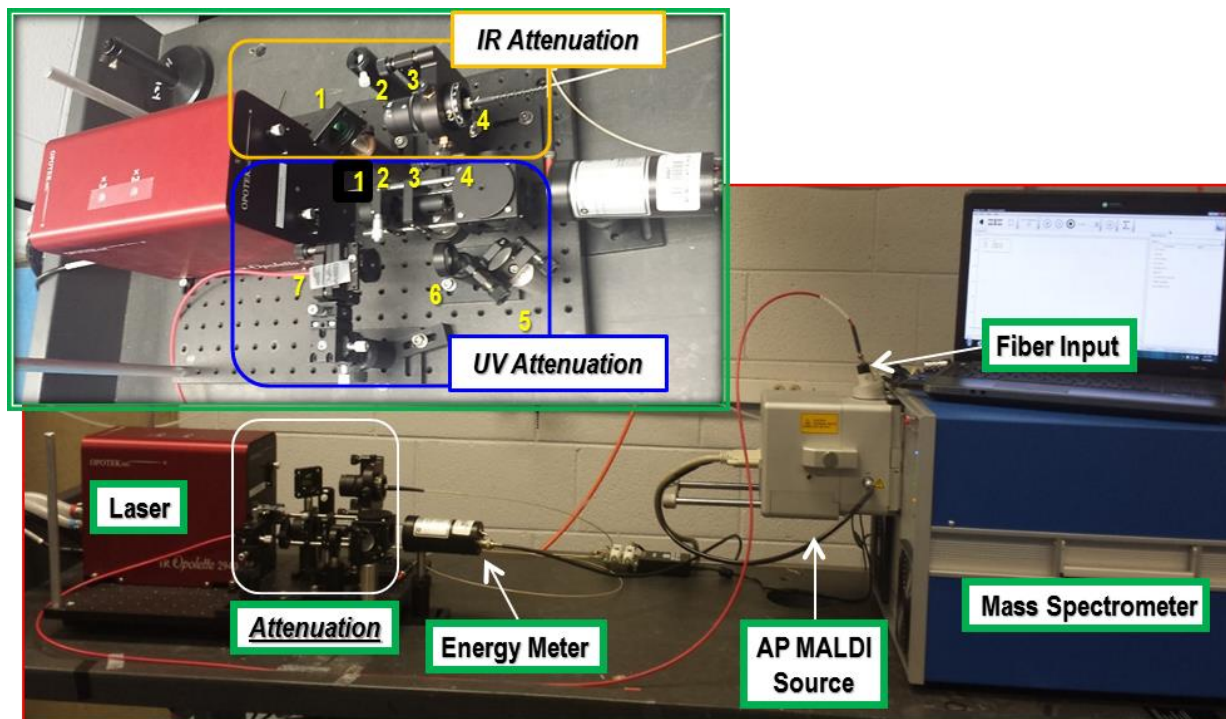


Figure 9. Atmospheric pressure matrix assisted laser desorption ionization (AP-MALDI) setup on a field-deployable quadrupole ion trap (QIT) mass spectrometer. Bottom: side view of entire AP-MALDI setup. Top: Optical components for (a) IR and (b) UV attenuation. IR attenuation consist of (1) beamsplitter, (2) neutral density filter, (3) focusing lens, and (4) germanium oxide fiber patch, which all transmit mid-IR. UV attenuation consist of (1) neutral density filter, (2) half-wave plate, (3) polarizer, (4) beamsplitter, (5) UV-enhanced Al mirror, (6) focusing lens, and (7) fiber patch, which all transmit UV.

The second configuration consisted of the AP-MALDI source fiber-coupled to a Nd:YAG laser with 355 nm output (Minilite, Continuum, San Jose, CA) with a UV fiber collimator and the fiber patch (Figure 10a). The laser was enclosed within the retractable hollow cube and lens tube setup. A modified extrusion piece, which extends from the laser head, was designed for the lens tube to fit over the extrusion piece (Figure 10b). This setup was directly interfaced to a 7 Tesla FTICR mass spectrometer located in the Research Resources Center at UIC (LTQ-FTICR, ThermoFisher Scientific, San Jose CA).

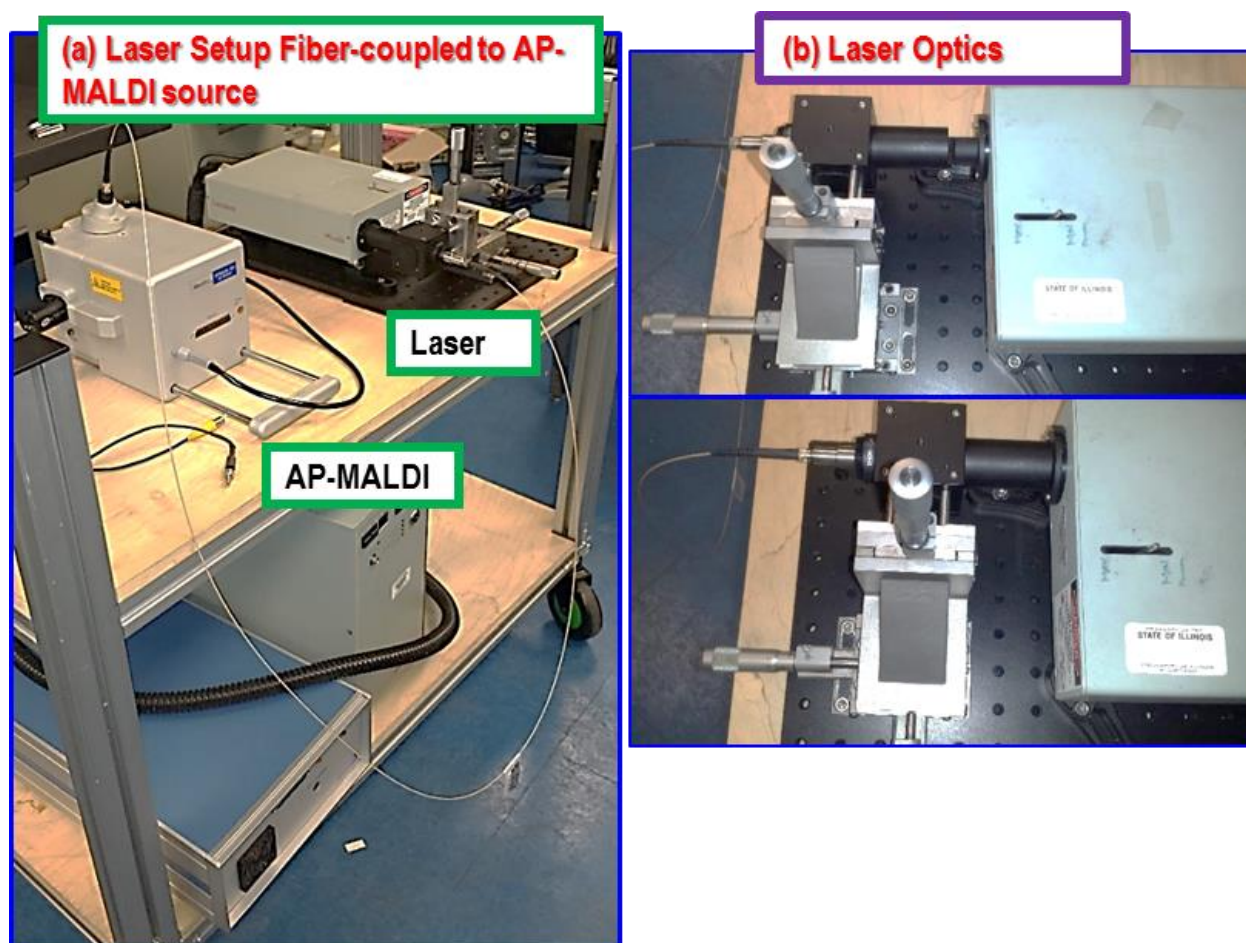


Figure 10. Components for interfacing AP-MALDI source onto a Fourier transform ion cyclotron resonance (FTICR) mass spectrometer. (a) Fiber-coupling between the 355 nm output of the Nd:YAG laser and the AP-MALDI source. (b) Laser enclosure and fiber collimator.

3.2.2 Sample Preparation

α -Cyano-4-hydroxycinnamic acid (CHCA) matrix, trypsin, proteins and peptides were all purchased from Sigma Aldrich (St. Louis, MO). The peptides were a mixture of angiotensin II, P14R, and bradykinin which were analyzed on the QIT mass spectrometer. Bovine serum albumin and lysozyme from hen egg were the proteins analyzed on the FTICR mass spectrometer. Proteins were tryptically-digested overnight with trypsin-to-protein ratio of 1:50 for albumin and 1:15 for lysozyme, then the resulting peptide fragments were analyzed. Dried droplet application of CHCA

followed by the addition of these protein/peptide standards were deposited onto a 96 spot MALDI plate.

A different sample preparation strategy was employed for vacuum MALDI-MS. A universal matrix consisting a mixture of CHCA and DHB was purchased from Sigma Aldrich. Overnight culture of *P. aeruginosa* clinical isolate (215) culture grown in a nutrient-defined *Clostridium Staphylococcus Pseudomonas* (CSP) medium was inoculated (1 μ L of 0.1 OD600) onto a polycarbonate membrane and grown on CSP agar plates for three days with nutrients replenished in between. Biofilms were fixed with 0.1% trifluoroacetic acid and exposed to 70%, 90%, and 95% ethanol washings, 5 mM dithiothreitol, and incubated at 37°C with 1g/L and trypsin for 4-18 hrs. Biofilms were then blotted onto the MALDI stainless steel target plate and flash frozen with the polycarbonate membrane removed (Figure 11a). Matrix was directly applied via a 53 μ m stainless steel sieve (Hogentogler & Co., Inc., Columbia, MD) on the thawed biofilm sample and allowed to dry (Figure 11b). Unfixed and unwashed biofilms were embedded in 1% agar with trypsin spotted on areas of the agar and the bottom two biofilms designated “T” (Figure 12a). Angiotensin II and CSP were also spotted on biofilms, designated “A” and “C,” respectively (Figure 12a). The biofilms embedded in agar were coated in matrix using the sieve and allowed to dry to completeness prior to analysis (Figure 12b). All imaging experiments were performed on a vacuum MALDI-TOF mass spectrometer (Autoflex Speed LRF, Bruker Daltonics, Billerica, MA).

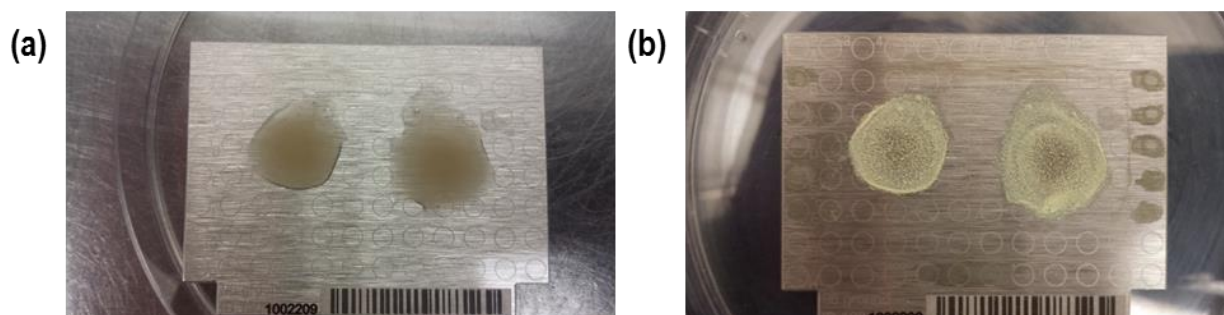


Figure 11. Images of blotted fixed biofilms and results. (a) Thawed blotted biofilms on MALDI plate. (b) Completely dried biofilms after matrix application.

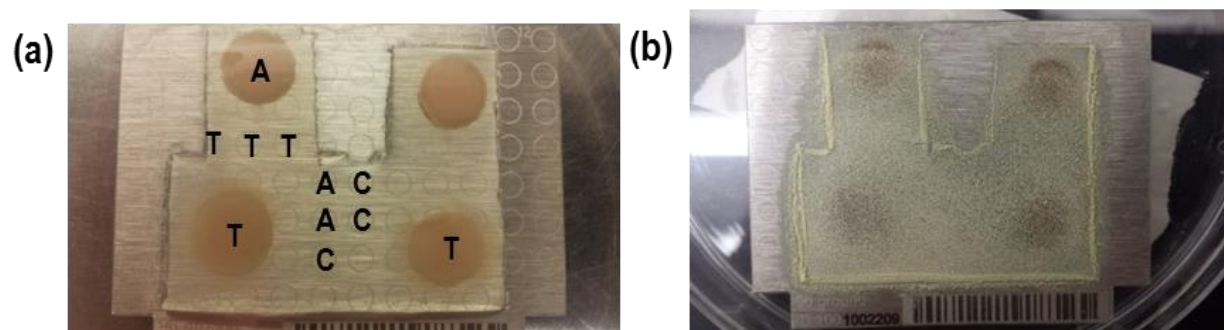


Figure 12. Images of agar embedded biofilms. (a) Blotted biofilms embedded in agar - top two biofilms were not treated with trypsin and bottom two are treated with trypsin. Letters indicate angiotensin II (A), trypsin (T), and *Clostridium Staphylococcus Pseudomonas* (CSP) medium (C) spotted on agar prior to matrix application. (b) Semi-dried biofilm following matrix application.

3.3 Results and Discussion

3.3.1 Non-Imaging UV-AP-MALDI-MS on a Quadrupole Ion Trap (QIT) Instrument

Femtomolar concentrations of peptides were detected by the QIT instrument using 355 nm UV-AP-MALDI. Protonated peptides of bradykinin (m/z 757.6), angiotensin II (m/z 1046.9), and P14R (m/z 1533.9) displayed peaks with high signal-to-noise ratios (Figure 13). The experimental molecular mass of the $[M+H]^+$ produced mass errors ranging from 40 to 400 ppm consistent with the typical ± 0.5 Da mass accuracy of this QIT instrument.

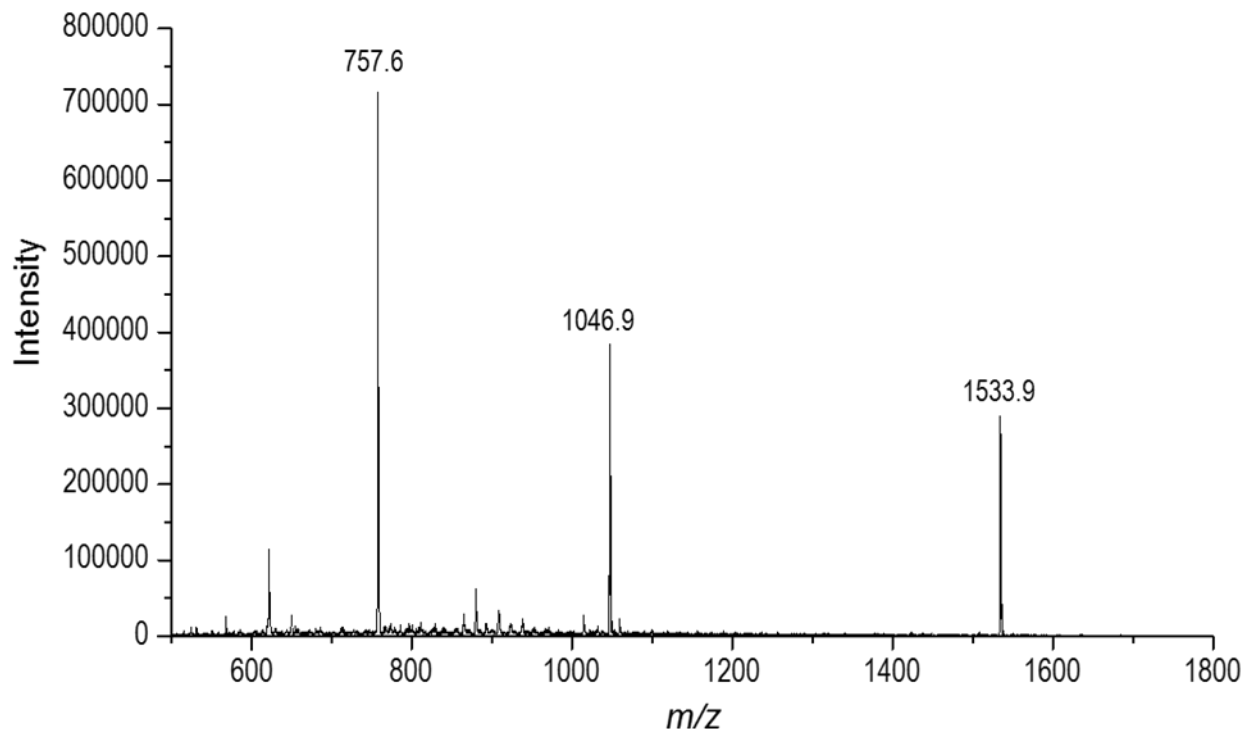


Figure 13. Mass spectrum of peptides – bradykinin (m/z 757.6), angiotensin II (m/z 1046.9), and P14R (m/z 1533.9).

3.3.2 Non-Imaging IR-AP-MALDI-MS on a QIT Instrument

No spectrum was obtained for IR-AP-MALDI. It was hypothesized that the optical design was not sufficient to produce ion signal by IR-AP-MALDI. It was found that the fiber numerical aperture ($N/A = 0.3$) for IR was incompatible with the fiber attachment tube (refer to Figure 14). This resulted in ~50% transmission loss due the three times larger N/A of the germanium oxide fiber. In addition, the laser beam could not be optimally focused on the MALDI plate for sample desorption/ionization as the fiber output could not be situated close enough to the focusing lens within the commercial apparatus.

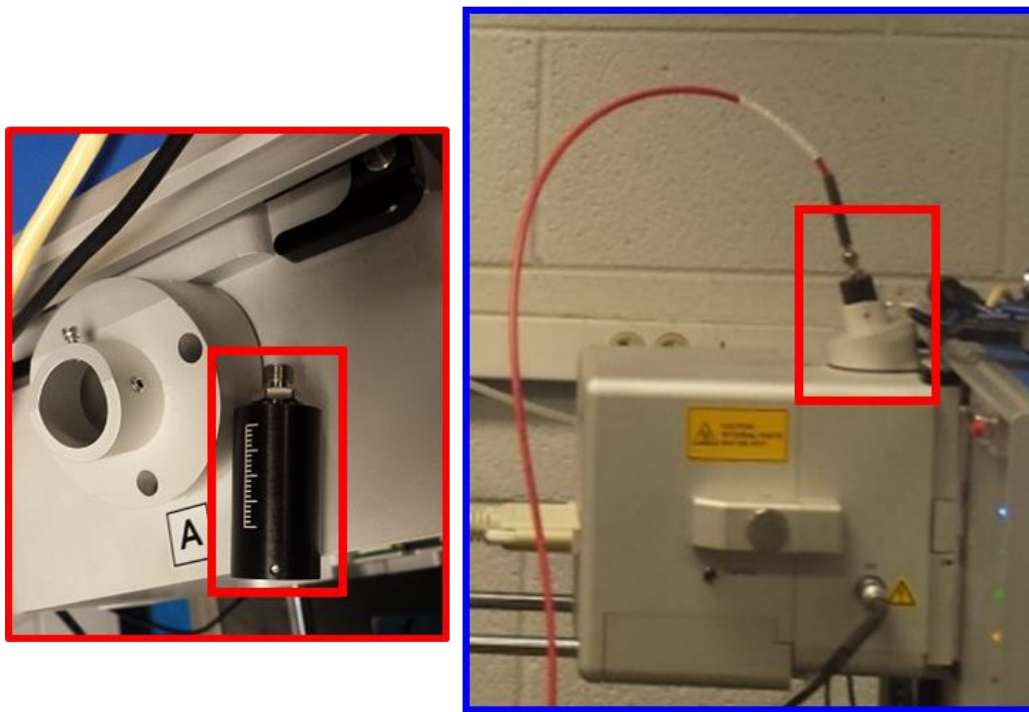


Figure 14. Fiber attachment piece on the AP-MALDI source. Left: Adjustable fiber attachment tube removed from the MALDI source. Right: Fiber attachment piece relative to the AP-MALDI setup.

3.3.3 Non-Imaging UV-AP-MALDI-MS on an Fourier Transform Ion Cyclotron

Resonance (FTICR) Instrument

AP-MALDI for molecular identifications required analyses to be performed on a high-resolution mass analyzer such as the FTICR. Trypsically-digested lysozyme and albumin were all detected with UV-AP-MALDI on the FTICR instrument with improved mass accuracy (< 10 ppm mass error). Figure 15 highlights all peptide fragments observed from trypsin digestion using the FTICR configuration. Soon after these results were obtained, a pre-existing cryogenic leak and a circuit board failure led to permanent decommissioning the FTICR instrument, preventing further use of this configuration.

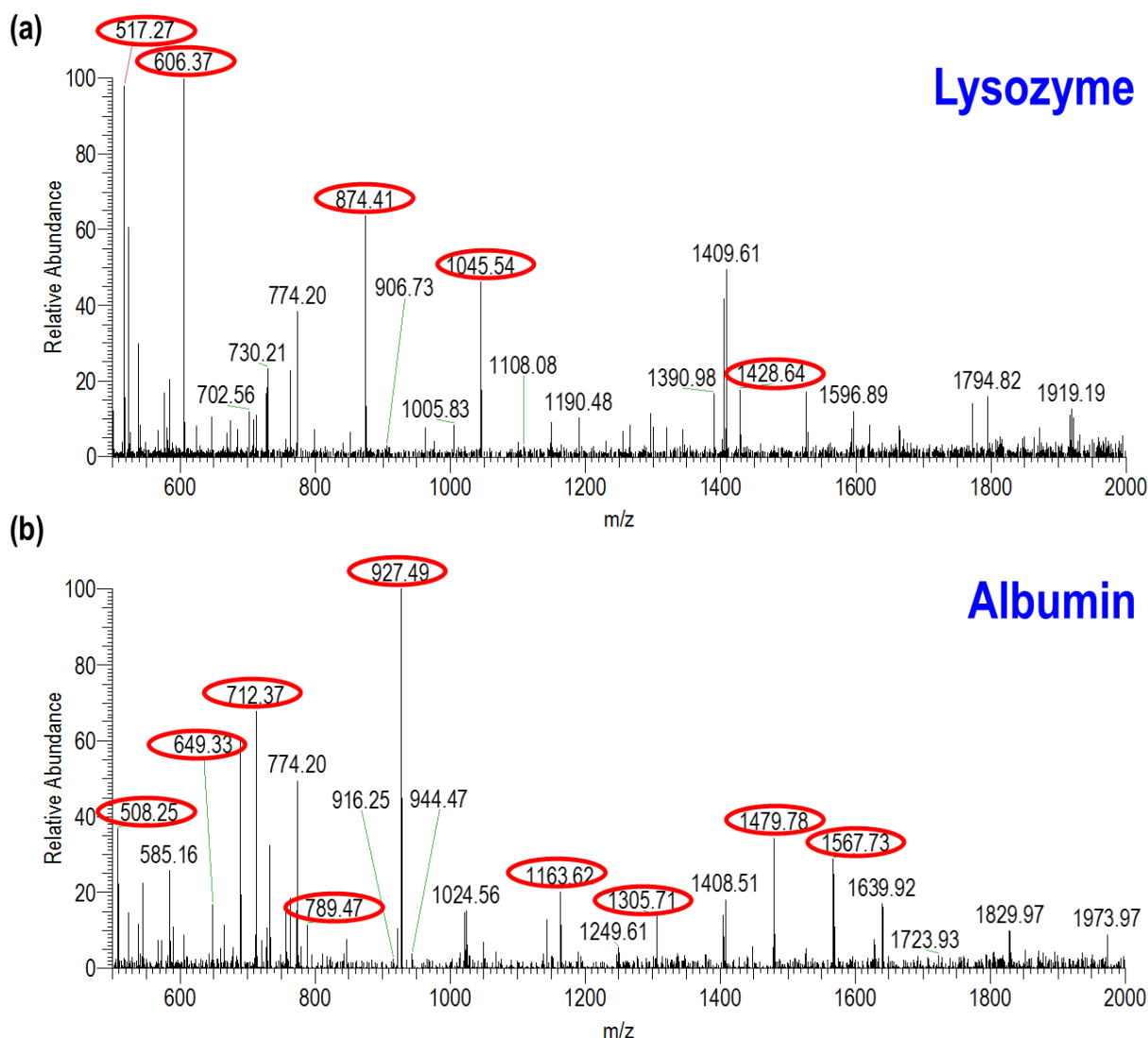


Figure 15. Mass spectra of (a) lysozyme and (b) albumin tryptic digests. Peaks corresponding to fragments from trypsin digestion are circled in red.

3.3.4 Imaging Vacuum UV-MALDI-MS on a Time-of-Flight (TOF) Instrument

Biofilms utilizing MALDI MS imaging were also attempted on a vacuum MALDI-TOF instrument (Autoflex Speed LRF, Bruker Daltonics, Billerica, MA). Results for the fixed biofilms displayed low intensity mass spectra throughout the regions of the biofilm. The mass spectrum obtained from an intact and fixed biofilm is shown in Figure 16a, but common metabolites

typically found in *P. aeruginosa* were not observed [69, 111-113]. For all peak intensities, only m/z 1424 displayed spatial differences throughout the biofilms, however, its identity and whether it is a false positive remains unknown (Figure 16a). It was hypothesized that the few hundred microns thickness of the biofilms and their high surface heterogeneity contributed to the poor signal. Previously analyses (not shown here) with biofilms on polycarbonate membranes which were adhered onto the MALDI plate with double-sided copper tape yielded similarly noisy spectra and also contributed to mass error. Ethanol washings may also have removed common metabolites, reducing signal levels.

Alternatively, unfixed biofilms were embedded in 1% agar to help with sample surface heterogeneity. For biofilms grown directly in agar with minimal salt concentrations, the Dorrestein group found that saturation of the universal MALDI matrix helped keep agar biofilms adhered onto the MALDI plate [68]. Since biofilms grown here were in a high salt concentrated medium, agar was used to help embed the biofilms to minimize flaking. For the motivation of ensuring signals were not coming from trypsin in the tryptically-digested biofilms or the CSP growth medium, trypsin and the CSP medium were spotted on agar, labelled “T” and “C,” respectively, in Figure 12a. Angiotensin II was also spotted above the agar, designated “A” directly above one of the untreated biofilm as a standard check (Figure 12a). Figure 12b shows the biofilm mostly dried. After complete drying, it was observed that one of the biofilms flaked, so the flaked region was not analyzed (Figure 16bc). The MS baseline of the agar embedded biofilms (Figure 16c) improved in comparison to the intact fixed biofilms without embedding (Figure 16a). Results for angiotensin II showed diffusion within the agar based on the intensity of m/z 1047 (Figure 16b), but no angiotensin II was observed in the region above the biofilm. Of all the peaks, only m/z 655 shows

spatial distributions in the regions where biofilms are embedded, however the identity of the compound is unknown (Figure 16c).

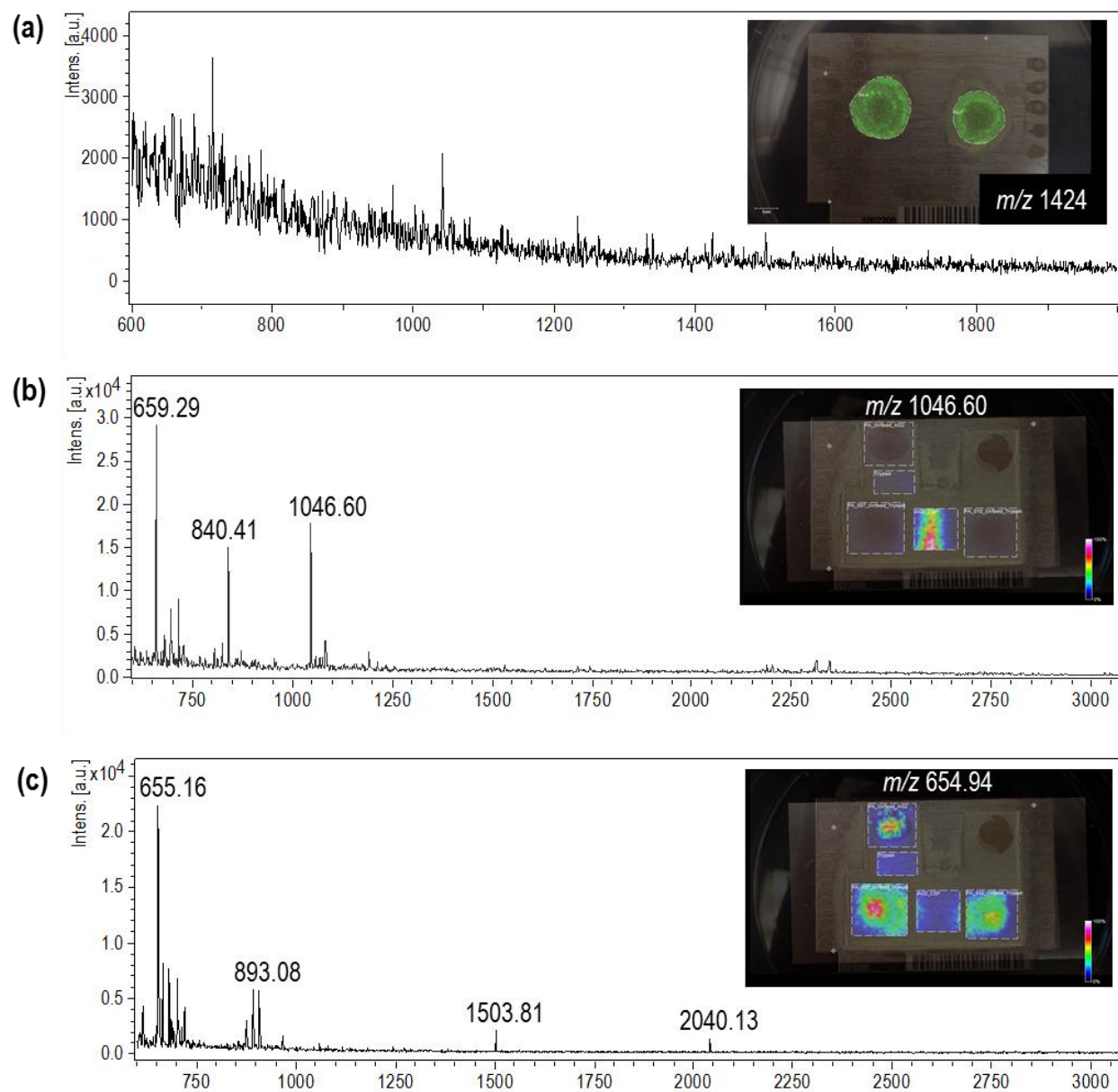


Figure 16. Mass spectra and images of biofilms. (a) Fixed *P. aeruginosa* mass spectrum with heat intensity of m/z 1424. (b) Mass spectrum and image of m/z 1046 for angiotensin II as a standard check. (c) Unfixed *P. aeruginosa* mass spectrum and image of m/z 655.

3.4 Conclusion

The successful fiber-coupling of both UV (355 nm) lasers – Nd:YAG pumped OPO and frequency-tripled Nd:YAG – to the QIT and FTICR instruments, respectively, were demonstrated. The UV-AP-MALDI on the QIT instrument detected all peptide standards with good signal/noise. However, mass accuracy may be problematic especially for biological applications that commonly require high mass accuracy for identification of unknown compounds. IR-AP-MALDI on the QIT instrument was also attempted but was unsuccessful presumably due to insufficient laser density (or possibly the IR-matrix used was not optimal). UV-AP-MALDI on the FTICR instrument on two tryptically-digested proteins, lysozyme and albumin, were demonstrated with a significantly improved mass accuracy. However, the upgrade to high-resolution MS was not sustained when the FTICR instrument became permanently unavailable.

Vacuum MALDI-TOF imaging analyses on biofilms grown in CSP medium were unable to determine common *P. aeruginosa* metabolites. Subsequent optimizations of sample preparation showed improved mass spectra with greater intensities. Nevertheless, actual identification of some of the detected compounds remain indeterminate as this vacuum MALDI-TOF instrument does not have tandem MS capability. For tissues, a thickness of 10-20 μm is thought to be optimal for MALDI analyses, whereas thicker tissue becomes more insulating which can affect the mass analyzer performance adversely [114, 115]. Limitations here were apparently the thickness and heterogenous surface of the biofilms. A future direction would be to cryosection biofilms into thinner slices to offset these challenges with sample preparation, but such cryosectioning and associated washing steps would first need to be refined.

4. SOLID SAMPLING WITH A DIODE LASER FOR PORTABLE AMBIENT MASS SPECTROMETRY

Reproduced in part with permission from [Yeni P. Yung, Raveendra Wickramasinghe, Anu Vaikkinen, Tiina J. Kauppila, Igor V. Veryovkin, and Luke Hanley. Solid Sampling with a Diode Laser for Portable Ambient Mass Spectrometry. *Analytical Chemistry* (2016) 89 (14), 7297–7301. DOI: 10.1021/acs.analchem.7b01745] Copyright 2017 American Chemical Society.

4.1 Introduction

There has been a rapid increase in the development of portable mass spectrometers (MS) and their application to the analysis of gaseous, liquid, and solid samples [116]. Potential applications of portable MS include in-field sampling of native plants [117, 118] or as in the case of this thesis, microbial communities [25, 119, 120]. For example, portable MS could be used to identify microbial colonies on medical devices for the purpose of disease prevention [121].

Along with other classes of ion sources used for MS [22], ambient or atmospheric pressure sources have been investigated for use in portable MS due to the convenience imparted by direct sampling without the extraction, pyrolysis, and/or desiccation required by traditional MS sample preparation methods [122]. Desorption electrospray ionization (DESI) [123-125] and plasma discharge-based ion sources [126-128] are both well established for direct sampling of solids in portable ambient MS. However, such ion sources can suffer from fluctuations in the efficiency with which analytes are extracted/volatilized then ionized. For example, the efficiency with which plasma-based sources will detect analytes in a solid sample will depend upon the specific plasma conditions and source-to-sample distance as well as sample volatility and thermal stability [126-128].

Laser sampling induces desorption/ablation of analyte from the surface of a solid sample and can additionally permit MS imaging at relatively high lateral resolution [22]. Laser desorption/ablation is also well established for sampling at atmospheric pressure, especially using UV or IR lasers with pulse lengths ranging from ~10 ns to <100 fs [22, 31, 85, 88, 129]. However, such lasers are usually too expensive, delicate, and/or complicated for routine application in portable ambient MS, especially when compared with DESI, paper spray, or other plasma-based methods. A potential portable solution can be found in laser diode thermal desorption (LDTD) [130] which uses continuous wave (CW) or pseudo-CW near-IR diode lasers to volatilize solid samples.

This chapter demonstrates the implementation of a handheld diode laser for solid sampling in portable ambient MS and more importantly its application to biofilm studies. A battery-powered surgical laser diode is employed for portable LDTD at 940 nm and compared with laser ablation by a laboratory-based nanosecond pulsed laser operating at 2940 nm. Postionization is achieved using atmospheric pressure photoionization (APPI) [88]. Experiments that used the 940 nm, portable laser diode are referred to as LDTD-APPI while those that used the pulsed 2940 nm laboratory laser are referred to as LAAPPI, for consistency with published nomenclature [88, 130]. A preliminary version of the LDTD-APPI source was previously reported [131]. These experiments compare the analysis of metabolites from sage leaves of *Salvia officinalis* and *Pseudomonas aeruginosa* biofilms by LDTD-APPI with the established method of LAAPPI [88, 130], demonstrating the feasibility of laser-based APPI methods for in-field sampling of native plant or microbial biofilm communities.

4.2 Experimental Details

4.2.1 Ion Source and Ambient Mass Spectrometry

The home-built LDTD-APPI source shown in Figure 17 was based on an APPI source [86] which consisted of a VUV photoionization lamp and dopant gas nebulizer, to which a laser had been added for desorption/ablation. A radiofrequency-powered krypton gas discharge VUV lamp (KrLM-LQD12, Resonance Ltd., Barrie, Ont., Canada) that outputs at 10.0/10.6 eV was used for photoionization. Dopant vapor was used in most of the experiments presented here as it had been previously shown to improve ionization efficiency in APPI through charge transfer and/or proton exchange [87, 132]. The nebulizer for dopant delivery was inspired by a published design [86] and consisted of a stainless-steel tee-junction (VICI Valco, Houston, TX) that was fitted to a stainless-steel heater block adapter machined in-house to incorporate a heater cartridge (Watlow FIREROD, Ash Equipment Co., Batavia, IL). The tee-junction had two inputs for dopant delivery from a syringe pump and nitrogen gas delivery, and an output to an effluent capillary tip that delivered the heated dopant vapor close to the intersection of the laser desorption/ablation spot on the sample, the VUV ionization region, and the atmospheric pressure aperture of the MS.

This LDTD-APPI source used a CW diode laser operating at 940 nm for sample desorption (iLase, Biolase Tech, Irvine, CA). This handheld laser (100 gm, 21 cm long), designed for dental surgical applications, was equipped with one-hour lifetime rechargeable batteries, had a 3W peak power optical output, and was typically operated in a pseudo-CW mode (0.1 ms on / 0.2 ms off). The laser beam was guided to the ablation area via a disposable, 400 μm fiber optic tip that can be bent to accommodate spatially constricted samples. A diode laser output of ~ 700 mW output (power density ~ 140 W/cm²) was generally used to collect the LDTD-APPI mass spectra.

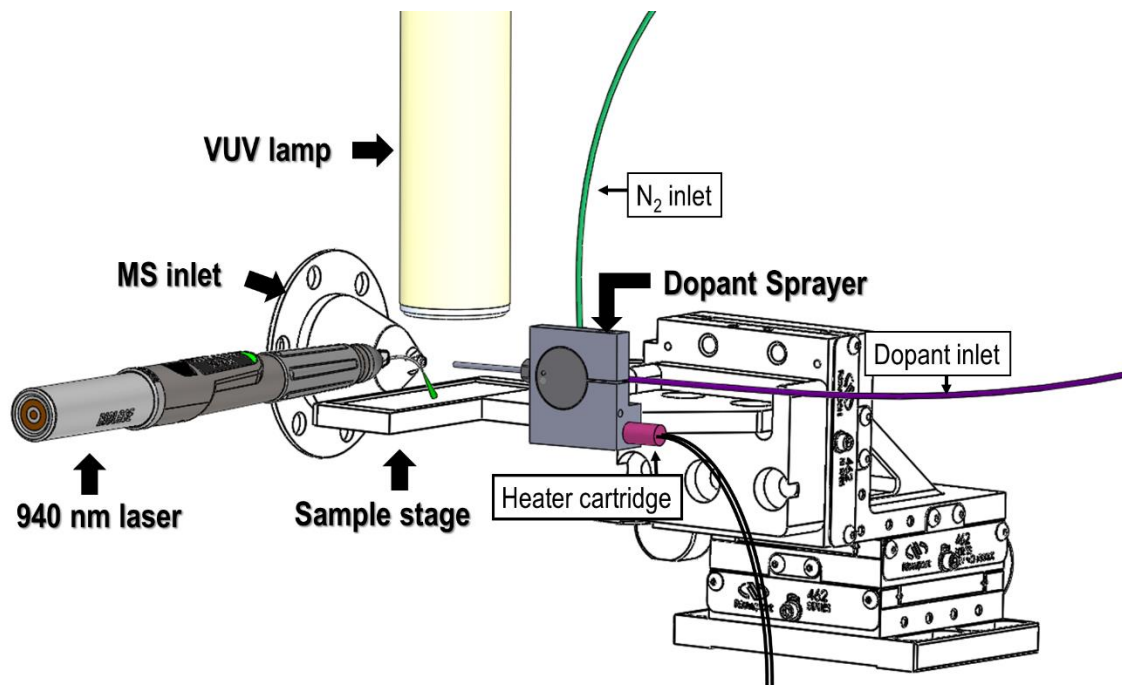


Figure 17. A schematic diagram of the laser diode thermal desorption atmospheric pressure photoionization (LDTD-APPI) source with a battery-powered, portable, pseudo-continuous wave (CW) near-IR at 940nm diode laser.

The LAAPPI source followed a previously reported configuration [88], but with the same VUV lamp and dopant vapor delivery scheme described above and shown in Figure 18 and LAAPPI employed a ~ 7 ns, 20 Hz pulsed, laboratory laser operating at 2940 nm composed of an optical parametric oscillator pumped by a Nd:YAG laser (Opolette 2940, Oportek, Carlsbad, CA). The laser output was focused via a biconvex CaF_2 lens into a 450 μm core GeO_2 fiber patch (Infrared Fiber Systems, Silver Springs, MD) and the fiber output beam was collimated and focused through two plano-convex CaF_2 lenses directly onto the sample. The output from the fiber optic in LAAPPI was generally ~ 2 mJ/pulse (power density ~ 25 W/cm²).

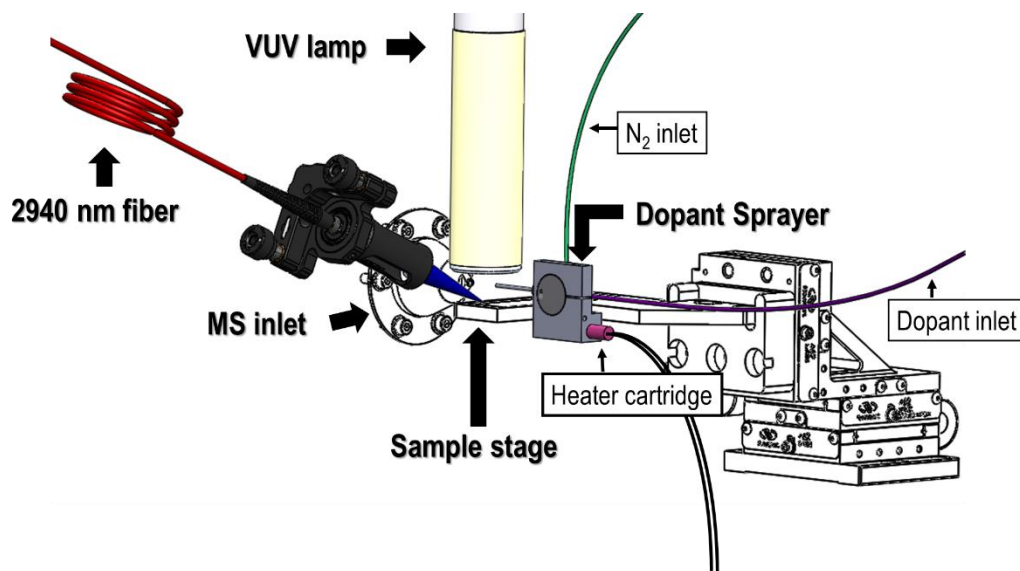


Figure 18. A schematic diagram of the laser ablation atmospheric pressure photoionization (LAAPPI) source with a fiber coupled laboratory mid-IR laser at 2940 nm.

The mass spectrometric analyses were performed using a field-deployable 3D quadrupole ion trap (MT Explorer 50, MassTech, Columbia, MD) [110]. The inlet cone was set to 120°C and the capillary voltage at 10 VDC, with automatic gain control enabled with target value set at 100,000. A high transmission wire grid was also mounted on the output end of the VUV lamp (not shown in Figure 17 nor Figure 18) and connected to both the sample plate and the capillary (including the aperture cone to the mass spectrometer) so that all three sat at the same voltage during analysis. The resultant electric field-free region in the vicinity of the MS aperture was an attempt to minimize signal losses due to possible ion deflection away from the aperture caused by sample charging effects and/or an electric field gradient. Minimum and maximum injection times for individual mass scans were 1 and 1000 ms, respectively, for the sage analysis. Biofilm analyses used a fixed injection time of 100 ms. Spectra were averaged over one min of individual scans for sage and two min for biofilms.

4.2.2 Chemicals, Samples, and Replicates

Anisole (99.7%) and toluene ($\geq 99.9\%$) were used as purchased (Sigma-Aldrich, St. Louis, MO). 4-amino-5-chloro-2-methoxybenzoic acid ($C_8H_8ClNO_3$, 97%) (Sigma Aldrich, St. Louis, MO) was dissolved in spectroscopic grade methanol to a concentration of 10 mg/mL then deposited onto chitosan-alginate polyelectrolyte multilayers adsorbed onto gold coated silicon wafers, prepared as described previously [133]. LDTD-APPI and LAAPPI analyses of the resultant standard samples were replicated at least four times while rastering the sample with respect to the laser spot at a rate of 0.2 mm/s.

Organic sage leaves (*Salvia officinalis*) were purchased from a local supermarket and stored at $\sim 4^\circ\text{C}$ prior to analysis. The leaves were washed with deionized, distilled water to remove dirt, blotted dry, and then mounted onto a glass slide using double-sided copper tape with the abaxial side facing up. LDTD-APPI and LAAPPI analyses were replicated on at least five replicates rastering at 0.3 mm/s with 5 $\mu\text{L}/\text{min}$ anisole dopant and $\sim 80\text{ mL}/\text{min}$ nitrogen flow rates.

10 μL of *Pseudomonas aeruginosa* chronic wound clinical isolate (215) overnight culture at 0.1 OD_{600} were inoculated onto a polycarbonate membrane placed on top of nutrient-defined CSP agar plate and grown for three days. The resultant biofilms were exposed to 0.1% trifluoroacetic acid for 1 hour for sterilization, transferred onto a stainless-steel plate, and frozen to remove the membrane prior to analysis. LDTD-APPI and LAAPPI analyses were performed on at least seven distinct biofilm samples, rastering at 0.03 mm/s with 0.2 $\mu\text{L}/\text{min}$ toluene dopant flow rate and $\sim 50\text{ mL}/\text{min}$ nitrogen flow rate.

4.3 Results and Discussion

LAAPPI (2940 nm, ~7 ns pulsed) and LDTD-APPI (940 nm, pseudo-CW) mass spectra of the 4-amino-5-chloro-2-methoxybenzoic acid (MACA, 201.02 Da) standard both show intense MH^+ ions in Figure 19, although LDTD-APPI displayed more fragmentation. The dopant vapor was not required to assist with ionization and was therefore not used. Both LAAPPI and LDTD-APPI displayed the 3:1 peak intensity ratio at m/z 201.6 and 203.6 attributed to the MH^+ ion that is characteristic of the $^{35}Cl/^{37}Cl$ isotopic ratio expected for MACA. Tandem MS experiments detected ions resulting from losses of $ClCOOH$ and $ClCH_2COOH$ from MH^+ , confirming this assignment (data not shown). Direct laser desorption ionization (without VUV lamp) of MACA was also observed for the 2940 nm laser, but not for 940 nm LDTD. The VUV lamp generated a signal via postionization for LDTD-APPI and enhanced the signal with LAAPPI (see Figure 19). Also observed in the LDTD-APPI mass spectra of Figure 19 were peaks at m/z 215.4, $[M+14]^+$ and m/z 189.3, $[M-12]^+$. The characteristic chlorine isotopic distributions of these two peaks indicate they derive from ion molecule reactions and/or fragmentation and rearrangement of precursor ions.

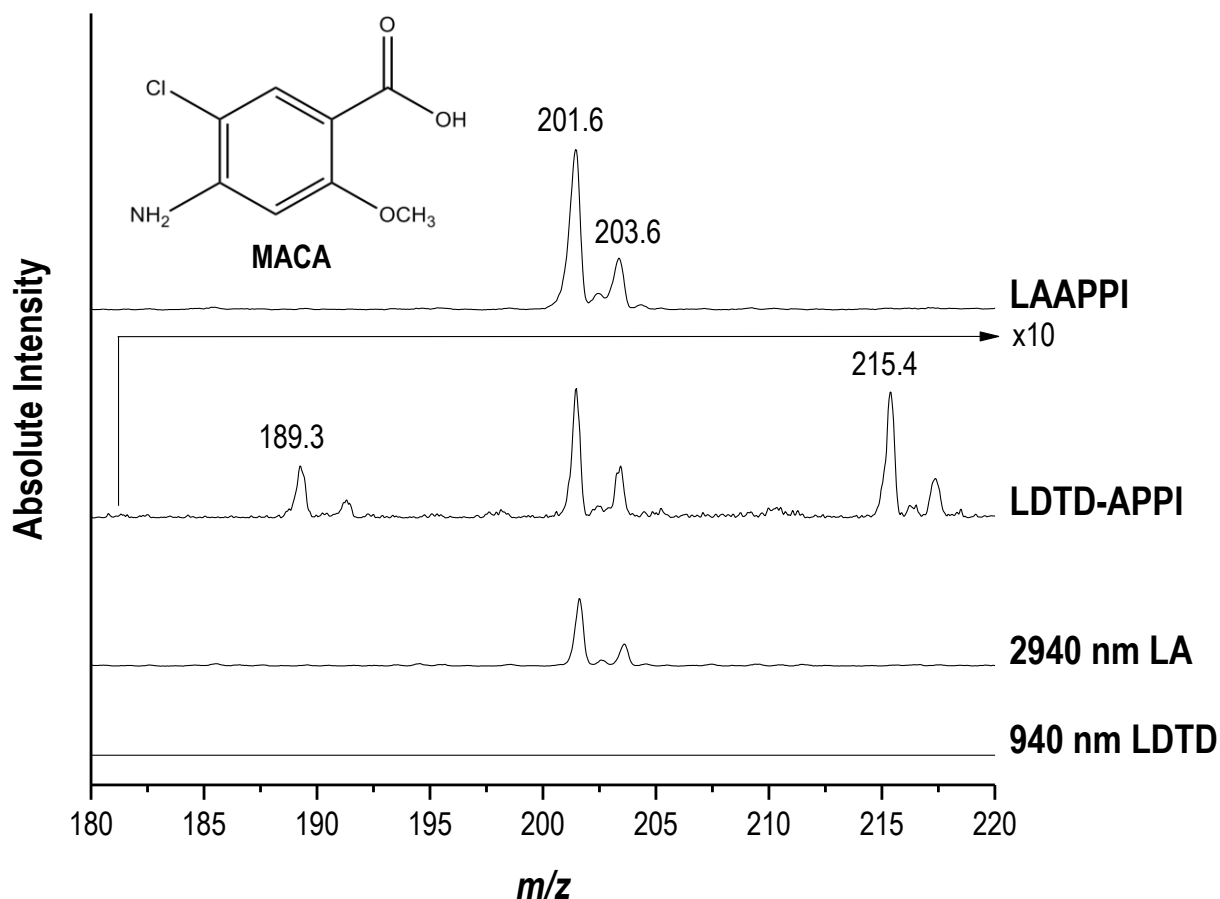


Figure 19. Mass spectra of the 4-amino-5-chloro-2-methoxybenzoic acid (MACA) standard (inset shows chemical structure) analyzed by (from top to bottom) 2940 nm laser ablation atmospheric pressure photoionization (LAAPPI), LDTD-APPI, 2940 nm laser ablation (without VUV lamp), and 940 nm LDTD (without VUV).

LAAPPI was previously used to analyze phytochemicals of sage leaves [89], so this analysis was repeated here as a proof-of-principle and compared in Figure 20 with an analysis of sage leaves by LDTD-APPI. Both anisole and toluene were used as dopants given that their low ionization energies (8.20 and 8.83 eV, respectively) are well below the photon energy of the VUV source (10.0/10.6 eV). However, Figure 20 displays only the results with anisole due to its lower background.

The LAAPPI and LDTD-APPI mass spectra of sage leaves shown in Figure 20 appear rather similar to a cursory visual examination. Table I outlines the twelve common peaks that were observed from sage leaves by both methods, as well as the three additional peaks observed exclusively by only one of the two methods, obtained by averaging all five replicates. The letters “(a)” to “(e)” annotate peaks observed by both LAAPPI and LDTD-APPI (see Table I) for whom tentative assignments were additionally made based on phytochemicals previously reported from sage leaves or extracts thereof [89, 134].

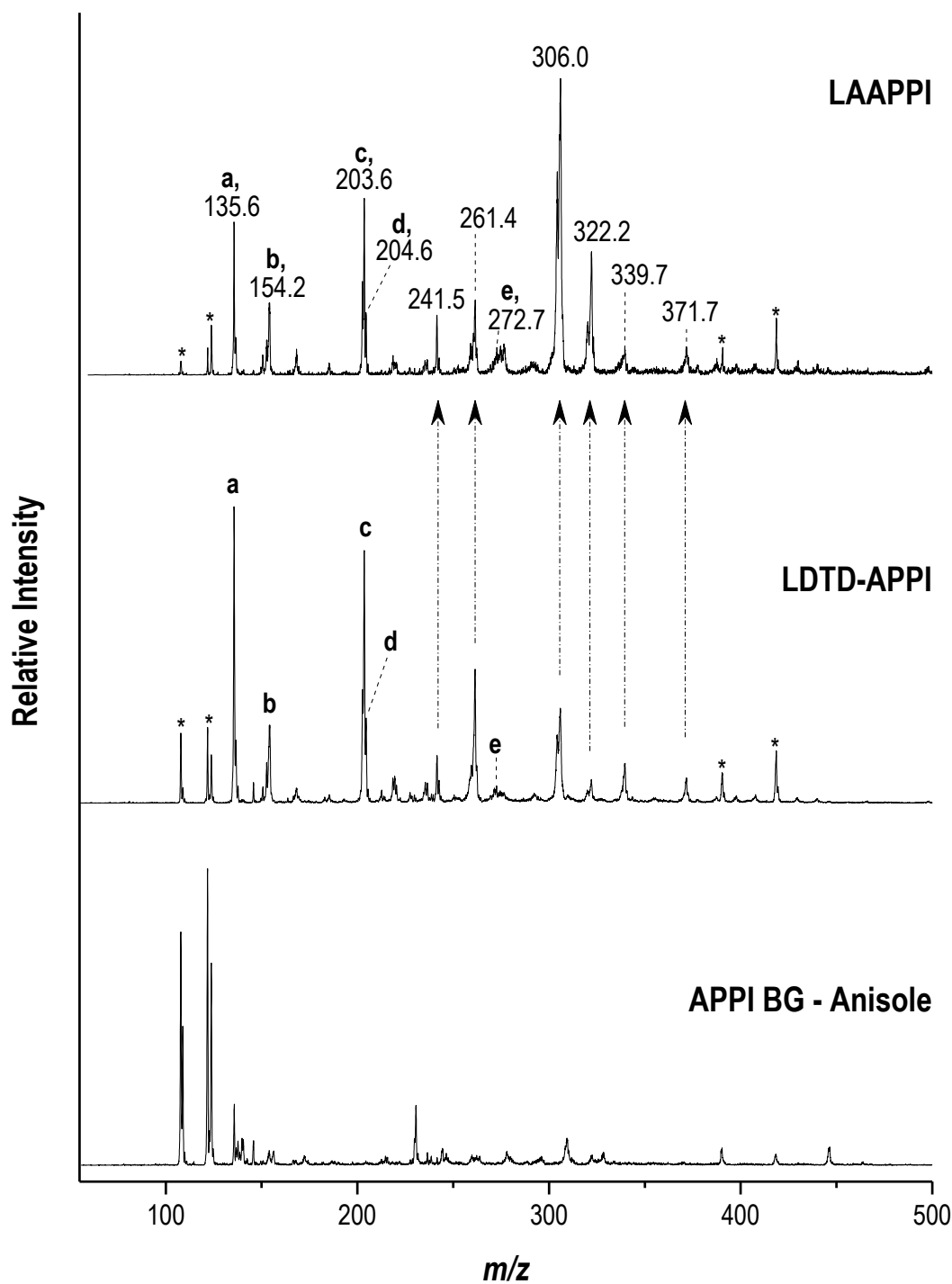


Figure 20. Representative analyses of sage leaves by (top) LAAPPI and (middle) LDTD-APPI with anisole dopant. Anisole dopant background in APPI (bottom). The letters “(a)” to “(e)” annotate peaks observed by both LAAPPI and LDTD-APPI for whom with tentative assignments were possible based on phytochemicals previous detected by LAAPPI (see Table 1) [89, 134]. The arrows indicate other peaks observed in the LDTD-APPI mass spectrum that are labelled in the LAAPPI mass spectrum. * indicates background peaks.

However, it is important to note that all the peak assignments are only tentative and are based on prior GC-MS, LC-MS, and LAAPPI studies [89, 134]. The ± 0.5 Da mass error of the field deployable ion trap used here limited the peak assignment accuracy. Furthermore, attempts to collect tandem MS data directly from the sage leaves were unsuccessful, presumably due to the low sensitivity of the ion trap mass analyzer. Peaks that were not observed here, but were observed previously [89] by LAAPPI include m/z 169.1, 286.2, 300.2, 315.1, 316.2, 331.2, 332.2, and 346.2. Differences in the peaks observed here and previously by LAAPPI [89] might be attributed to the use of different mass analyzers, MS source conditions, and/or sage leaf growth conditions, storage conditions, and/or genetics.

Table I. Peaks observed in LAAPPI- and LDTD-APPI-MS spectra of sage leaves with anisole as the dopant. *The letters “(a)” to “(e)” annotate the same peaks so noted in Figure 20 while italicized peaks in LDTD-APPI are those that also appeared with toluene dopant.

| LAAPPI ($\pm m/z$ 0.1) | LDTD-APPI ($\pm m/z$ 0.1) | LAAPPI (m/z) [89] | Tentative Peak Assignments [89, 134] |
|----------------------------|-------------------------------|--------------------------|--|
| (a) 135.6 | (a) 135.6 *** | 135.1 | p-cymene MH ⁺ monoterpenes (e.g., α -pinene/ β -pinene/ limonene/camphene) [M-H] ⁺ monoterpenoids (e.g., camphor/ α -thujone/ β -thujone) [MH-H ₂ O] ⁺ |
| 136.6 | | 136.1 | monoterpenes (e.g., α -pinene/ β -pinene/ limonene/camphene) M ⁺ monoterpenoids (e.g., borneol/1,8-cineole/terpinen-4-ol) [M-H ₂ O] ⁺ |
| (b) 154.2 | (b) 154.2 | 154.1 | monoterpenoids (e.g., borneol/1,8-cineole/terpinen-4-ol) M ⁺ |
| (c) 203.6 | (c) 203.6 | 203.2 | sesquiterpenes (e.g., α -humulene/ β -caryophyllene) [M-H] ⁺ caryophyllene oxide [MH-H ₂ O] ⁺ |
| (d) 204.6 | (d) 204.5 | 204.2 | sesquiterpenes (e.g., α -humulene/ β -caryophyllene) M ⁺ viridiflorol [M-H ₂ O] ⁺ |
| | 219.5 | 219.2 | caryophyllene oxide [M-H] ⁺ |
| 241.5 | 241.4 | | |
| 261.4 | 261.4 | | |
| (e) 272.7 ** | (e) 272.6 | 272.2 | monoterpenes (e.g., α -pinene/ β -pinene/ limonene/camphene) [2M] ⁺ manool [M-H ₂ O] ⁺ |
| | 304.3 | | |
| 306.0 | 306.0 | | |
| 320.3 | 320.2 | | |
| 322.2 | 322.1 | | |
| 339.7 | 339.7 | | |
| | 340.7 | | |
| 371.7 | 371.7 | | |

*Peaks were included in Table I only if they were observed in $\geq 50\%$ of the samples with >5 signal to noise (S/N) when compared against the anisole background.

**Denotes low S/N peak.

***LDTD-APPI peaks that appear with both anisole and toluene dopant are italicized in Table I.

The LAAPPI and LDTD-APPI mass spectra shown in Figure 21 of membrane-grown *P. aeruginosa* biofilms are also quite similar by visual inspection. Table II lists 21 peaks observed by both methods and an additional two peaks observed exclusively by only one method, obtained by averaging all seven replicates. Of these 21 common peaks, those annotated with the lower case letters “(a)” to “(g)” in Figure 21 and Table II were those that could additionally be tentatively assigned to metabolites previously reported for *P. aeruginosa* cultures by various MS strategies [25, 70, 113, 135, 136]. Overall, peaks were observed whose m/z values can be attributed to phenazines, homoserine lactones (HSL), *Pseudomonas* quinolone signal (PQS) and hydroxy-alkyl-quinolones (HAQs) that were previously detected by various mass spectrometric methods and are thought to participate in inter- and intraspecies cellular communication known as QS (see Table II) [137]. However, the same caveats regarding peak assignments stated above for the sage leaf MS also apply to the biofilms.

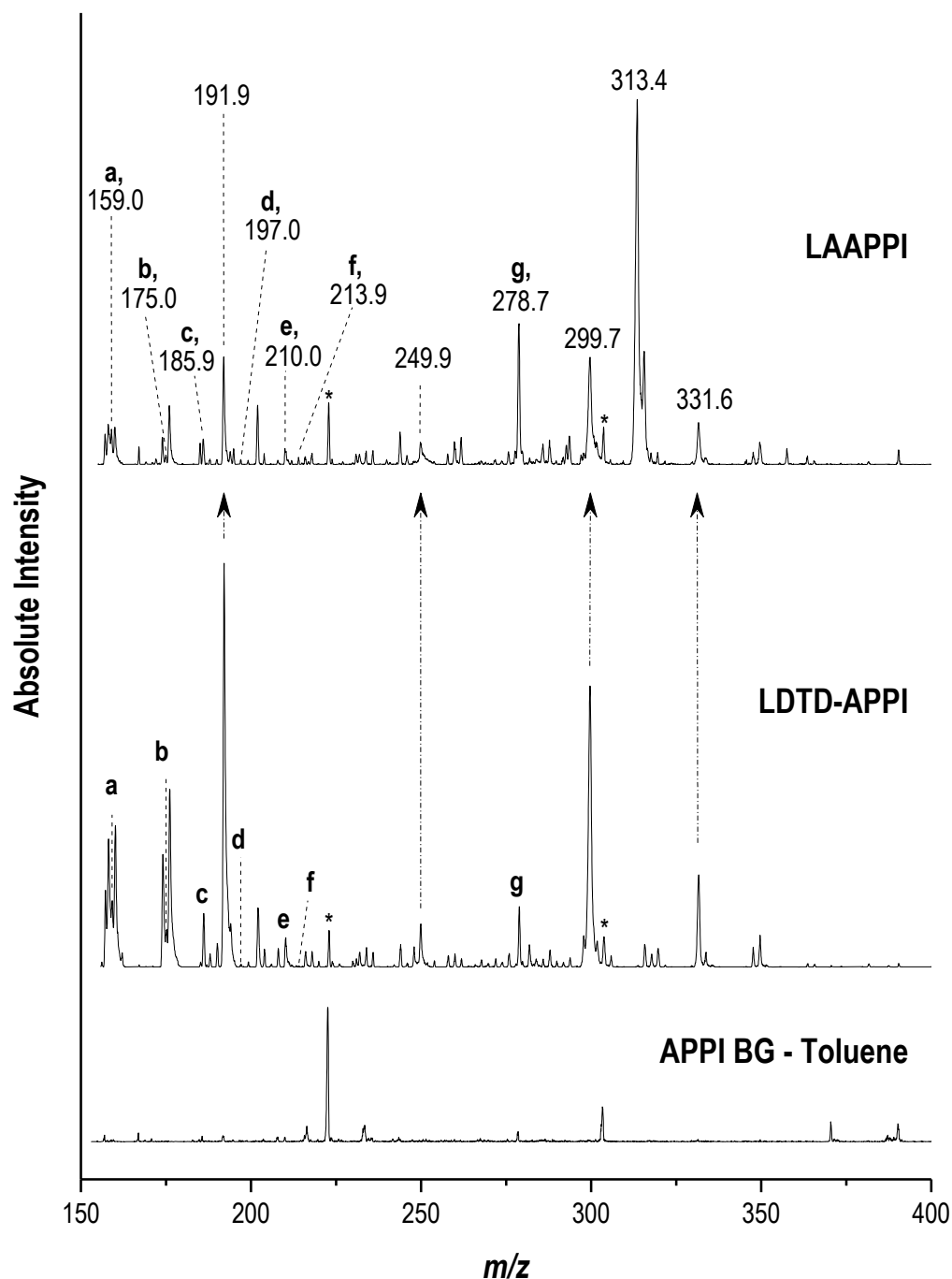


Figure 21. Representative analyses of *P. aeruginosa* membrane grown biofilms by (top) LAAPPI and (middle) LDTD-APPI with toluene. Toluene dopant background in APPI (bottom). The peaks annotated with “(a)” to “(g)” annotated in the figure correspond to peaks observed in both LAAPPI and LDTD-APPI that have been tentatively assigned to known metabolites reported in literature (see Table II) [25, 70, 113, 135, 136]. The arrows indicate other peaks observed in the LDTD-APPI mass spectrum that are labelled in the LAAPPI mass spectrum. * indicates background peaks.

Table II. Peaks observed in LAAPPI and LDTD-APPI spectra of *P. aeruginosa* biofilms with toluene as the dopant*The letters “(a)” to “(g)” annotate the same peaks so noted in Figure 21.

| LAAPPI ($\pm m/z$ 0.1) | LDTD-APPI ($\pm m/z$ 0.1) | Tentative Peak Assignments | Monoisotopic Mass (Da) of Assignment | References |
|----------------------------|-------------------------------|---|--|------------|
| 157.1 | 157.1 | | | |
| 158.0 | 158.1 | | | |
| (a) 159.0 | (a) 159.1 | HAQ (hydroxy-alkyl-quinolones) fragment ion of HHQ (4-hydroxy-2-heptylquinoline) | 159.1 | [70, 135] |
| 160.0 | 160.0 | | | |
| 173.9 | 174.0 | | | |
| (b) 175.0 | (b) 175.1 | HAQs fragment ion of PQS (<i>Pseudomonas</i> quinolone signal; 2-heptyl-3-hydroxyquinolone) | 175.1 | [70, 135] |
| 176.0 | 176.0 | | | |
| 185.0 | 185.1 | | | |
| (c) 185.9 | (c) 186.0 ** | HAQs fragment ion of HQNO (4-hydroxy-2-heptylquinoline-N-oxide) | 186.1 | [135] |
| 191.9 | 192.0 | | | |
| (d) 197.0 | (d) 197.0 | 1-HP (1-hydroxyphenazine) MH ⁺ | 197.1 | [70] |
| 199.1 | 199.2 | | | |
| 201.9 | 202.0 | | | |
| | 203.9 ** | | | |
| (e) 210.0 | (e) 210.1 | 1-MP (1-methoxyphenazine) M ⁺ PYO (pyocyanin) M ⁺ | 210.1 | [25] |
| (f) 213.9 | (f) 214.0 | 4-hydroxy-2-pentenylquinoline MH ⁺ | 214.1 | [135] |
| 230.8 | 230.9 | | | |
| 249.9 | 249.9 | | | |
| (g) 278.7 | (g) 278.8 | C6-HSL (N-hexanoyl-homoserine lactone) oxidative product MH ⁺ | 279.1 | [136] |
| 287.7 ** | 287.8 | 2-nonyl-3-hydroxyquinolone (C9-PQS) MH ⁺ 4-hydroxy-2-nonylquinolone-N-oxide (C9-NQNO) MH ⁺ | 288.2 | [70, 135] |
| 299.7 | 299.5 | | | |
| 313.4 | | | | |
| 331.6 | 331.5 | | | |

*Peaks were included in Table II only if they were observed in $\geq 50\%$ of the samples with >5 signal to noise (S/N) when compared against the toluene background.

**denotes low S/N peak.

4.4 Conclusion

The LDTD-APPI method should be useful for solid sampling in portable ambient MS in in-field sampling of microbial communities [25, 119-121] or native plant [117, 118] as well as other potential applications. The direct detection of metabolites could prove useful for metabolomics studies on intact bacterial biofilms. The feasibility of many portable MS applications is facilitated by the availability of low cost, portable, battery-powered diode lasers. Furthermore, the fact that LDTD-APPI gives similar results to LAAPPI – at least for sage leaves and *P. aeruginosa* biofilms – highlights the use of LDTD-APPI in cases where portability and lower cost are desirable.

The similarity of spectra is also fundamentally interesting given that sample volatilization in LDTD presumably occurs via thermal desorption [130], whereas LAAPPI is thought to proceed via explosive evaporation of water that ejects a hydrated sample into the gas phase [88, 138]. The separation of the desorption/ablation and ionization steps indicates that photoionization of similar volatilized species is occurring in both LDTD-APPI and LAAPPI.

LDTD-APPI is expected to enhance sample volatilization via thermal heating, when compared with desorption atmospheric pressure photoionization (DAPPI), which proceeds via a hot solvent jet impinging upon the sample [139]. LDTD might also be effective when coupled to plasma-based ion sources that are used for solid sampling [127, 128, 140], since LDTD might be used to reduce fluctuations in volatilization efficiency that arise from sample heating by the plasma, which will vary with specific plasma conditions and source-to-sample distance [126, 140]. Plasma power has a direct relationship with sample surface heating, but also affects the extent of molecular fragmentation [126] as well as ionization efficiency. It is speculated that the addition of

LDTD might be more reproducible than plasma-based ionization alone by enhancing sample volatilization. Finally, LDTD could readily be coupled to electrospray ionization for LDTD-ESI, a portable method analogous to laser ablation electrospray ionization (LAESI) [129].

5. USING PROTEOMICS TO ILLUMINATE METABOLIC PROCESSES IN BACTERIAL COMMUNITIES

5.1 Introduction

Chronic wounds are categorized as nonhealing wounds that remain open for an extended period of time [141]. Such nonhealing wounds impact over eight million Medicare patients and cost up to \$28 billion in healthcare costs annually [142]. The various types of common chronic wounds include diabetic foot ulcers, arterial or venous leg ulcers, pressure ulcers, and burn wounds [143, 144]. As many as 20 microorganisms are typically found in chronic wounds and of those, up to 60% are biofilm-forming [145]. *Pseudomonas aeruginosa* is a pathogenic biofilm-forming microorganism best known for the role it plays in cystic fibrosis and medical device-related infections [146, 147] that is also commonly isolated in chronic wounds [144]. *P. aeruginosa* has been widely studied for its ability to adapt to various environmental conditions and coordinate genes based on cell-to-cell communications and surface adhesions [148-150].

Microorganisms have been shown to prioritize the catabolism of preferred carbon sources while repressing the utilization of non-preferred carbon sources, a process known as carbon catabolite repression (CCR) or diauxic growth [151]. CCR can influence bacterial metabolic states, communication, biofilm formation and virulence. During stress, resource allocation [152] allows bacteria to maximize biological fitness and survival while adapting to changing environments. A preference for glucose over organic acids (e.g., lactate or citric acid cycle “TCA” intermediates), referred to as diauxie, is exhibited in *Escherichia coli* [151, 153]. By contrast, a preference for organic acids over glucose, reverse diauxie, is exhibited in *P. aeruginosa* [151, 153].

While always abundant in humans, lactate is reported at elevated levels amongst obese patients with type II diabetes when compared to normal healthy patients [154]. Chronic wound models show lactate production increases with oxidative stress [155]. These elevated levels of lactate correlate with disease severity and are used for medical prognosis [156]. Wound healing can be impaired at lactate concentrations exceeding 20 mM where cell viability is severely compromised [157]. Lactate can be produced from carbohydrates, then oxidized to pyruvate to serve as a substrate for the electron transport chain and as an energy source for growth [158]. It has been postulated that lactate is needed for microbial invasion and replication [158]. Lactate utilization contributes to pathogenesis and infection processes by enhancing resistance to O₂-dependent bactericidal mechanisms by competing for O₂, stimulating metabolism to enhance growth rates, and providing a more direct and faster pathway for pathogenic determinants (e.g., polysialic acid capsule and sialylated lipopolysaccharide) in *Neisseria spp.* [159]. Furthermore, lactate utilization enhances *Staphylococcus aureus* resistance to NO[•], an innate host effector essential for removing various pathogenic bacteria [160]. The single step conversion of lactate to pyruvate is catalyzed by the enzyme, lactate dehydrogenase, and the effects of lactate conversion on microbial metabolism and adaptative mechanisms are often complex and diverse [158].

One popular approach is to analyze how gene expression is correlated to metabolic reactions [161]. These genomic to metabolomic strategies have been used to determine cellular phenotype from intra- or extra-cellular metabolites in bacteria [162], identify metabolic networks from substrate consumption in yeast [163], and differentiate between planktonic and biofilm differences in bacterial cultures [164].

However, the direct genomic to metabolomic approach ignores the rich information on the actual expression of enzymes and other proteins provided by bottom-up proteomics via liquid

chromatography mass spectrometry (LC-MS/MS) [165, 166]. For example, LC-MS/MS proteomics have been used to directly link expressional changes in enzymes to metabolic reactions in a demonstration of its potential for studying chronic wounds in humans [167, 168]. Proteomic strategies have also been used to differentiate exudates in acute and chronic wounds of human skin [169] as well as planktonic vs. biofilm cultures of *Halobacterium salinarum* [24].

The integration of proteomics with metabolomics can uncover important drivers of cellular metabolism in microbial communities. A label-free proteomic approach is used here as it has been demonstrated to generate the deepest proteome coverage on an Orbitrap mass spectrometer [170]. Bottom-up proteomics by LC-MS/MS was used to examine the phenotype of planktonic *P. aeruginosa* clinical isolate (215) as a function of culturing conditions, where cellular protein expression delineates active metabolic processes and link them to genes. Planktonic consumption of carbon sources (glucose and lactate) was examined by exogenous metabolome data and correlated to representative metabolic proteins. Finally, the potential application of these strategies to surface associated bacterial and fungal communities such as biofilms are discussed.

5.2 Experimental Details

5.2.1 Bacterial Strains and Culturing Conditions

Overnight cultures of *P. aeruginosa* chronic wound clinical isolate strain (215) [171] were grown in 10 mL of CSP nutrient-defined medium containing 4 g/L glucose, 0.7 g/L sodium citrate, 0.1 g/L EDTA tetrasodium salt, 1.7 g/L yeast nitrogen base, minimum essential media non-essential amino acid (100× solution), minimum essential media amino acid (50× solution), 4.7 g/L

KH₂PO₄, 8.2 g/L Na₂HPO₄, 0.02 g/L adenine, 0.02 g/L uracil, 0.02 g/L cytosine, 0.02 g/L guanine, 0.15 g/L glutamine, 2.0×10^{-6} g/L vitamin B12, 2.8×10^{-3} g/L FeSO₄·7H₂O, and 1.2×10^{-5} g/L CoCl₂·6H₂O or CSP supplemented with 2 g/L lactate (LCSP) [172]. Aliquots of the overnight cultures were diluted to an OD₆₀₀ of ~0.010 with fresh medium in a baffled shake flask covered with a gas permeable sponge cap and grown under aerobic condition at 37°C and 150 RPM.

5.2.2 Exogenous Metabolomics

Details of the exogenous metabolomic analyses will be published elsewhere [172] and are therefore only summarized here. Supernatant was first collected from *P. aeruginosa* planktonic cultures. For extracellular metabolite analyses, 1.5 mL of culture supernatant was filtered using a 0.22 µm syringe filter, mixed with fucose as internal standard and separated through LC (1200 series, Agilent, Santa Clara, CA) equipped with both a variable wavelength detector and refractive index detector with an ion exclusion column (Aminex HPX-87H, 9 µm particle size, 300 mm length × 7.8 mm internal diameter, Bio-Rad, Hercules, CA) using a 0.03% H₂SO₄ isocratic mobile phase, at 0.6 mL/min, for a total run time of 25 min at 45°C to detect glucose and organic acids.

5.2.3 Sample Preparation for Proteomics

Planktonic *P. aeruginosa* cells (N = 3) cultured in CSP and LCSP were sampled at 4, 7, 11, and 21 h. Cells were transferred into a 2 mL microcentrifuge vial with a screw cap, required for mechanical bead beating, and centrifuged at $3600 \times g$ with three phosphate buffered solution wash steps to remove residual media. Cells were re-suspended in 1.25 mL radioimmunoprecipitation assay buffer (50 mM Tris-HCl, pH 8.0, 150 mM sodium chloride, 1.0% Igepal CA-630 (NP-40), 0.5% sodium deoxycholate 0.1% sodium dodecyl sulfate, Sigma Aldrich)

with 12.5 μ L of protease inhibitors (Halt Protease Cocktail Inhibitor, Thermo Fisher Scientific, Rockford, IL) for the prevention of enzyme degradation upon cell lysis, 0.1 mg/ml lysozyme for solubilization of the peptidoglycan layer, and 5 mM dithiothreitol (DTT) for disulfide bond cleavage. The remainder of the vial was filled with 0.1 mm diameter zirconia/silica beads. Cells were mechanically lysed at 4800 oscillations/min in a mini bead beater (Mini-beadbeater-1, BioSpec Products, Inc, Bartlesville, OK) for five 30 s cycles with ice water bath chilling in between cycles.

A detergent compatible protein assay kit (DC Bradford Reagent, Thermo Fisher Scientific) was used to determine protein concentrations. Equal amount of proteins was transferred to centrifugal filter units (Microcon-30kDa Centrifugal Filter Unit with Ultracel-30 membrane, Millipore Sigma, Billerica, MA) for sample processing following the protocol for filter aided sample preparation (FASP) [173]. Briefly, the steps involved buffer exchange with urea for detergent removal, DTT for protein reduction of disulfide bonds, iodoacetamide for alkylation preventing reformation of disulfide bonds, and overnight trypsin digestion at 37°C with 1:50 enzyme:substrate (w:w) ratio for proteolytic cleavage. The tryptic digests were acidified with formic acid, desalted using a C18 column (Macro SpinColumn, Harvard Apparatus, Holliston, MA), and dried through centrifugal evaporation. Prior to analyses, peptides were re-suspended in 5% acetonitrile with 0.1% formic acid.

5.2.4 Liquid Chromatography Tandem Mass Spectrometry (LC-MS/MS)

Planktonic (200 ng, $N_{(L)CSP} = 3$, single replicate injection) peptide resuspensions were separated in a high-performance LC system (1260 Infinity LC System, Agilent, Santa Clara, CA) and a C18 column (3.5 μ m particle size, 150 mm length \times 75 μ m internal diameter, Zorbax 300SB,

Agilent) through a 60 min mobile phase gradient ranging from 5 - 85% organic (0.1% formic acid in water to 0.1% formic acid in acetonitrile) at 250 nL/min flow rate for a total run time of 75 min. Following LC separation, peptides were simultaneously ionized through nanoelectrospray with a spray voltage at 1.90 kV and 275°C capillary temperature, then analyzed in a high resolution Orbitrap mass spectrometer located in the Research Resources Center at UIC (Orbitrap Velos Pro purchased in 2007, Thermo Fisher Scientific, Waltham, MA) with automatic gain control set at 10^6 ions and injection times of 1 - 200 ms. Full scan mass spectra from m/z 400 - 2000 at 30,000 mass resolution were collected in data-dependent acquisition mode. Ten precursor ions were selected from each full mass scan for analysis by tandem mass spectrometry (MS/MS, using 30% energy in HCD mode for fragmentation).

Raw mass spectra data files were directly uploaded and processed for protein identification and quantitation using the MaxQuant software (v. 1.5.3.30) [174] with main search parameters set at 4.5 ppm peptide tolerance, 20 ppm MS/MS match tolerance, 10 ppm MS/MS *de novo* tolerance, 7 min peptide length, 0.01 FDR, carbamidomethyl fixed modification, oxidation and acetylation variable modifications, and enabled contaminant search. Protein abundances were evaluated by Student's paired sample t-test with p -value < 0.05 using the Perseus software (v.1.5.4.0) [175] for statistical significance. Proteins with significant expression differential (fold change $\geq |1.5|$) and at least ~10% sequence coverage were functionally annotated using the Search Tool for Retrieval of Interacting Genes (STRING) database (v. 10.5) [176] for protein-protein interactions (set at medium confidence of 0.4) and Pseudomonas Genome Database [177]. For lactate, glucose, and acetate metabolic pathways, the Kyoto Encyclopedia of Genes and Genome (KEGG) database was also used for reference [178].

5.3 **Results**

Proteins facilitate metabolic reactions via catalysis or enzyme regulation. Elucidating protein expression can highlight metabolic acclimations to different culturing conditions, such as the presence or absence of a carbon source. *P. aeruginosa* clinical isolate strain (215) cultures grown on either glucose only CSP or glucose and lactate containing LCSP medium were sampled here at time points corresponding to primary growth (4 h), secondary growth (7 h), early stationary (11 h), and intermediate stationary (21 h) phases for bottom-up proteomic analyses. Bottom-up proteomics utilized LC-MS/MS to sequence peptides that were then used to reconstruct entire proteins via comparison with protein databases [165, 166].

5.3.1 **LldD (L-Lactate Dehydrogenase) Protein Identification and Quantification**

The typical workflow started with digestion of proteins into peptide fragments by enzymatic cleavage with trypsin at the carboxyl side of lysine and arginine residues. The resulting tryptic digests were separated by LC, then ionized via electrospray ionization for subsequent analysis in an Orbitrap mass spectrometer. Figure 22 depicts typical mass spectra collected in bottom-up proteomics, with data shown for the protein LldD (L-lactate dehydrogenase). A full scan mass spectrum is shown in Figure 22a, displaying all peptide ions detected from a single elution time off the LC column with the inset expanding the region of the m/z 600.83 ion to include its natural abundance isotope peaks (all marked with stars). Higher intensity peptide ions observed in the full scan were then fragmented by gas phase collision induced dissociation to determine their individual amino acid sequence based upon backbone cleavage. The fragment ion peaks in the tandem mass spectrum of the m/z 600.83 ion in Figure 22c are labelled using the standard notation that is displayed in Figure 22b. These fragment ions allowed identification of the m/z

600.83 ion as derived from the NVEDLSAIALR peptide, which by matching against a protein database (along with other peptides), was in turn identified as deriving from the LldD enzyme with 14 unique peptides and ~44% sequence coverage.

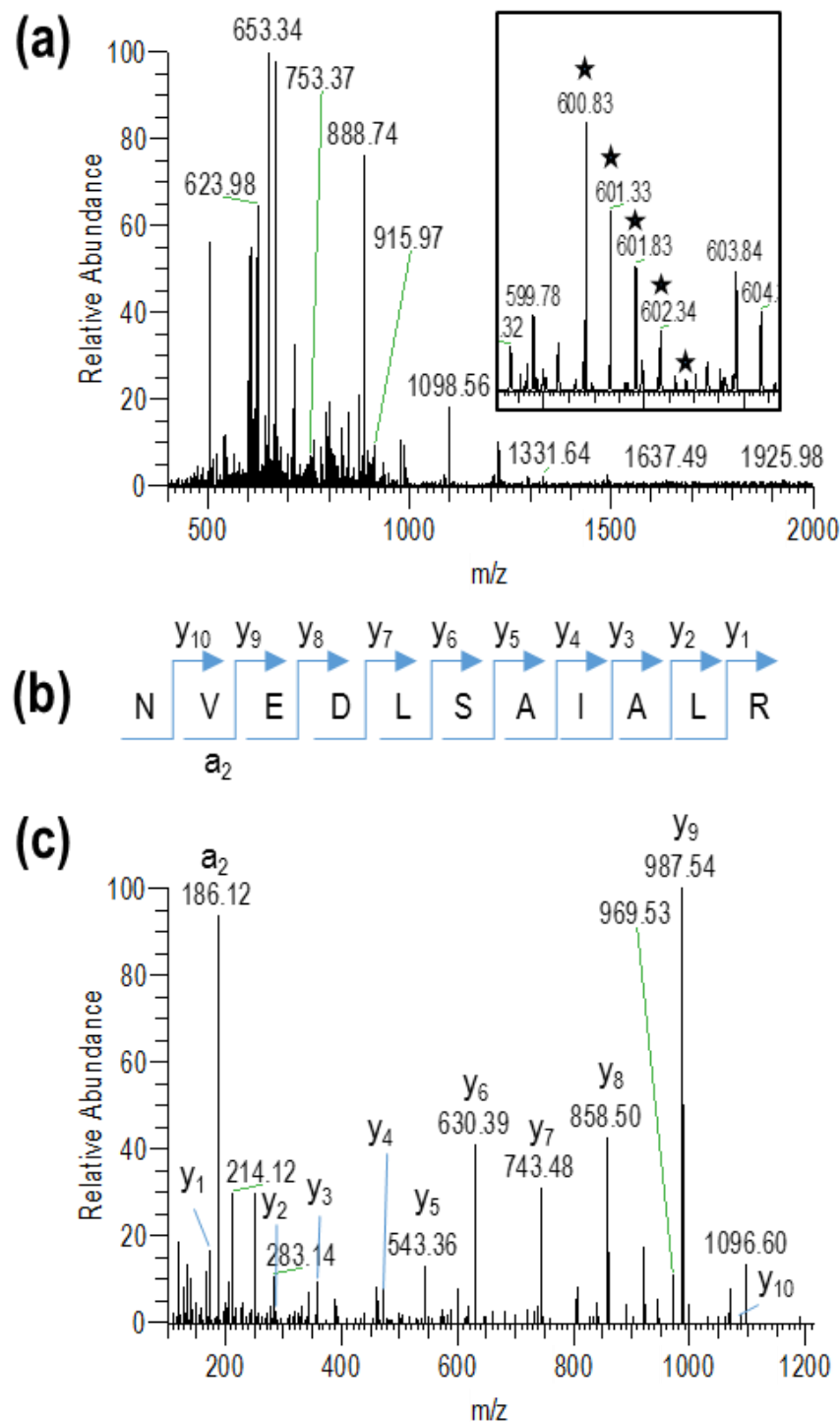


Figure 22. Mass spectra used to identify L-lactate dehydrogenase (LldD). (a) Full scan mass spectrum at a specific elution time from liquid chromatography (LC), with inset showing expanded region around with m/z 600.83 along with its isotope peaks (marked by stars). (b) Schematic of peptide sequence of NVEDLSAIALR and standard notation for its backbone fragmentation by tandem MS. (c) Tandem mass spectrum of m/z 600.38 labelled with a- and y- fragment ions that identifies it as NVEDLSAIALR, a peptide sequence from LldD enzyme.

Processing the entire mass spectral data set with the MaxQuant software [174] led to the identification of ~500 proteins from all digested peptides from the LCSP and CSP media. An intensity-based quantification method by the MaxQuant and Perseus software [174, 175] was then used to determine relative protein abundances by summing all unique peptide ion intensities within each sample: this analysis first converted ion intensities into logarithmic scale (base 2) for normalization, then applied Student's paired t-test to obtain p -values used to distinguish statistically significant differences in expressed protein abundances between the LCSP and CSP media, which is based on peptide ion abundances from the LC-MS/MS full scans (i.e., Figure 22a). Student's t-test was used to calculate the protein expression differential using $\log_2(x_{\text{LCSP}}/x_{\text{CSP}})$, where $x_{\text{(L)CSP}}$ is a given peptide ion intensity from LC-MS/MS data from each timepoint (i.e., Figure 22a) and the results are described below.

5.3.2 Overall Protein Identifications and Differential Expressions

As noted above, a total of ~500 proteins were identified for all culturing conditions. Significant protein expression differentials for LCSP vs. CSP media for each time point are shown in Figure 23 as scatter plots of the $-\log_{10}(p\text{-values})$ for statistical significance versus the expression differential. The horizontal black line corresponds to $p\text{-value} = 0.05$, where proteins above line ($p\text{-value} < 0.05$) are deemed statistically significant and below the line ($p\text{-value} > 0.05$) are statistically non-significant. Approximately 51, 14, 51, and 62 proteins were statistically significant at 4, 7, 11, and 21 h, respectively. Expression differentials indicated both upregulated (positive scale) and downregulated (negative scale) proteins, where only protein expression differentials $> |1.5|$ are highlighted in red (upregulated) or blue (downregulated) in Figure 23 with at least ~10% sequence coverage were considered and are listed in Table III.

Five of the 51 proteins – AtpA (ATP synthase subunit alpha), Hpd (4-hydroxyphenylpyruvate dioxygenase), GlnA (glutamine synthetase), UvrB (UvrABC system protein B) and PA4667 (TPR repeat-containing protein) – at 4 h, six of the 14 proteins – LldD, HutU (urocanate hydratase), AtoB (acetyl-CoA acetyltransferase), HupA (DNA-binding protein HU-alpha), BkdB (lipoamide acyltransferase component of branched-chain alpha-keto acid dehydrogenase complex), and AcsA1 (acetyl-CoA synthetase 1) – at 7 h, fifteen of the 51 proteins – LldD, MmsA (methylmalonate-semialdehyde dehydrogenase [acylating]), MmsB (3-hydroxyisobutyrate dehydrogenase), HutH (histidine ammonia-lyase), Glk (glucokinase), OprB (glucose/carbohydrate outer membrane, porin B), HutU, Zwf (glucose-6-phosphate 1-dehydrogenase), HupA, AtoB, Gap (glyceraldehyde 3-phosphate dehydrogenase), MaiA (maleylacetoacetate isomerase), HutI (imidazolonepropionase), Pgl (6-phosphogluconolactonase), and Hfq (RNA-binding protein in *P. aeruginosa*) – at 11 h, and two of the 62 proteins – LldD and RpoZ (DNA-directed RNA polymerase subunit omega) – at 21 h displayed significant expression differentials. The remaining proteins and its associated KEGG IDs with non-significant expression differentials are listed in Table IV.

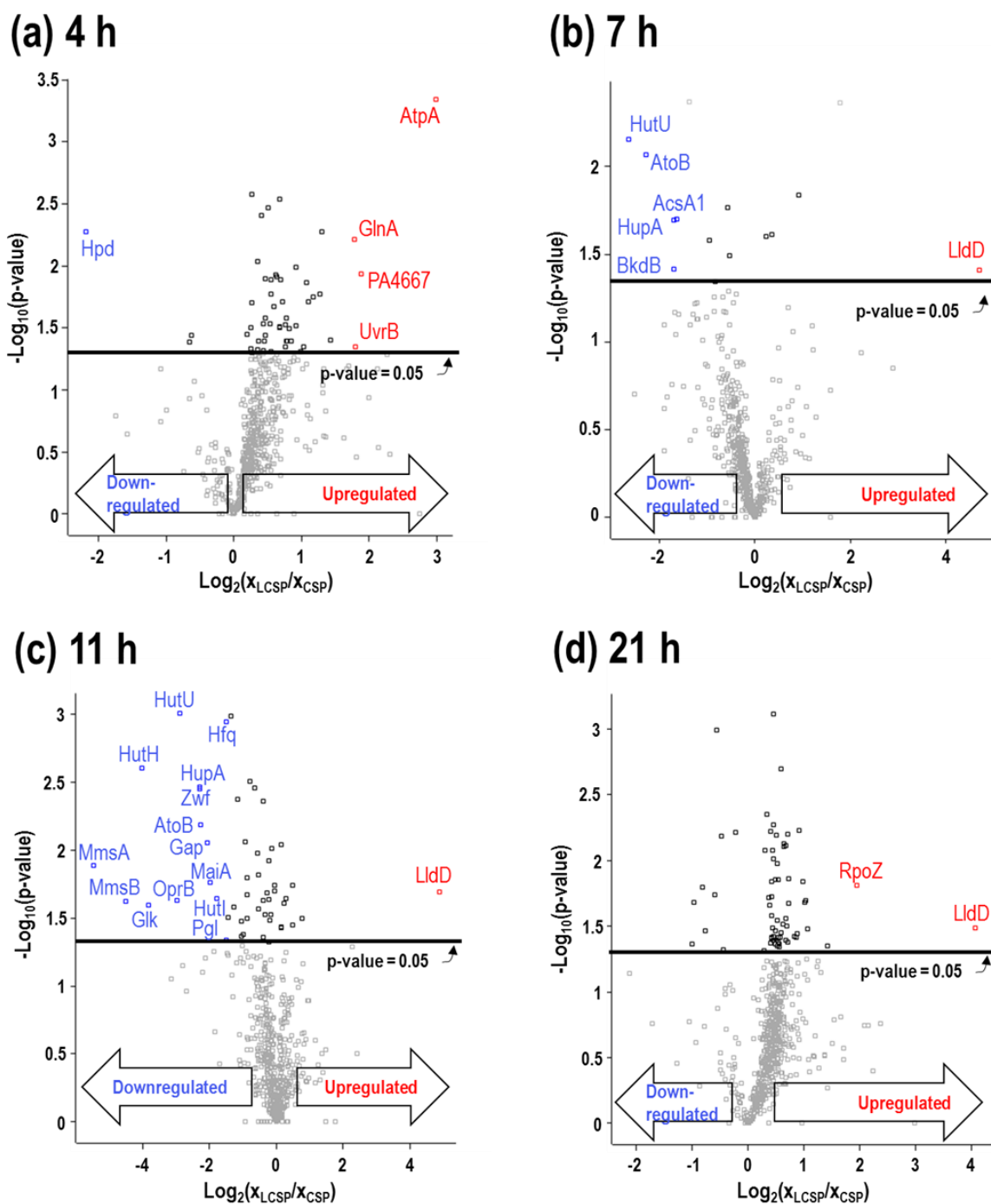


Figure 23. Scatter plots of significant protein expression differentials, $\log_2(x_{\text{LCSP}}/x_{\text{CSP}})$, where x = peptide ion intensities from LC-MS/MS data at (a) 4 h, (b) 7 h, (c) 11 h, and (d) 21 h for LCSP vs. CSP media. Proteins deemed statistically significant (p -values < 0.05) are highlighted above the horizontal black line and non-significant proteins below the black line. Protein expression differentials, with at least ~10% sequence coverage, highlighted in blue (less than -1.5) were downregulated and proteins highlighted in red (greater than 1.5) were upregulated.

Table III. List of up- and downregulated proteins, with its Kyoto Encyclopedia of Genes and Genome identification (KEGG ID), protein name, unique peptides, sequence coverage percentage, molecular weight (kDa), and $\log_2(x_{\text{LCSP}}/x_{\text{CSP}})$ differential value (LCSP vs CSP culture media) observed at 4, 7, 11, and 21 h for planktonic *P. aeruginosa* cultures. *indicates protein homology

| Time (h) | Protein | KEGG ID | Protein Name | Unique Peptides | Seq Cov (%) | Mol Wt (kDa) | Log2(x) Diff |
|----------|---------|---------|---|-----------------|-------------|--------------|--------------|
| 4 | AtpA | PA5556* | ATP synthase subunit alpha | 2 | 41.8 | 55.3 | 3 |
| | Hpd | PA0865 | 4-hydroxyphenylpyruvate dioxygenase | 18 | 57.7 | 39.9 | -2.2 |
| | GlnA | PA5119 | glutamine synthetase | 23 | 66.7 | 51.9 | 1.8 |
| | UvrB | PA3138 | UvrABC system protein B | 3 | 4.9 | 76.1 | 1.8 |
| | PA4667 | PA4667 | TPR repeat-containing protein | 6 | 13.4 | 66.3 | 1.9 |
| 7 | LldD | PA4771 | L-lactate dehydrogenase | 14 | 44.4 | 41.1 | 4.7 |
| | HutU | PA5100 | urocanate hydratase | 23 | 55.3 | 61.2 | -2.6 |
| | AtoB | PA2001 | acetyl-CoA acetyltransferase | 15 | 62.6 | 40.4 | -2.3 |
| | HupA | PA5348 | DNA-binding protein HU-alpha | 9 | 73.3 | 9.7 | -1.7 |
| | BkdB | PA2249 | lipoamide acyltransferase component of branched-chain alpha-keto acid dehydrogenase complex | 15 | 47.9 | 45.8 | -1.7 |
| | AcsA1 | PA0887 | acetyl-CoA synthetase 1 | 29 | 63.3 | 71.8 | -1.6 |
| 11 | LldD | PA4771 | L-lactate dehydrogenase | 14 | 44.4 | 41.1 | 4.9 |
| | MmsA | PA3570 | methylmalonate-semialdehyde dehydrogenase [acylating] | 18 | 50.1 | 53.7 | -5.5 |
| | MmsB | PA3569 | 3-hydroxyisobutyrate dehydrogenase | 9 | 52.7 | 30.5 | -4.5 |
| | HutH | PA5098 | histidine ammonia-lyase | 8 | 27.5 | 53.8 | -4.0 |
| | Glk | PA3193 | glucokinase | 2 | 12.1 | 34.6 | -3.8 |
| | OprB | PA3186 | porin B | 15 | 44.3 | 50.8 | -3.0 |
| | HutU | PA5100 | urocanate hydratase | 23 | 55.3 | 61.2 | -2.9 |
| | Zwf | PA3183 | glucose-6-phosphate 1-dehydrogenase | 18 | 53.0 | 55.6 | -2.3 |
| | HupA | PA5348 | DNA-binding protein HU-alpha | 9 | 73.3 | 9.7 | -2.3 |
| | AtoB | PA2001 | acetyl-CoA acetyltransferase | 15 | 62.6 | 40.4 | -2.3 |
| | Gap | PA3195 | glyceraldehyde 3-phosphate dehydrogenase | 16 | 59.0 | 36.2 | -2.1 |
| | MaiA | PA2007 | maleylacetoacetate isomerase | 5 | 39.2 | 23.7 | -2.0 |
| | HutI | PA5092 | imidazolonepropionase | 3 | 11.2 | 43.4 | -1.8 |
| | Pgl | PA3182 | 6-phosphogluconolactonase | 9 | 52.1 | 25.6 | -1.5 |
| | Hfq | PA4944* | RNA-binding protein in <i>P. aeruginosa</i> | 16 | 51.3 | 66.2 | -1.5 |
| 21 | LldD | PA4771 | L-lactate dehydrogenase | 14 | 44.4 | 41.1 | 4.1 |
| | RpoZ | PA5337 | DNA-directed RNA polymerase subunit omega | 4 | 52.9 | 9.7 | 1.9 |

Table IV. Statistically significant proteins and KEGG IDs with non-significant differential values (LCSP vs CSP) at 4 (blue region), 7 (red region), 11 (yellow region), and 21 h (green region).
*indicates protein homology

| 4 h | | | | | | | | | |
|---------|---------|---------|---------|---------|---------|--------|---------|---------|---------|
| Protein | KEGG ID | Protein | KEGG ID | 11 h | | 21 h | | | |
| HisA | PA5141 | ClpB | PA4542 | Protein | KEGG ID | | | Protein | KEGG ID |
| MsrA | PA5018 | HslV | PA5053 | AspA | PA5429 | | | | |
| HldE | PA4996 | RpsU | PA0579 | SpuD | PA0300 | HupA | PA5348 | Frr | PA3653 |
| DnaJ | PA4760 | HemN | PA1546 | BraF | PA1071 | PA3922 | PA3922 | RpoA | PA4238 |
| CysS | PA1795 | Tal | PA2796 | GdhB | PA3068 | PA0587 | PA0587 | RpsE | PA4246 |
| RpsH | PA4249 | MucD | PA0766* | PhhB | PA0872 | BraF | PA1071 | RpmG | PA5315 |
| RpsE | PA4246 | ArcA | PA5171 | BraG | PA1070 | HutI | PA5092 | RpsM | PA4241 |
| SecB | PA5128 | SecF | PA3820 | DavT | PA0266 | AstB | PA0899 | TrpB | PA0036 |
| Gap | PA5215 | PctA | PA4309 | TyrS | PA4138* | LeuC | PA3121* | LpxC | PA4406 |
| Ssb | PA4232 | Eta | PA1148 | GltA | PA1580 | BkdA2 | PA2248 | SecD | PA3821 |
| SerC | PA3167 | AcnA | PA1562 | AhcY | PA0432 | GcvH1 | PA2446 | RpsR | PA4934 |
| Zwf | PA3183 | ArcC | PA5173 | NfuA | PA1847 | SerC | PA3167 | RnpA | PA5569 |
| OprF | PA1777 | NirS | PA0519 | AhpC | PA0139* | BamD | PA4545 | NqrF | PA2994 |
| PA4465 | PA4465 | 7 h | | PA5475 | PA5475 | HslU | PA5054 | HscA | PA3810 |
| LeuS | PA3987 | | | PA1673 | PA1673 | GreA | PA4755 | FabA | PA1610 |
| FadB | PA3014 | Protein | KEGG ID | Hom | PA3736 | RpsH | PA4249 | RpmE2 | PA3601 |
| NqrA | PA2999 | KdsD | PA4457 | ArgB | PA5323 | Hcp1 | PA0085 | HisZ | PA4939 |
| ZipA | PA1528 | PhhA | PA0872 | ProS | PA0956 | PurD | PA4855 | RpsP | PA3745 |
| UbiG | PA3171 | TrmB | PA0382 | MexA | PA0425 | CoaX | PA4279 | Hom | PA3736 |
| CoaX | PA4279 | ClpX | PA1802 | RnpA | PA5569 | TrpE | PA0609 | PrfC | PA3903 |
| AlgP | PA5253 | TatA | PA5068 | CysS | PA1795 | RecA | PA3617 | HemC | PA5260 |
| RsmC | PA4627 | AtpB | PA5560 | LpdG | PA1587 | PA0170 | PA0170 | PA5217 | PA5217 |
| Eda | PA3181 | PA5217 | PA5217 | KatA | PA4236 | RpsF | PA4935 | PA3453 | PA3453 |
| ParE | PA4967 | RpoB | PA4270* | Pta | PA0835 | RpsJ | PA4264 | TruB | PA4742 |
| DnaK | PA4761* | | | AlgU | PA0762 | RpsG | PA4267 | RplD | PA4262 |
| PscF | PA1719 | | | RplV | PA4258 | SucD | PA1589 | FtsZ | PA4407 |
| Gap | PA3195 | Protein | KEGG ID | ArgG | PA3525 | Psd | PA4957 | FptA | PA4221 |
| RpoN | PA4462 | Eda | PA3181 | PckA | PA5192* | AroC | PA1681 | SecF | PA3820 |
| HslU | PA5054 | GlyA2 | PA2444 | RplP | PA4256 | FliN | PA1444 | GlnS | PA4742 |
| HemB | PA5243 | BPI | | SpeE1 | PA1687 | LeuS | PA3987 | SerS | PA2612 |
| PdxH | PA1049 | PhhC | PA0870 | DsbA | PA5489 | RpsD | PA4239 | CspA | PA3266 |
| PurK | PA5425 | AstE | PA0901 | RapA | PA3308 | HslU | PA5054* | Cmk | PA3163 |

5.3.3 **Glucose and Lactate Metabolism vs. LldD Differential Expression**

Metabolomic study also measured two media-supplied carbon sources – glucose and lactate – with 25 mM lactate in LCSP being the only difference between the two culturing conditions (Figure 24ab). The extracellular metabolomics data showed that the LCSP grown cultures had consumed all the lactate by 11 h and there was substantial glucose remaining in the medium until glucose is completely consumed by 13 h – see starting glucose and lactate concentrations (Figure 24a). The CSP cultures catabolized glucose and did not secrete lactate as demonstrated by the absence of lactate in the culture supernatant in Figure 24b. Upon glucose depletion, the production and consumption of acetate was observed at levels greater than in LCSP than CSP (Figure 24ab). Additionally, the abundance of the LldD enzyme is greater in LCSP than CSP media (Figure 24c).

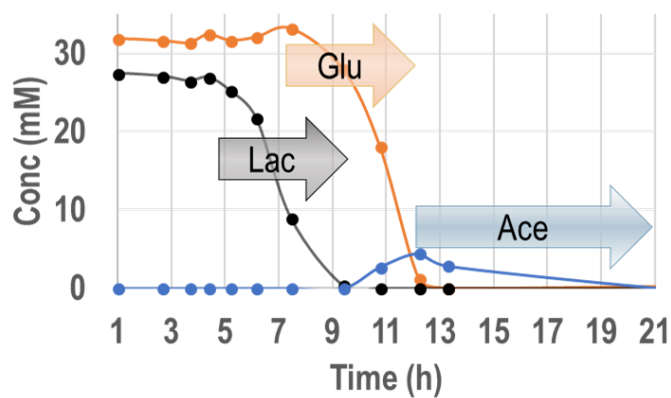
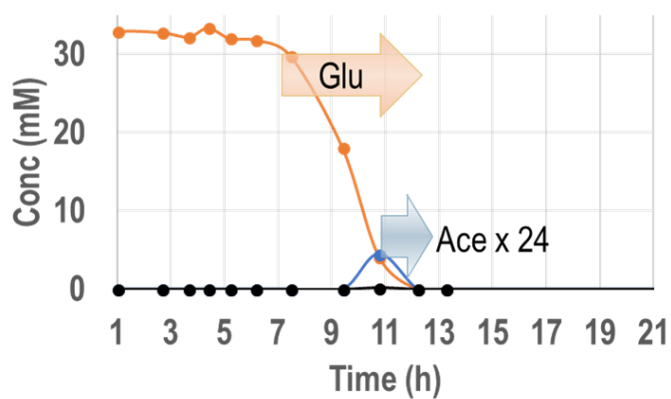
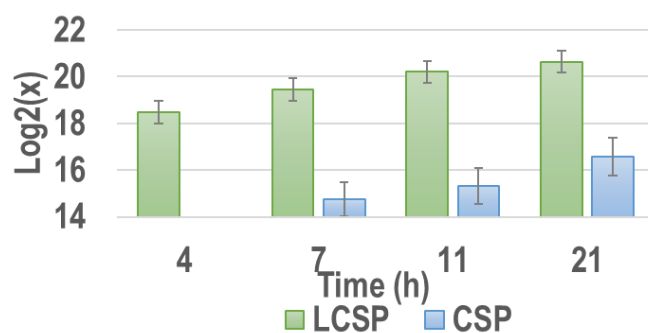
(a) LCSP**(b) CSP****(c) LldD**

Figure 24. Millimolar concentrations of extracellular glucose and lactate taken from growth media (supernatant) at time (a) 0 and (b) 11 h. (c) Protein expression at 11 h of LldD based on log₂(x) values of peptide abundances from LldD.

5.4 **Discussion**

The regulated metabolism of glucose and lactate as carbon sources is important for cellular growth, maintenance, and structural support [179, 180]. Bottom-up proteomics via LC-MS/MS was used here to distinguish differences in the phenotypes of planktonic *P. aeruginosa* clinical isolate (215) that resulted from the presence or absence of a single, auxiliary carbon source, lactate. Lactate dehydrogenase enzyme (LldD) catalyzes the specific conversion of L-lactate to pyruvate (Figure 25). The cultures grown in the presence of lactate and glucose had a higher abundance of LldD, but lower abundance of glycolysis enzymes. The cultures grown in the presence of only glucose had high abundance of glycolysis enzymes and only low abundance of LldD. These protein expression differentials were consistent with the extracellular metabolite analyses which showed that lactate was consumed preferentially to glucose; the cultures consuming lactate had protein abundances consistent with lactate consumption, and the cultures catabolizing glucose had protein abundances consistent with glycolysis including enzymes from the Entner-Doudoroff pathway [181]. Collectively, Figure 24 demonstrated that the *P. aeruginosa* strain (215) examined here has a catabolite repression regulatory system that prefers lactate consumption over glucose consumption, a reverse diauxic metabolic strategy, which is different from many Gram-negative bacteria such as *E. coli* with diauxie [172].

5.4.1 **Lactate, Glucose, and Acetate Metabolisms**

Figure 25 depicts acetate, lactate, and glucose conversion to pyruvate as a series of metabolic reactions or pathways [158, 178-180]. The yellow stars in Figure 25 highlight proteins that are key to the metabolic reactions that have been found here to be statistically significant and with significant expression differentials at 7 and 11 h. With the induction of LldD in the LCSP

medium, several proteins were repressed during the times of lactate (secondary growth phase, 7 h) and glucose (early stationary phase, 11 h) consumption (Figure 23bc). During lactate consumption in the LCSP medium, two of the five proteins, AcsA1 and AtoB, were related to acetate metabolism and were repressed. During glucose consumption in the LCSP medium, four of the fourteen proteins, Glk, Zwf, Gap, and Pgl were related to glucose metabolism [151] and were repressed. Several additional metabolites shown in Figure 25 are acetate and glucose intermediates (also highlighted in green text): acetyl-CoA, acetoacetyl-CoA, G6P (glucose-6P), 6-PGDL (6-phosphogluconolactone), Gln-6P (gluconate-6P), and 13-DPG (phosphoglyceroyl-P) [151, 178, 181]. No intracellular metabolomic analyses were performed on these intermediates, but they are displayed in Figure 25 to illustrate the metabolic pathways with key successive enzymes involved in glucose and acetate conversion. These multienzyme pathways can be contrasted with the single LldD enzyme implicated in lactate conversion to pyruvate. Contrasting with the protein repressions during lactate and glucose consumption, four proteins, GlnA, UvrB, PA4667, and AtpA, prior to lactate consumption (primary growth phase, 4 h) and one protein, RpoZ, following glucose depletion (intermediate stationary phase, 21 h) were induced.

5.4.2 Determination of Protein Associations and Metabolic Pathways

These protein associations were determined using the STRING database [176] based on known, predicted, and other protein-protein interactions. Protein associations are described below and derived respectively from curated databases or experiments; gene neighborhood, fusions, or co-occurrence; and text mining, co-expression, or protein homology. Functional enrichment analysis from the STRING database were also performed using the KEGG pathway reference database [178], which annotates enzymes related to a metabolic pathway for predicting phenotypes

in large-scale datasets. The *Pseudomonas* Genome Database [177] was consulted for additional annotations of unassociated proteins.

The STRING database is useful for determining the protein-protein interactions by revealing how a single protein can be associated – either directly or indirectly – in a metabolic pathway [176]. Protein-protein interactions [176] were found at timepoints 4 (GlnA and AtpA), 7 (AcsA1 and AtoB), 11 (Glk, Zwf, Pgl, and Gap), and 21 h (LldD and RpoZ) where thicker red-dotted lines indicate more interactions in Figure 25 for 7 and 11 h (4 and 21 h are not shown).

Functional enrichment analysis of the proteins and its enzymatic involvement in KEGG metabolic pathways was also performed [176]. The enzymes involved with specific KEGG metabolic pathways (listed in the KEGG database as “Matching proteins in network” with false discovery rates, FDR, less than 0.05), are listed in Table V. Functional enrichment was found at the times of lactate (7 h) and glucose (11 h) consumption. During lactate consumption, four KEGG metabolic pathways were found: AcsA1 and AtoB in pyruvate and propanoate metabolism and AtoB and BkdB in valine, leucine, and isoleucine degradation as well as biosynthesis of secondary metabolites. The remaining unassociated enzymatic proteins were HupA and HutU. During glucose consumption, six KEGG metabolic pathways were found where Glk, Zwf, Pgl, and Gap were involved in three of the six KEGG metabolic pathways: carbon metabolism, microbial metabolism in diverse environments, and biosynthesis of secondary metabolites. Furthermore, Zwf and Pgl were involved in the pentose phosphate pathway. Other KEGG pathways were valine, leucine and isoleucine degradation and histidine metabolism. Of the remaining three enzymatic proteins, two apparently have regulatory roles, HupA and Hfq, and the third is a metabolite transport protein, OprB [177].

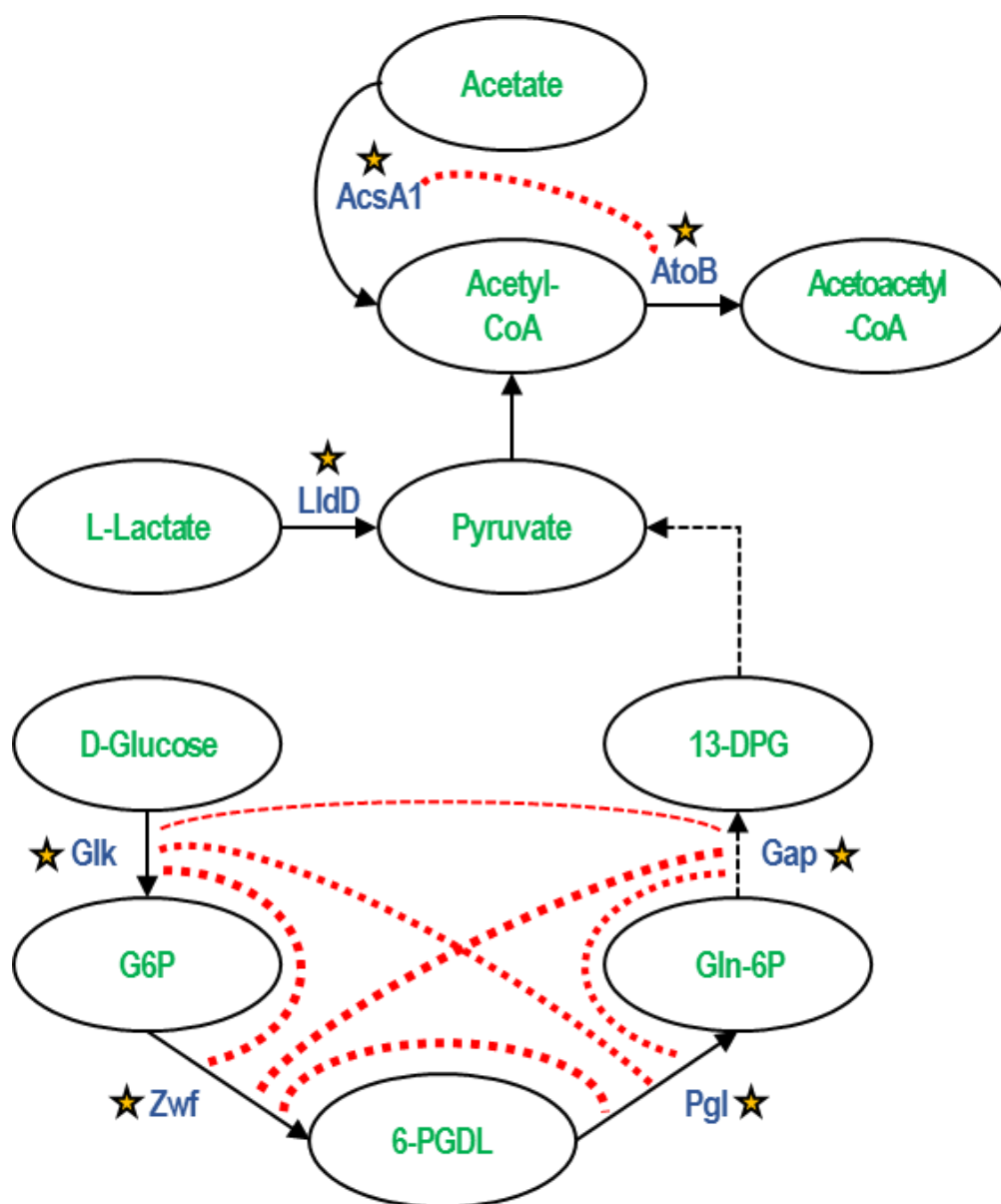


Figure 25. Schematic of the abbreviated metabolic pathways [178] of small molecule (green) metabolism en route to pyruvate, lactate and acetate. Black arrows with associated proteins (blue) indicate reactions involving single reaction (solid) or multiple reactions (dotted). Yellow stars indicate key proteins that showed significant expression differentials at 7 and 11 h (refer to Table III and text for protein names). Red dotted lines represent STRING protein-protein interactions, with thicker lines indicating more associations. Additional metabolites noted are G6P, 6-PGDL, Gln-6P, and 13-DPG (see text).

Table V. KEGG metabolic pathway functional annotation of proteins at 7 and 11 h planktonic *P. aeruginosa* cultures. FDR are false discovery rates with protein networks listed in the KEGG pathways.

| Time (h) | KEGG pathway description | FDR | Matching proteins in network |
|----------|--|------------------------|---|
| 7 | Metabolic pathways | 1.57×10^{-02} | <i>AcsA1, AtoB, BkdB, HutU, LldD</i> |
| | Pyruvate metabolism | 2.62×10^{-02} | <i>AcsA1, AtoB</i> |
| | Valine, leucine and isoleucine degradation | 2.89×10^{-02} | <i>AtoB, BkdB</i> |
| | Propanoate metabolism | 2.89×10^{-02} | <i>AcsA1, AtoB</i> |
| 11 | Metabolic pathways | 1.75×10^{-06} | <i>AtoB, Gap, Glk, HutH, HutI, HutU, LldD, MaiA, MmsA, MmsB, Pgl, Zwf</i> |
| | Carbon metabolism | 2.84×10^{-05} | <i>AtoB, Gap, Glk, MmsA, Pgl, Zwf</i> |
| | Histidine metabolism | 1.32×10^{-03} | <i>HutH, HutI, HutU</i> |
| | Microbial metabolism in diverse environments | 2.01×10^{-03} | <i>AtoB, Gap, Glk, MaiA, Pgl, Zwf</i> |
| | Valine, leucine and isoleucine degradation | 5.39×10^{-03} | <i>AtoB, MmsA, MmsB</i> |
| | Biosynthesis of secondary metabolites | 2.72×10^{-02} | <i>AtoB, Gap, Glk, Pgl, Zwf</i> |
| | Pentose phosphate pathway | 3.16×10^{-02} | <i>Pgl, Zwf</i> |

5.5 Conclusion

LC-MS/MS based bottom-up proteomics was used to examine metabolic acclimation to different culturing conditions of planktonic *P. aeruginosa* clinical isolate (215). The application of proteomics to differentiate metabolic changes in protein expression were found to be consistent with the different nutrients in the medium - the presence or absence of lactate - and the uptake of

preferred carbon sources such as glucose based on a regulatory process known as catabolite repression. The ability of lactate to modulate LldD, acetate metabolic, and glycolysis enzymes has significance to how *P. aeruginosa* will grow in diverse environments such as multispecies biofilms.

6. DELINEATING *PSEUDOMONAS AERUGINOSA* METABOLISM IN PLANKTONIC AND BIOFILM CULTURES THROUGH MULTI-OMICS

6.1 Introduction

Immobilized, interphase associated bacterial biofilms play important roles in both human health and disease. Biofilms play a positive role as part of the human microbiome aiding digestion and nutrient acquisition [182], but can also be antagonistic to human health by contributing to inflammation and degradation of host tissue [1, 3]. For example, many studies have examined the role of biofilms in prolonged infections of the lungs of cystic fibrosis patients and on the surfaces of medical devices [1].

Biofilm removal has been pursued via mechanical abrasion, increasing temperature, chemical treatment (i.e., peroxide, quaternary amines, or chlorine), electrochemical treatment [183], and electrical gaseous plasma discharges [184, 185]. An alternative strategy in biofilm control is to interrupt factors that enhance their growth, such as manipulation of available nutrients [1, 3]. Such a control strategy is supported by the observation that culturing conditions can have a dramatic effect on the response of biofilms to specific antibiotics [186]. It follows that development of such control strategies requires further understanding of spatially resolved phenotypes and interspecies interactions in microbial communities.

A multi-omics strategy can help delineate the underlying changes in lactate-related metabolisms in microbial communities. Bottom-up proteomics is used here with guided exogenous metabolomics to determine phenotypic changes of the clinical chronic wound isolate *P. aeruginosa* in both free-flowing planktonic culture and sessile biofilms, both grown in amino acid rich media

containing glucose with and without auxiliary lactate. The proteomics results will eventually be used to inform computational metabolic models of polymicrobial chronic wound biofilms which will elucidate spatially resolved phenotypes and interspecies interactions [187]. Understanding these mechanisms is essential for devising effective therapies for patients suffering from chronic wound infections.

6.2 Experimental Details

6.2.1 Bacterial Strains and Growth Conditions

Planktonic *P. aeruginosa* growth details can be found in Chapter 5, Section 5.2.1. For biofilm growth, diluted overnight cultures ($OD_{600} \sim 0.010$) were inoculated on tissue culture inserts and suspended on 6-well plates above fresh medium at 37°C.

6.2.2 Exogenous Metabolomics

Refer to Chapter 5, Section 5.2.2 for details.

6.2.3 Sample Preparation for Proteomics

For planktonic *P. aeruginosa* ($N = 3$) sample preparations, refer to Chapter 5, Section 5.2.3 for details. Biofilms ($N = 2$) were prepared following the same steps as planktonic cultures but with no washings.

6.2.4 LC-MS/MS

Planktonic ($N_{(L)CSP} = 3$, single replicate injection) and biofilm ($N_{(L)CSP} = 2$, triple replicate injections) *P. aeruginosa* peptide resuspensions were analyzed with LC-MS/MS (refer to Chapter 5, Section 5.2.4. for details).

6.3 Results

6.3.1 Metabolomics

Glucose and lactate concentrations from planktonic (Figure 26a) and biofilm (Figure 26b) cultures were detected in the supernatant at 0 and 11 h of culture growth. Glucose was measured for both planktonic and biofilm cultures in both CSP and lactate supplemented CSP (LCSP) media at 0 h, but lactate was only detected in LCSP and not in CSP, as expected. The planktonic culture at 11 h displayed a greater decrease in glucose concentration for CSP than LCSP media, whereas lactate was completely depleted in the LCSP media. The 11 h timepoint correlates to the early stationary phase in planktonic culture. By comparison, biofilms displayed a slightly lower glucose concentration in CSP media and a marked decrease with lactate concentration in the LCSP media.

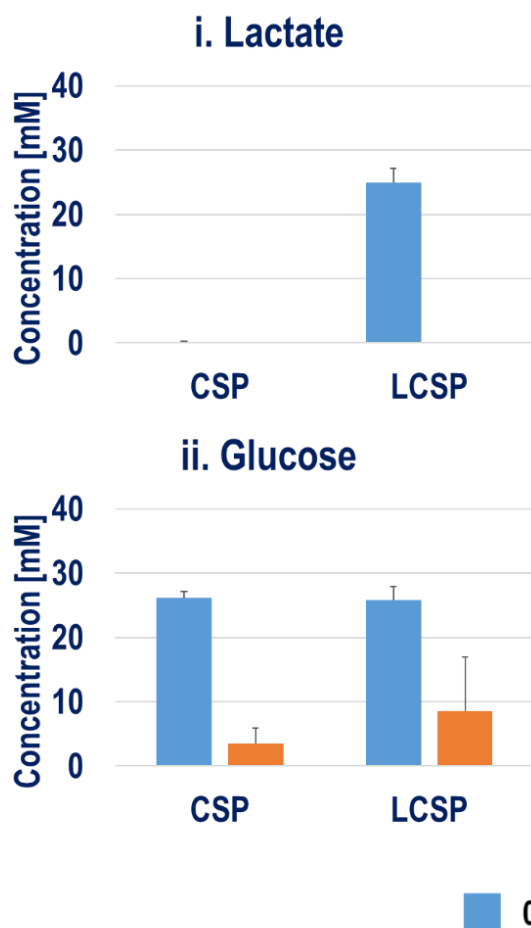
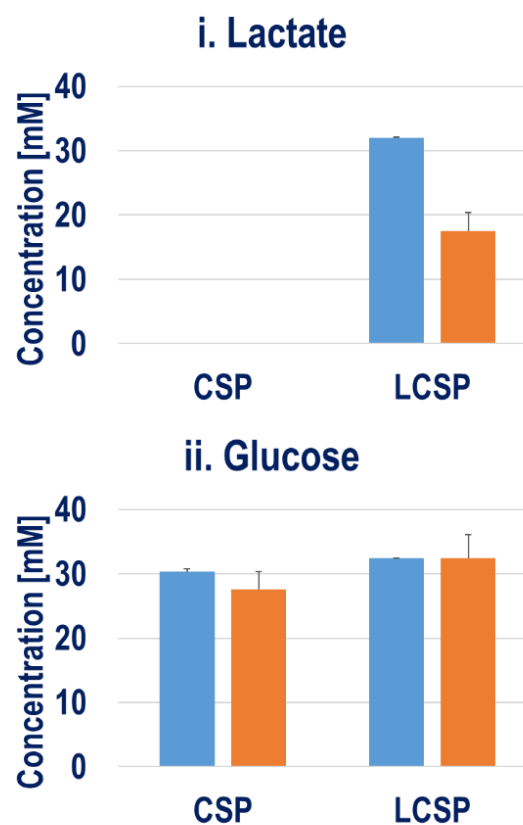
(a) Planktonic**(b) Biofilm**

Figure 26. Metabolite profiling of (i) lactate & (ii) glucose in (a) planktonic and (b) biofilm *P. aeruginosa* cultures grown in CSP and lactate-supplemented CSP media (LCSP) for 0 h and 11 h.

6.3.2 Proteomics

Untargeted label-free quantitative processing of the entire Orbitrap mass spectral data set led to the identification of ~500 proteins cumulatively from all digested peptides from the LCSP and CSP media. However, planktonic and biofilm cultures had only 51 and 48 statistically significant proteins, respectively (see below). Intensity-based quantification by the MaxQuant software [174] was used to determine relative protein abundances by summing all unique peptide ion intensities from the LC-MS/MS full scans.

Expression differentials indicated both upregulated (positive scale) and downregulated (negative scale) proteins, where proteins were significantly up- or down-regulated are annotated in the gray area to the right and left, respectively in Figure 27. These proteins are also listed in Table VI along with the protein name, KEGG ID, number of unique peptides, sequence coverage percentage, and molecular weight (kDa). Fifteen of the 51 proteins in planktonic cultures displayed significant expression differentials: LldD, MmsA, MmsB, HutH, Glk, OprB, HutU, Zwf, HupA, AtoB, Gap, MaiA, HutI, Pgl, and Hfq. Nine of the 48 proteins in the biofilms displayed significant expression differentials: LldD, FolE2 (GTP cyclohydrolase), PvdA (L-ornithine N(5)-monooxygenase), SpeE1 (polyamine aminopropyltransferase 1), Mqo1 (probable malate:quinone oxidoreductase 1), SodA (superoxide dismutase [Mn]), HisA (1-(5-phosphoribosyl)-5-[(5-phosphoribosylamino)methylideneamino] imidazole-4-carboxamide isomerase), PA5217 (probable binding protein component of ABC iron transporter), and FumC1 (fumarate hydratase). The remaining proteins and associated KEGG IDs with non-significant expression differentials are listed in Table VII.

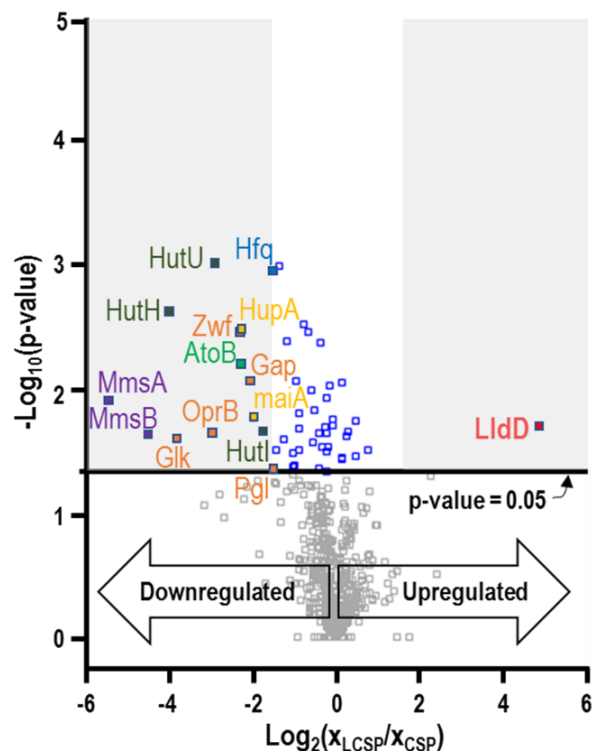
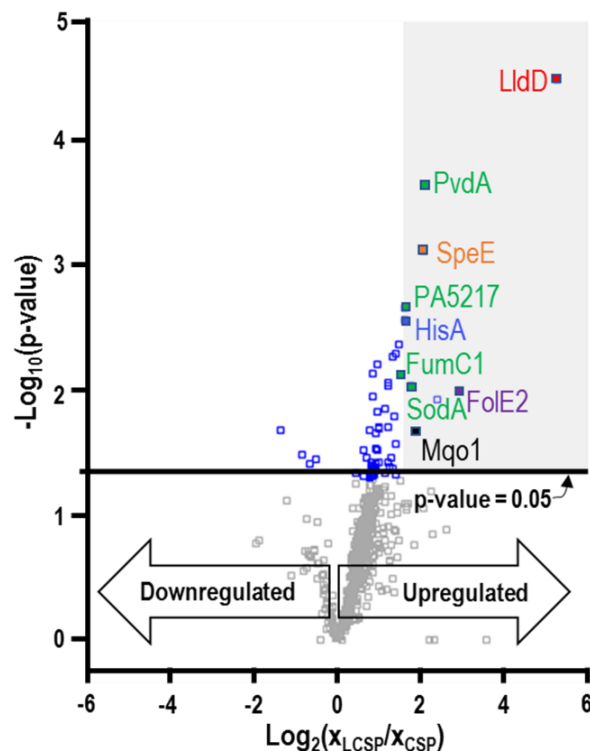
(a) Planktonic**(b) Biofilm**

Figure 27. Protein expression in LCSP vs. CSP for planktonic and biofilm *P. aeruginosa* growth at 11 h. Scatter plots of \log_2 fold-change [$\log_2(x_{\text{LCSP}}/x_{\text{CSP}})$] vs $-\log_{10}(p\text{-value})$. Statistically significant proteins ($p\text{-value} < 0.05$) are highlighted above horizontal black line. Significant down- or up-regulation with greater than 1.5-fold change and at least ~10% sequence coverage are annotated in the gray regions.

Table VI. List of up- and downregulated proteins, with its KEGG ID, protein name, unique peptides, sequence coverage percentage, molecular weight (kDa), and $\log_2(X_{LCSP}/X_{CSP})$ differential value (LCSP vs CSP culture media) observed from planktonic and biofilm *P. aeruginosa* cultures. *indicates protein homology

| Culture | Protein | KEGG ID | Protein Name | Unique peptides | Sequence coverage | Mol Wt (kDa) | $\log_2(x)$ Diff |
|------------|---------|---------|---|-----------------|-------------------|--------------|------------------|
| Planktonic | LldD | PA4771 | L-lactate dehydrogenase | 14 | 44.4% | 41.1 | 4.9 |
| | MmsA | PA3570 | methylmalonate-semialdehyde dehydrogenase [acylating] | 18 | 50.1% | 53.7 | -5.5 |
| | MmsB | PA3569 | 3-hydroxyisobutyrate dehydrogenase | 9 | 52.7% | 30.5 | -4.5 |
| | HutH | PA5098 | histidine ammonia-lyase | 8 | 27.5% | 53.8 | -4.0 |
| | Glc | PA3193 | glucokinase | 2 | 12.1% | 34.6 | -3.8 |
| | OprB | PA3186 | porin B | 15 | 44.3% | 50.8 | -3.0 |
| | HutU | PA5100 | urocanate hydratase | 23 | 55.3% | 61.2 | -2.9 |
| | Zwf | PA3183 | glucose-6-phosphate 1-dehydrogenase | 18 | 53.0% | 55.6 | -2.3 |
| | HupA | PA5348 | DNA-binding protein HU-alpha | 9 | 73.3% | 9.7 | -2.3 |
| | AtoB | PA2001 | acetyl-CoA acetyltransferase | 15 | 62.6% | 40.4 | -2.3 |
| | Gap | PA3195 | glyceraldehyde 3-phosphate dehydrogenase | 16 | 59.0% | 36.2 | -2.1 |
| | MaiA | PA2007 | maleylacetoacetate isomerase | 5 | 39.2% | 23.7 | -2.0 |
| | HutI | PA5092 | imidazolonepropionase | 3 | 11.2% | 43.4 | -1.8 |
| | Pgl | PA3182 | 6-phosphogluconolactonase | 9 | 52.1% | 25.6 | -1.5 |
| | Hfq | PA4944* | RNA-binding protein in <i>P. aeruginosa</i> | 16 | 51.3% | 24.0 | -1.5 |
| Biofilm | LldD | PA4771 | L-lactate dehydrogenase | 12 | 39.6% | 41.1 | 5.3 |
| | FolE2 | PA5539 | GTP cyclohydrolase | 6 | 36.2% | 32.4 | 2.9 |
| | PvdA | PA2386 | L-ornithine N(5)-monooxygenase | 4 | 12.4% | 49.5 | 2.1 |
| | SpeE1 | PA1687 | polyamine aminopropyltransferase 1 | 3 | 23.8% | 32.2 | 2.0 |
| | Mqo1 | PA3452 | probable malate:quinone oxidoreductase 1 | 4 | 11.1% | 57.2 | 1.9 |
| | SodA | PA4468 | superoxide dismutase [Mn] | 3 | 25.1% | 22.5 | 1.8 |
| | PA5217 | PA5217 | probable binding protein component of ABC iron transporter | 12 | 36.1% | 36.3 | 1.6 |
| | HisA | PA5141 | 1-(5-phosphoribosyl)-5-[(5-phosphoribosylamino) methylideneamino] imidazole-4-carboxamide isomerase | 6 | 32.7% | 25.9 | 1.6 |
| | FumC1 | PA4470 | fumarate hydratase | 19 | 59.6% | 48.7 | 1.5 |

Table VII. Statistically significant proteins and KEGG IDs with non-significant differential values (LCSP vs CSP) in planktonic and biofilm *P. aeruginosa* cultures. *indicates protein homology

| Planktonic Culture | | | | Biofilm Culture | | | |
|--------------------|---------|---------|---------|-----------------|---------|---------|---------|
| Protein | Protein | Protein | Protein | Protein | KEGG ID | Protein | KEGG ID |
| AhcY | PA0432 | MexA | PA0425 | ArgF | PA3537 | PA1295 | PA1295 |
| AhpC | PA0139* | NfuA | PA1847 | AtpA | PA5556* | PA2271 | PA2271 |
| AlgU | PA0762 | PA1673 | PA1673 | BamD | PA4545 | PA2634 | PA2634 |
| ArgB | PA5323 | PA5475 | PA5475 | ClpP1 | PA1801 | PckA | PA5192* |
| ArgG | PA3525 | PckA | PA5192* | CspA | PA3266 | PstS | PA5369 |
| AspA | PA5429 | PhhB | PA0872 | CysS | PA1795 | PurC | PA1013* |
| AstE | PA0901 | PhhC | PA0870 | DsbA | PA5489 | PyrH | PA3654 |
| BPI | | ProS | PA0956 | Eco | PA2755 | RdgC | PA3263 |
| BraF | PA1071 | Pta | PA0835 | FtsA | PA4408 | RplL | PA4271 |
| BraG | PA1070 | RapA | PA3308 | HchA | PA1135 | SecB | PA5128 |
| CysS | PA1795 | RnpA | PA5569 | Hcp1 | PA0085 | SecD | PA3821 |
| DavT | PA0266 | RplP | PA4256 | HemC | PA5260 | SthA | PA2991 |
| DsbA | PA5489 | RplV | PA4258 | HmuV | PA4706 | Thil | PA5118 |
| Eda | PA3181 | SpeE1 | PA1687 | HutI | PA5092 | ThrB | PA5495 |
| GdhB | PA3068 | SpuD | PA0300 | LepB | PA0768 | TrpC | PA0651 |
| GltA | PA1580 | TyrS | PA4138* | LeuC | PA3121 | TrpE | PA0609 |
| GlyA2 | PA2444 | | | MurG | PA4412 | TrpS | PA4439 |
| Hom | PA3736 | | | NqrC | PA2997 | TyrS1 | PA4138 |
| KatA | PA4236 | | | OprB | PA3186 | Xpt | PA5298 |
| LpdG | PA1587 | | | PA0423 | PA0423 | | |

6.4 Discussion

6.4.1 Protein Associations

Twelve of the fifteen proteins from planktonic cultures and six of the nine proteins from biofilms listed in Table VI were found to be enzymes involved with specific KEGG “Metabolic pathways,” where associated enzymes are listed in Table VIII as “Matching proteins in network” with KEGG Pathway descriptions and false discovery rates (FDR) < 0.05 . From the remaining three of the fifteen proteins in planktonic cultures, two apparently are known to have regulatory roles: HupA and Hfq while the third is a metabolite transport associated protein, OprB (see below). The remaining three of the six proteins in biofilms are PA5217, SodA, and PvdA.

Table VIII. KEGG metabolic pathway functional annotation on enzymatic proteins from planktonic and biofilm *P. aeruginosa* cultures. FDR are false discovery rates with protein networks listed in the KEGG pathways.

| Culture | KEGG Pathway description | FDR | Matching proteins in network |
|------------|--|------------------------|---|
| Planktonic | Metabolic pathways | 1.75×10^{-06} | <i>AtoB, Gap, Glk, HutH, HutI, HutU, LldD, MaiA, MmsA, MmsB, Pgl, Zwf</i> |
| | Carbon metabolism | 2.84×10^{-05} | <i>AtoB, Gap, Glk, MmsA, Pgl, Zwf</i> |
| | Histidine metabolism | 1.32×10^{-03} | <i>HutH, HutI, HutU</i> |
| | Microbial metabolism in diverse environments | 2.01×10^{-03} | <i>AtoB, Gap, Glk, MaiA, Pgl, Zwf</i> |
| | Valine, leucine and isoleucine degradation | 5.39×10^{-03} | <i>AtoB, MmsA, MmsB</i> |
| | Biosynthesis of secondary metabolites | 2.72×10^{-02} | <i>AtoB, Gap, Glk, Pgl, Zwf</i> |
| | Pentose phosphate pathway | 3.16×10^{-02} | <i>Pgl, Zwf</i> |
| Biofilm | Metabolic Pathways | 2.37×10^{-02} | <i>FumC1, HisA, LldD, Mqo1, FolE2, SpeE1</i> |
| | Pyruvate metabolism | 1.08×10^{-02} | <i>FumC1, LldD, Mqo1</i> |
| | Citrate cycle (TCA cycle) | 4.77×10^{-02} | <i>FumC1, Mqo1</i> |

6.4.2 Carbon Catabolite Repression

Carbon catabolite repression (CCR) regulatory effects are important to drive cellular growth, maintenance, and structural support [180, 181]. Metabolomics data indicate changes that are occurring at a given instant [161] and are complementary to proteomic data and changes in protein expression differentials that can be used to elucidate metabolic acclimations [188]. LldD is the enzyme responsible for the single step conversion of lactate to pyruvate (Figure 28, green

text) [158, 178]. The 11 h time point was chosen specifically to determine the metabolic changes following lactate consumption for the planktonic growth in LCSP compared with the CSP medium. The integration of metabolomic and proteomic data found that as lactate was consumed, LldD was significantly induced (Figure 28, red upward arrow) in both planktonic and biofilm *P. aeruginosa*. However, differences for planktonic vs. biofilm were observed in the downstream effects as shown in Figure 28 and are further described below.

Planktonic culture underwent an upregulation of LldD along with a downregulation of enzymes involved in glucose utilization. Figure 28a depicts the downregulated enzymes (blue downward arrows) and protein-protein interactions from the STRING database (thicker dashed lines correlate with stronger association evidence). Downregulation was observed for the outer membrane transport protein OprB and the four enzymes Glk, Zwf, Pgl, and Gap that carry out the conversion of glucose to their four respective intermediate metabolites: G6P, 6-PGDL, Gln-6P, and 13-DPG [151, 178, 181]. No intracellular metabolomic analyses were performed to detect any of these four intermediate metabolites, but all four are nevertheless displayed in Figure 28a to illustrate the metabolic pathways with key successive enzymes involved in glucose conversion to pyruvate (as well as for contrast with the simpler pathway for lactate conversion to pyruvate by LldD).

In addition to the repression of glucose metabolism in the presence of lactate in planktonic culture, other more specific metabolisms that were also repressed include histidine metabolism (HutH, HutI, and HutU) and the degradation of valine, leucine, and isoleucine (AtoB, MmsA, and MmsB, see Table VIII). Several unassociated proteins were also repressed: MaiA as well as the regulatory binding proteins Hfq and HupA. MaiA is involved in aromatic acid metabolism [177]. The repression of Hfq was previously found to upregulate genes encoding proteins involved in

CCR in the PAO1 strain of *P. aeruginosa* [189]. While repression of HupA was found to increase aggregation and adhesion in *E. coli* [190], the role of HupA in *P. aeruginosa* has not been determined [191].

Biofilms display upregulation of LldD along with induction of two additional TCA cycle enzymes: Mqo1, involved in fumarate conversion to S-malate, and FumC1, involved in S-malate conversion to oxaloacetate (Figure 28b, depicted with red upward arrows). Results indicate little to no glucose uptake is observed during lactate utilization, suggesting glucose uptake is deferred until lactate is near depletion. Mqo1, FumC1, and LldD are also associated as part of the pyruvate metabolism (Table VIII). The role of Mqo1 has not yet been determined for *P. aeruginosa*, but Mqo2 is known to be essential for *P. aeruginosa* growth in acetate and ethanol [192].

Other proteins were also upregulated in the biofilms. Upregulated proteins associated with increased biological fitness and virulence [193] include HisA, PA5217, SodA, PvdA, FolE2, and SpeE1 (Table VI). HisA is part of the subpathway for L-histidine biosynthesis [177]. FumC1 with PA5217, SodA, and PvdA are typically induced in iron-deficient conditions that are the hallmark of burn-wound infections [193]. The effect of iron levels plays a role in biofilm formation, in which either too low or too high iron concentrations results in thin or flat biofilm phenotypes [194]. PvdA catalyzes the first step in the biosynthesis of pyoverdine siderophores, a virulence factor which are typically induced under iron-starvation conditions along with exotoxin A and endoproteases [194]. Induction of FolE2 has been found to occur under zinc-deficient conditions [195] in which significant changes in gene expressions have been reported for *P. aeruginosa* survivability and promulgation for zinc homeostasis [195]. SpeE1 catalyzes the synthetic pathway of putrescine to spermidine and it has been found that spermidine functions in protecting bacterial membranes from

antibiotics and oxidative damage [196]. Although spermidine was not measured here, it might be considered a promising target metabolite.

The effect of CCR in *P. aeruginosa* is diverse and impacts various phenotypic changes. Extensive studies have been done on planktonic *P. aeruginosa* metabolite uptake [197] as well as on the translational regulatory protein, catabolite repression control (Crc) and its effect on biofilm development [198], antimicrobial-tolerate subpopulations [199], and quorum sensing regulations [200]. The repression of glucose utilization for the preferred lactate uptake is consistent with the reverse diauxic growth typically found in planktonic *Pseudomonas spp.* studies [151, 197]. Like planktonic cultures, biofilms also display reverse diauxie characteristics with lactate, which lead to the induction of proteins that are typically upregulated under zinc and iron limited conditions. This is expected given the diffusion constraints of biofilms. While reverse diauxie is generally inferred and understood based on planktonic growth, the authors have not been able to identify a prior report of reverse diauxic growth with *P. aeruginosa* biofilms with respect to lactate preference.

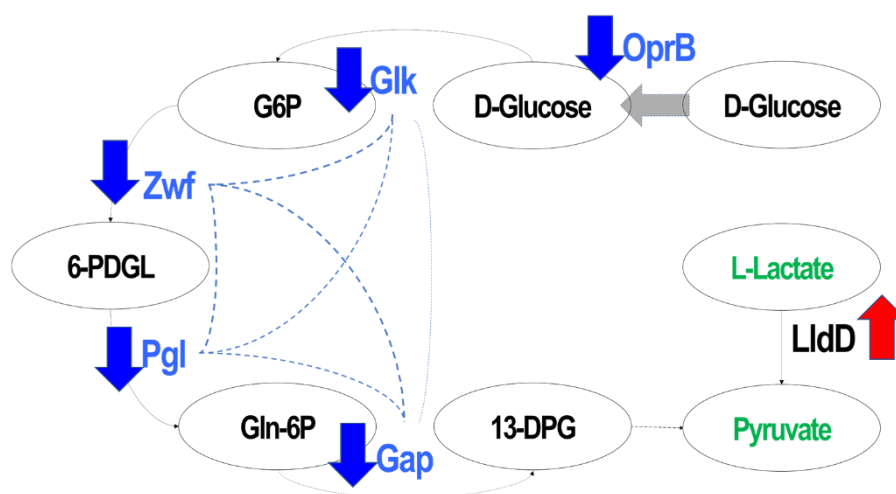
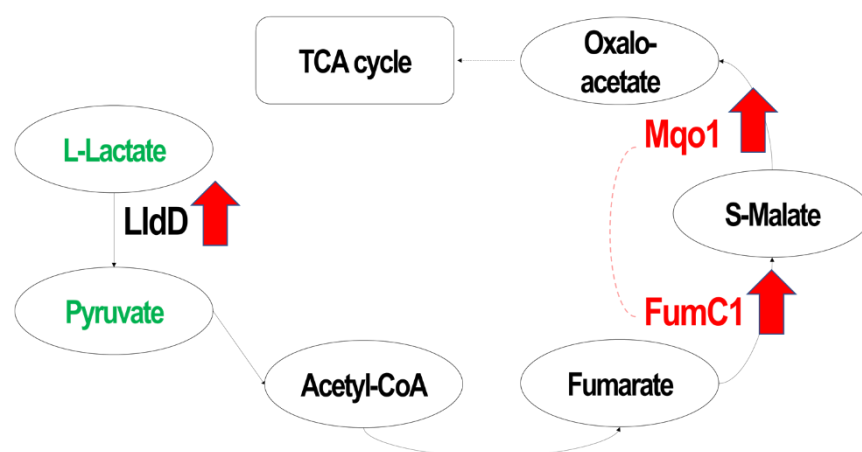
(a) Planktonic**(b) Biofilm**

Figure 28. Schematic of glucose and lactate metabolisms in (a) planktonic and (b) biofilm *P. aeruginosa* cultures. Dashed lines indicate protein-protein associations, where thickness correlates to stronger associations. Upregulated and downregulated proteins are represented by red upward facing arrows and blue downward facing arrows, respectively. (a) Planktonic culture: lactate conversion to pyruvate by LldD is upregulated. Downregulation is observed for proteins, OprB, Glk, Zwf, Pgl, Gap, involved in glucose conversion (see text or Table VI for full protein names). (b) Biofilms: LldD is similarly upregulated. Upregulation is observed for proteins within the citric acid (TCA) cycle: FumC1, in fumarate conversion to S-malate, and Mqo1, in S-malate conversion to oxaloacetate.

6.5 Conclusion

Glucose and lactate are both important carbon sources, but they are utilized in bacterial cultures via a hierarchical order of carbon utilization for growth, maintenance, and sustenance [151]. Nutrient resource allocation influences metabolic networks, where nutrient scarcity acclimation can shift phenotype [152]. Reverse diauxic growth for primary carbon source, lactate, followed by glucose is showcased in metabolomics, resulting in an upregulation of LldD in both planktonic and biofilm *P. aeruginosa* cultures observed by proteomics. LldD upregulation affected metabolisms in planktonic cultures with glucose related repressions and in biofilm cultures with inductions relating to the TCA cycle, pathogenesis, and virulence. Reverse diauxie present in both planktonic and biofilm *P. aeruginosa* clinical isolate (215) are demonstrated here.

Mentioned previously, resource allocation allows bacteria to increase biological fitness and survival [151, 152]. Lactate utilization stimulates metabolism to enhance growth rates and contributes to pathogenesis [158]. The excretion of acetate increased in the presence of lactate, despite the decreased protein expression among glucose and acetate related proteins (data not shown). Cells utilize acetate when nutrients are depleted, a process referred to as the acetate switch [201]. Additionally, planktonic cell densities are greater when grown in the presence of lactate (data not shown). This suggests lactate is a more efficient means for growth and sustenance. In biofilm cultures, iron and zinc mass transfer limitations induce protein expressions for virulence (PvdA) and survivability (FolE2) [194, 195]. With the addition of lactate, these features are induced. Furthermore, under magnesium limitations, spermidine binds to the lipopolysaccharides which stabilize and protect the outer membrane as a defensive mechanism against antibiotics [196]. The addition of lactate induces SpeE1, which is involved in spermidine production.

7. CONCLUSION

Biofilms differ from their planktonic forms as they confer greater resistance to antibiotic or antimicrobial treatments. However, the dynamics of biofilms are not well understood and are of current interest especially since biofilms contribute to prolonged infections in patients with chronic wounds.

Non-imaging and imaging MALDI-MS have been integral in metabolomics and proteomics studies, which has been demonstrated on microbial systems. For untargeted biological studies, the use of a high-resolution mass analyzer is essential for accurate identifications however the FTICR mass spectrometer was decommissioned halting the progression of biofilm studies with UV-AP-MALDI-MS. Biofilm imaging on a vacuum-based MALDI-TOF mass spectrometer was attempted in which some proteins/peptides from the biofilms were detected but remain indeterminate as the instrument did not have tandem MS capability. As demonstrated, sample preparation proved challenging and is not trivial, therefore cryosectioning the biofilms into thinner sections can be an alternative direction for imaging with vacuum MALDI-MS.

The development of a laser-based APPI was intended to study metabolites. LDTD-APPI with a portable handheld 800 nm near-IR laser was developed and compared with LAAPPI. This experimentally simpler configuration of LDTD-APPI was verified for metabolite analyses and can additionally be used for field analyses. Spatially resolved analyses could have been achieved, except for the low sensitivity of the QIT mass spectrometer. Furthermore, the QIT is a low-resolution instrument, which is a major disadvantage for untargeted analyses with LDTD-APPI. Therefore, knowledge of expected or known metabolites might be needed for field analyses.

Nonetheless, QS molecules typically detected in MALDI and ESI studies were also detected with LDTD-APPI. Among these were homoserine lactones, quinolones, and phenazines which are involved bacterial cell signaling. The metabolites detected in this study can serve as a guidance for a more targeted proteome approach which can reveal underlying metabolism changes such as with interspecies interactions.

When it comes to studying complex biological systems, multi-omics are especially needed. While gene modeling is based on genomes, various pathways can lead to the same metabolic results. However, proteomics can help identify a more specific pathway in which the metabolism can occur. The second half of this thesis involved the development of a MS-based proteomics workflow used to study *P. aeruginosa* cultures. This development was utilized with metabolomics as a guidance for changes in metabolism with an additional nutrient source, lactate. Changes in protein abundances between these two conditions indicate a preferential use of different substrates, which in turn suggests shifts in metabolic strategies as a function of nutrient environment. This was first demonstrated in planktonic cultures and then applied to biofilms, in which distinct changes in metabolisms were discovered. The identified proteins with significant expression differentials can be used to target specific metabolites (i.e. spermidine, fumarate, S-malate) in future studies of bacterial pathogenesis.

However, there are caveats to this approach. Cell physiology in planktonic conditions is highly homogenous whereas cells in biofilms are relatively heterogeneous resulting from differences in spatial location within the biofilm, nutrient availability, and exposure to other environmental factors. Because there was no direct method to compare relative growth phases between the two cultures, the same time point was simply used to compare metabolic state. Additionally, the intensity-based quantification method used by the Perseus software relies upon

the sum of peptide ion intensities to determine relative protein abundances. This strategy assumes no differences in protein extraction efficiency from the initial sample preparation as well as uniform ionization efficiencies of different peptide ions in ESI-MS. However, these assumptions may not be that significant to the order of magnitude comparisons of protein expression differentials measured here.

The proteomic strategies described here is now being applied to the study of biofilms and other surface associated microbial communities by application of laser ablation sample transfer (LAST). The mid-infrared pulsed laser in LAST samples proteins from selected small volumes of biofilms for determining spatially resolved phenotypes, additional information not provided from whole cell lysates. LAST brings the high protein coverage of bottom-up LC-MS/MS based proteomics to spatially resolved analysis of bacterial communities as demonstrated from preliminary LAST results. While the bottom-up proteomics strategies employed here do not reveal the posttranslational modifications of proteins known to play an important role in microbial metabolism [180], bottom-up strategies have been described to explore posttranslational modifications [202]. Protein imaging based upon matrix assisted laser desorption ionization MS typically offers much higher lateral resolution than LAST, but can suffer from relatively poor protein coverage and a frequently challenging sample preparation for biofilms and other bacterial communities [27, 59, 203].

In conclusion, *P. aeruginosa* clinical isolate studied here is part of a three species polymicrobial biofilm, along with clinical isolates of methicillin-resistant *S. aureus* and *Clostridium perfringens*, that was initially developed to understand *in vitro* growth of chronic wounds [171]. The proteomic results reported here are now being applied to refining computational metabolic models of multi-species interactions, such as between *P. aeruginosa* and

methicillin-resistant *S. aureus* [187], and eventually with all three species. This will help understand the dynamics and responses to environmental perturbations for the broader impact of devising better therapeutic treatments for chronic wound patients.

CITED LITERATURE

1. Hall-Stoodley, L., Costerton, J.W., and Stoodley, P.: Bacterial biofilms: from the natural environment to infectious diseases. Nat. Rev. Microbiol. 2:95-108, 2004.
2. Burmølle, M., Ren, D., Bjarnsholt, T., and Sørensen, S.J.: Interactions in multispecies biofilms: do they actually matter? Trends Microbiol. 22:84-91, 2014.
3. Flemming, H.-C., Wingender, J., Szewzyk, U., Steinberg, P., Rice, S.A., and Kjelleberg, S.: Biofilms: an emergent form of bacterial life. Nat Rev Micro 14:563-575, 2016.
4. Stoodley, P., Sauer, K., Davies, D.G., and Costerton, J.W.: Biofilms as complex differentiated communities. Annu. Rev. Microbiol. 56:187-209, 2002.
5. Lopez, D., Vlamakis, H., and Kolter, R.: Biofilms. Cold Spring Harb. Perspect. Biol. 2:a000398, 2010.
6. Elias, S. and Banin, E.: Multi-species biofilms: living with friendly neighbors. FEMS Microbiol. Rev. 36:990-1004, 2012.
7. Chen, M., Yu, Q., and Sun, H.: Novel Strategies for the Prevention and Treatment of Biofilm Related Infections. Int. J. Mol. Sci. 14:18488-18501, 2013.
8. Kostakioti, M., Hadjifrangiskou, M., and Hultgren, S., J.: Bacterial biofilms: development, dispersal, and therapeutic strategies in the dawn of the postantibiotic era. Cold Spring Harb. Perspect. Biol. 3:a010306, 2013.
9. Heeb, S., Fletcher, M.P., Chhabra, S.R., Diggle, S.P., Williams, P., and Cámara, M.: Quinolones: from antibiotics to autoinducers. FEMS Microbiol. Rev. 35:247-274, 2011.
10. Corona, F. and Martinez, J.: Phenotypic resistance to antibiotics. Antibiotics 2:237, 2013.
11. Amato, S., Fazen, C., Henry, T., Mok, W., Orman, M., Sandvik, E., Volzing, K., and Brynildsen, M.: The role of metabolism in bacterial persistence. Front. Microbiol. 5 2014.

12. Rodrigue, A., Quentin, Y., Lazdunski, A., Méjean, V., and Foglino, M.: Cell signalling by oligosaccharides. Two-component systems in *Pseudomonas aeruginosa*: why so many? Trends Microbiol. 8:498-504, 2000.
13. Mikkelsen, H., Sivaneson, M., and Filloux, A.: Key two-component regulatory systems that control biofilm formation in *Pseudomonas aeruginosa*. Environ. Microbiol. 13:1666-1681, 2011.
14. Green, J.-B.D., Fulghum, T., and Nordhaus, M.A.: Review of immobilized antimicrobial agents and methods for testing. Biointerphases 6:MR13-MR28, 2011.
15. Aydin Sevinc, B. and Hanley, L.: Antibacterial activity of dental composites containing zinc oxide nanoparticles. J. Biomed. Mater. Res. Part B 94B:22-31, 2010.
16. Feng, G., Cheng, Y., Wang, S.-Y., Borca-Tasciuc, D.A., Worobo, R.W., and Moraru, C.I.: Bacterial attachment and biofilm formation on surfaces are reduced by small-diameter nanoscale pores: how small is small enough? npj Biofilms and Microbiomes 1:15022, 2015.
17. Azeredo, J., Azevedo, N.F., Briandet, R., Cerca, N., Coenye, T., Costa, A.R., Desvaux, M., Di Bonaventura, G., Hébraud, M., Jaglic, Z., Kačániová, M., Knöchel, S., Lourenço, A., Mergulhão, F., Meyer, R.L., Nychas, G., Simões, M., Tresse, O., and Sternberg, C.: Critical review on biofilm methods. Crit. Rev. Microbiol. 43:313-351, 2017.
18. Merritt, J.H., Kadouri, D.E., and O'toole, G.A.: Growing and analyzing static biofilms. Curr. Protoc. Microbiol. 0 1:Unit-1B.1, 2005.
19. Denkhaus, E., Meisen, S., Telgheder, U., and Wingender, J.: Chemical and physical methods for characterization of biofilms. Mikrochim. Acta 158:1-27, 2007.
20. Spengler, B.: Mass Spectrometry Imaging of Biomolecular Information. Anal. Chem. 87:64-82, 2015.
21. Moore, J.L., Caprioli, R.M., and Skaar, E.P.: Advanced mass spectrometry technologies for the study of microbial pathogenesis. Curr. Opin. Microbiol. 19:45-51, 2014.
22. Bhardwaj, C. and Hanley, L.: Ion sources for mass spectrometric identification and imaging of molecular species Nat. Prod. Rep. 31:756-767, 2014.

23. Banerjee, S. and Mazumdar, S.: Electrospray ionization mass spectrometry: a technique to access the information beyond the molecular weight of the analyte. Int. J. Anal. Chem. 2012:1-40, 2012.
24. Losensky, G., Jung, K., Urlaub, H., Pfeifer, F., Fröls, S., and Lenz, C.: Shedding light on biofilm formation of *Halobacterium salinarum* R1 by SWATH-LC/MS/MS analysis of planktonic and sessile cells. Proteomics 17:1600111, 2017.
25. Moree, W.J., Phelan, V.V., Wu, C.-H., Bandeira, N., Cornett, D.S., Duggan, B.M., and Dorrestein, P.C.: Interkingdom metabolic transformations captured by microbial imaging mass spectrometry. Proc. Natl. Acad. Sci. U. S. A. 109:13811-13816, 2012.
26. Yang, Y.L., Xu, Y., Straight, P., and Dorrestein, P.C.: Translating metabolic exchange with imaging mass spectrometry. Nat. Chem. Biol. 5:885-887, 2009.
27. Blaze M.T., M., Aydin, B., Carlson, R.P., and Hanley, L.: Identification and imaging of peptides and proteins on *Enterococcus faecalis* biofilms by matrix assisted laser desorption ionization mass spectrometry. Analyst 137:5018-5025, 2012.
28. Bhardwaj, C., Moore, J.F., Gasper, G., Cui, Y., Bernstein, H., Carlson, R.P., and Hanley, L. *Imaging bacterial biofilms using laser desorption postionization mass spectroscopy: comparing 10.5 eV to 7.87 eV photoionization.* in *ASMS 59th Conf. on Mass Spectrom. Allied Topics*. 2011. Denver: ASMS.
29. Graham, R.L., Graham, C., and McMullan, G.: Microbial proteomics: a mass spectrometry primer for biologists. Microb. Cell. Fact. 6:1-14, 2007.
30. Russo, R.E., Mao, X., Gonzalez, J.J., Zorba, V., and Yoo, J.: Laser ablation in analytical chemistry. Anal. Chem. 85:6162-6177, 2013.
31. Flanigan, P. and Levis, R.: Ambient femtosecond laser vaporization and nanosecond laser desorption electrospray ionization mass spectrometry. Annu. Rev. Anal. Chem. 7:229-256, 2014.
32. Gessel, M.M., Norris, J.L., and Caprioli, R.M.: MALDI imaging mass spectrometry: spatial molecular analysis to enable a new age of discovery. J. Proteomics 107:71-82, 2014.

33. Nilsson, A., Goodwin, R.J.A., Shariatgorji, M., Vallianatou, T., Webborn, P.J.H., and Andrén, P.E.: Mass spectrometry imaging in drug development. Anal. Chem. 87:1437-1455, 2015.
34. Koch, J. and Gunther, D.: Review of the state-of-the-art of laser ablation inductively coupled plasma mass spectrometry. Appl. Spectrosc. 65:155A-162A, 2011.
35. Becker, J.S.: Imaging of metals in biological tissue by laser ablation inductively coupled plasma mass spectrometry (LA-ICP-MS): state of the art and future developments. J. Mass Spectrom. 48:255-268, 2013.
36. Limbeck, A., Galler, P., Bonta, M., Bauer, G., Nischkauer, W., and Vanhaecke, F.: Recent advances in quantitative LA-ICP-MS analysis: challenges and solutions in the life sciences and environmental chemistry. Anal. Bioanal. Chem. 407:6593-6617, 2015.
37. Cui, Y., Moore, J.F., Milasinovic, S., Liu, Y., Gordon, R.J., and Hanley, L.: Depth profiling and imaging capabilities of an ultrashort pulse laser ablation time of flight mass spectrometer. Rev. Sci. Instrum. 83:093702, 2012.
38. Zhang, B., He, M., Hang, W., and Huang, B.: Minimizing matrix effect by femtosecond laser ablation and ionization in elemental determination. Anal. Chem. 85:4507-4511, 2013.
39. Moreno-García, P., Grimaudo, V., Riedo, A., Tulej, M., Wurz, P., and Broekmann, P.: Towards matrix-free femtosecond-laser desorption mass spectrometry for in situ space research. Rapid Commun. Mass Spectrom. 30:1031-1036, 2016.
40. Gao, Y., Lin, Y., Zhang, B., Zou, D., He, M., Dong, B., Hang, W., and Huang, B.: Single-cell elemental analysis via high irradiance femtosecond laser ionization time-of-flight mass spectrometry. Anal. Chem. 85:4268-4272, 2013.
41. Grimaudo, V., Moreno-García, P., Riedo, A., Neuland, M.B., Tulej, M., Broekmann, P., and Wurz, P.: High-resolution chemical depth profiling of solid material using a miniature laser ablation/ionization mass spectrometer. Anal. Chem. 87:2037-2041, 2015.
42. Dreisewerd, K.: Recent methodological advances in MALDI mass spectrometry. Anal. Bioanal. Chem. 406:2261-2278, 2014.

43. Fuchs, B. and Schiller, J.: Application of MALDI-TOF mass spectrometry in lipidomics. Eur. J. Lipid Sci. Technol. 111:83-98, 2009.
44. Duncan, M.W., Nedelkov, D., Walsh, R., and Hattan, S.J.: Applications of MALDI mass spectrometry in clinical chemistry. Clin. Chem. 62:134-143, 2016.
45. Charles, L.: MALDI of synthetic polymers with labile end-groups. Mass Spectrom. Rev. 33:523-543, 2014.
46. Zhang, J., Ellis, H., Yang, L., Johansson, E.M.J., Boschloo, G., Vlachopoulos, N., Hagfeldt, A., Bergquist, J., and Shevchenko, D.: Matrix-assisted laser desorption/ionization mass spectrometric analysis of poly(3,4-ethylenedioxythiophene) in solid-state dye-sensitized solar cells: comparison of in situ photoelectrochemical polymerization in aqueous micellar and organic media. Anal. Chem. 87:3942-3948, 2015.
47. Laiko, V.V., Moyer, S.C., and Cotter, R.J.: Atmospheric pressure MALDI/ion trap mass spectrometry. Anal. Chem. 72:5239-5243, 2000.
48. Schneider, B.B., Lock, C., and Covey, T.R.: AP and vacuum MALDI on a QqLIT instrument. J. Am. Soc. Mass Spectrom. 16:176-182, 2005.
49. De Hoffmann, E. and Stroobant, V.: Mass Spectrometry: Principles and Applications, 3rd Edition. Wiley-Interscience, 2007.
50. Hoffmann, T. and Dorrestein, P.: Homogeneous Matrix Deposition on Dried Agar for MALDI Imaging Mass Spectrometry of Microbial Cultures. J. Am. Soc. Mass Spectrom. 26:1959-1962, 2015.
51. Toh-Boyo, G.M., Wulff, S.S., and Basile, F.: Comparison of sample preparation methods and evaluation of intra- and intersample reproducibility in bacteria MALDI-MS profiling. Anal. Chem. 84:9971-9980, 2012.
52. Liu, X. and Hummon, A.B.: Mass spectrometry imaging of therapeutics from animal models to three-dimensional cell cultures. Anal. Chem. 87:9508-9519, 2015.
53. Schwamborn, K. and Caprioli, R.M.: Molecular imaging by mass spectrometry — looking beyond classical histology. Nat. Rev. Cancer 10:639-646, 2010.

54. Weaver, E.M. and Hummon, A.B.: Imaging mass spectrometry: from tissue sections to cell cultures. Adv. Drug Delivery Rev. 65:1039-1055, 2013.
55. Caprioli, R.M.: Imaging mass spectrometry: enabling a new age of discovery in biology and medicine through molecular microscopy. J. Am. Soc. Mass Spectrom. 26:850-852, 2015.
56. Zavalin, A., Todd, E.M., Rawhouser, P.D., Yang, J., Norris, J.L., and Caprioli, R.M.: Direct imaging of single cells and tissue at sub-cellular spatial resolution using transmission geometry MALDI MS. J. Mass Spectrom. 47:1473-1481, 2012.
57. Zavalin, A., Yang, J., Hayden, K., Vestal, M., and Caprioli, R.: Tissue protein imaging at 1 μ m laser spot diameter for high spatial resolution and high imaging speed using transmission geometry MALDI TOF MS. Anal. Bioanal. Chem. 407:2337-2342, 2015.
58. Li, H. and Hummon, A.B.: Imaging mass spectrometry of three-dimensional cell culture systems. Anal. Chem. 83:8794-8801, 2011.
59. Spraggins, J.M., Rizzo, D.G., Moore, J.L., Rose, K.L., Hammer, N.D., Skaar, E.P., and Caprioli, R.M.: MALDI FTICR IMS of intact proteins: using mass accuracy to link protein images with proteomics data. J. Am. Soc. Mass Spectrom. 26:974-985, 2015.
60. Buck, A., Balluff, B., Voss, A., Langer, R., Zitzelsberger, H., Aichler, M., and Walch, A.: How suitable is matrix-assisted laser desorption/ionization-time-of-flight for metabolite imaging from clinical formalin-fixed and paraffin-embedded tissue samples in comparison to matrix-assisted laser desorption/ionization-Fourier transform ion cyclotron resonance mass spectrometry? Anal. Chem. 88:5281-5289, 2016.
61. Havlicek, V., Lemr, K., and Schug, K.A.: Current trends in microbial diagnostics based on mass spectrometry. Anal. Chem. 85:790-797, 2012.
62. Clark, A.E., Kaleta, E.J., Arora, A., and Wolk, D.M.: Matrix-assisted laser desorption ionization-time of flight mass spectrometry: a fundamental shift in the routine practice of clinical microbiology. Clin. Microbiol. Rev. 26:547-603, 2013.
63. Sandrin, T.R., Goldstein, J.E., and Schumaker, S.: MALDI TOF MS profiling of bacteria at the strain level: a review. Mass Spectrom. Rev. 32:188-217, 2013.

64. Fenselau, C.: Rapid characterization of microorganisms by mass spectrometry—what can be learned and how? J. Am. Soc. Mass Spectrom. 24:1161-1166, 2013.
65. Alves, L.a.C., Souza, R.C., Da Silva, T.M.C., Watanabe, A., Dias, M., Mendes, M.A., and Ciamponi, A.L.: Identification of microorganisms in biofluids of individuals with periodontitis and chronic kidney disease using matrix-assisted laser desorption/ionization time-of-flight mass spectrometry. Rapid Commun. Mass Spectrom. 30:1228-1232, 2016.
66. Fleurbaaij, F., Kraakman, M.E.M., Claas, E.C.J., Knetsch, C.W., Van Leeuwen, H.C., Van Der Burgt, Y.E.M., Veldkamp, K.E., Vos, M.C., Goessens, W., Mertens, B.J., Kuijper, E.J., Hensbergen, P.J., and Nicolardi, S.: Typing *Pseudomonas aeruginosa* isolates with ultrahigh resolution MALDI-FTICR mass spectrometry. Anal. Chem. 88:5996-6003, 2016.
67. Hohmann, S., Neidig, A., Kühl, B., Kirschhöfer, F., Overhage, J., and Brenner-Weiß, G.: A new data processing routine facilitating the identification of surface adhered proteins from bacterial conditioning films via QCM-D/MALDI-ToF/MS. Anal. Bioanal. Chem. 409:5965-5974, 2017.
68. Yang, J.Y., Phelan, V.V., Simkovsky, R., Watrous, J.D., Trial, R.M., Fleming, T.C., Wenter, R., Moore, B.S., Golden, S.S., Pogliano, K., and Dorrestein, P.C.: Primer on Agar-Based Microbial Imaging Mass Spectrometry. J. Bacteriol. 194:6023-6028, 2012.
69. Phelan, V., Fang, J., and Dorrestein, P.: Mass spectrometry analysis of *Pseudomonas aeruginosa* treated with azithromycin. J. Am. Soc. Mass Spectrom. 26:873-877, 2015.
70. Lanni, E.J., Masyuko, R.N., Driscoll, C.M., Dunham, S.J.B., Shrout, J.D., Bohn, P.W., and Sweedler, J.V.: Correlated imaging with C60-SIMS and confocal raman microscopy: visualization of cell-scale molecular distributions in bacterial biofilms. Anal. Chem. 86:10885-10891, 2014.
71. Leipert, J., Treitz, C., Leippe, M., and Tholey, A.: Identification and quantification of N-acyl homoserine lactones involved in bacterial communication by small-scale synthesis of internal standards and matrix-assisted laser desorption/ionization mass spectrometry. J. Am. Soc. Mass Spectrom. 28:2538-2547, 2017.
72. Kim, Y.-W., Sung, C., Lee, S., Kim, K.-J., Yang, Y.-H., Kim, B.-G., Lee, Y.K., Ryu, H.W., and Kim, Y.-G.: MALDI-MS-Based quantitative analysis for ketone containing momoserine lactones in *Pseudomonas aeruginosa*. Anal. Chem. 87:858-863, 2015.

73. Wakeman, C.A., Moore, J.L., Noto, M.J., Zhang, Y., Singleton, M.D., Prentice, B.M., Gilston, B.A., Doster, R.S., Gaddy, J.A., Chazin, W.J., Caprioli, R.M., and Skaar, E.P.: The innate immune protein calprotectin promotes *Pseudomonas aeruginosa* and *Staphylococcus aureus* interaction. Nat. Commun. 7:11951, 2016.
74. Wang, R.-Q., Druckenmüller, K., Elbers, G., Guenther, K., and Croué, J.-P.: Analysis of aquatic-phase natural organic matter by optimized LDI-MS method. J. Mass Spectrom. 49:154-160, 2014.
75. Jaschinski, T., Helfrich, E.J.N., Bock, C., Wolfram, S., Svatoš, A., Hertweck, C., and Pohnert, G.: Matrix-free single-cell LDI-MS investigations of the diatoms *Coscinodiscus granii* and *Thalassiosira pseudonana*. J. Mass Spectrom. 49:136-144, 2014.
76. Pirkel, A., Meier, M., Popkova, Y., Letzel, M., Schnapp, A., Schiller, J., and Dreisewerd, K.: Analysis of free fatty acids by ultraviolet laser desorption ionization mass spectrometry using insect wings as hydrophobic sample substrates. Anal. Chem. 86:10763-10771, 2014.
77. Stolee, J.A., Walker, B.N., Zorba, V., Russo, R.E., and Vertes, A.: Laser-nanostructure interactions for ion production. PCCP 14:8453-8471, 2012.
78. Hanley, L. and Zimmermann, R.: Light and molecular ions: the emergence of vacuum UV single-photon ionization in MS. Anal. Chem. 81:4174-4182, 2009.
79. Pan, Y., Yin, H., Zhang, T., Guo, H., Sheng, L., and Qi, F.: The characterization of selected drugs with infrared laser desorption/tunable synchrotron vacuum ultraviolet photoionization mass spectrometry. Rapid Commun. Mass Spectrom. 22:2515-2520, 2008.
80. Sabbah, H., Morrow, A.L., Pomerantz, A.E., and Zare, R.N.: Evidence for island structures as the dominant architecture of asphaltenes. Energy Fuels 25:1597-1604, 2011.
81. Bhardwaj, C., Cui, Y., Hofstetter, T., Liu, S.Y., Bernstein, H.C., Carlson, R.P., Ahmed, M., and Hanley, L.: Differentiation of microbial species and strains in coculture biofilms by multivariate analysis of laser desorption postionization mass spectra. Analyst 138:6844-6851, 2013.
82. Akhmetov, A., Moore, J.F., Gasper, G.L., Koin, P.J., and Hanley, L.: Laser desorption postionization for imaging MS of biological material. J. Mass Spectrom. 45:137-145, 2010.

83. Bhardwaj, C., Moore, J.F., Cui, Y., Gasper, G.L., Bernstein, H.C., Carlson, R.P., and Hanley, L.: Laser desorption VUV postionization MS imaging of a cocultured biofilm. Anal. Bioanal. Chem. 405:6969-6977, 2013.
84. Cui, Y., Bhardwaj, C., Milasinovic, S., Carlson, R.P., Gordon, R.J., and Hanley, L.: Molecular imaging and depth profiling of biomaterials interfaces by femtosecond laser desorption postionization mass spectrometry. ACS Appl. Mater. Interfaces 5:9269-9275, 2013.
85. Cui, Y., Veryovkin, I.V., Majeski, M.W., Cavazos, D.R., and Hanley, L.: High lateral resolution vs. molecular preservation in near-IR fs-laser desorption postionization mass spectrometry. Anal. Chem. 87:367-371, 2015.
86. Kauppila, T.J., Östman, P., Marttila, S., Ketola, R.A., Kotiaho, T., Franssila, S., and Kostiainen, R.: Atmospheric pressure photoionization-mass spectrometry with a microchip heated nebulizer. Anal. Chem. 76:6797-6801, 2004.
87. Kauppila, T.J., Kuuranne, T., Meurer, E.C., Eberlin, M.N., Kotiaho, T., and Kostiainen, R.: Atmospheric pressure photoionization mass spectrometry. Ionization mechanism and the effect of solvent on the ionization of naphthalenes. Anal. Chem. 74:5470-5479, 2002.
88. Vaikkinen, A., Shrestha, B., Kauppila, T.J., Vertes, A., and Kostiainen, R.: Infrared laser ablation atmospheric pressure photoionization mass spectrometry. Anal. Chem. 84:1630-1636, 2012.
89. Vaikkinen, A., Shrestha, B., Koivisto, J., Kostiainen, R., Vertes, A., and Kauppila, T.J.: Laser ablation atmospheric pressure photoionization mass spectrometry imaging of phytochemicals from sage leaves. Rapid Commun. Mass Spectrom. 28:2490-2496, 2014.
90. Wu, Q. and Zare, R.N.: Laser desorption lamp ionization source for ion trap mass spectrometry. J. Mass Spectrom. 50:160-164, 2015.
91. Peng, I.X., Ogorzalek Loo, R.R., Margalith, E., Little, M.W., and Loo, J.A.: Electrospray-assisted laser desorption ionization mass spectrometry (ELDI-MS) with an infrared laser for characterizing peptides and proteins. The Analyst 135:767-772, 2010.
92. Berisha, A., Dold, S., Guenther, S., Desbenoit, N., Takats, Z., Spengler, B., and Römpf, A.: A comprehensive high-resolution mass spectrometry approach for characterization of metabolites by combination of ambient ionization, chromatography and imaging methods. Rapid Commun. Mass Spectrom. 28:1779-1791, 2014.

93. Robichaud, G., Barry, J., and Muddiman, D.: IR-MALDESI mass spectrometry imaging of biological tissue sections using ice as a matrix. J. Am. Soc. Mass Spectrom. 25:319-328, 2014.
94. Cochran, K., Barry, J., Robichaud, G., and Muddiman, D.: Analysis of trace fibers by IR-MALDESI imaging coupled with high resolving power MS. Anal. Bioanal. Chem. 407:813-820, 2015.
95. Nazari, M. and Muddiman, D.: Cellular-level mass spectrometry imaging using infrared matrix-assisted laser desorption electrospray ionization (IR-MALDESI) by oversampling. Anal. Bioanal. Chem. 407:2265-2271, 2015.
96. Bokhart, M., Rosen, E., Thompson, C., Sykes, C., Kashuba, A.M., and Muddiman, D.: Quantitative mass spectrometry imaging of emtricitabine in cervical tissue model using infrared matrix-assisted laser desorption electrospray ionization. Anal. Bioanal. Chem. 407:2073-2084, 2015.
97. Li, H., Balan, P., and Vertes, A.: Molecular imaging of growth, metabolism, and antibiotic inhibition in bacterial colonies by laser ablation electrospray ionization mass spectrometry. Angew. Chem. Int. Ed. 55:15035-15039, 2016.
98. Donnarumma, F. and Murray, K.K.: Laser ablation sample transfer for localized LC-MS/MS proteomic analysis of tissue. J. Mass Spectrom. 51:261-268, 2016.
99. Donnarumma, F., Cao, F., and Murray, K.: Laser ablation with vacuum capture for MALDI mass spectrometry of tissue. J. Am. Soc. Mass Spectrom. 27:108-116, 2016.
100. Wang, K., Donnarumma, F., Herke, S.W., Herke, P.F., and Murray, K.K.: Infrared laser ablation sample transfer of tissue DNA for genomic analysis. Anal. Bioanal. Chem. 409:4119-4126, 2017.
101. Donnarumma, F., Camp, E.E., Cao, F., and Murray, K.K.: Infrared laser ablation with vacuum Capture for fingerprint sampling. J. Am. Soc. Mass Spectrom. 28:1958-1964, 2017.
102. Hayes, J.M. and Murray, K.K.: Ambient laser ablation sample transfer with nanostructure-assisted laser desorption ionization mass spectrometry for bacteria analysis. Rapid Commun. Mass Spectrom. 28:2382-2384, 2014.

103. Brauer, J., Beech, I., and Sunner, J.: Mass spectrometric imaging using laser ablation and solvent capture by aspiration (LASCA). J. Am. Soc. Mass Spectrom. 26:1538-1547, 2015.
104. Ghorai, S., Seneviratne, C.A., and Murray, K.K.: Tip-enhanced laser ablation sample transfer for biomolecule mass spectrometry. J. Am. Soc. Mass Spectrom. 26:63-70, 2015.
105. Watrous, J.D. and Dorrestein, P.C.: Imaging mass spectrometry in microbiology. Nat. Rev. Microbiol. 9:683-694, 2011.
106. Li, B., Comi, T.J., Si, T., Dunham, S.J.B., and Sweedler, J.V.: A one-step matrix application method for MALDI mass spectrometry imaging of bacterial colony biofilms. J. Mass Spectrom. 51:1030-1035, 2016.
107. Pereira, F.D.E.S., Bonatto, C.C., Lopes, C.a.P., Pereira, A.L., and Silva, L.P.: Use of MALDI-TOF mass spectrometry to analyze the molecular profile of *Pseudomonas aeruginosa* biofilms grown on glass and plastic surfaces. Microb. Pathog. 86:32-37, 2015.
108. Van Berkel, G., J., Pasilis Sofie, P., and Ovchinnikova, O.: Established and emerging atmospheric pressure surface sampling/ionization techniques for mass spectrometry. J. Mass Spectrom. 43:1161-1180, 2008.
109. Harris, G.A., Galhena, A.S., and Fernández, F.M.: Ambient sampling/ionization mass spectrometry: applications and current trends. Anal. Chem. 83:4508-4538, 2011.
110. Misharin, A., Novoselov, K., Laiko, V., and Doroshenko, V.M.: Development and characterization of a field-deployable ion-trap mass spectrometer with an atmospheric pressure interface. Anal. Chem. 84:10105-10112, 2012.
111. Fang, J. and Dorrestein, P.C.: Emerging mass spectrometry techniques for the direct analysis of microbial colonies. Curr. Opin. Microbiol. 19:120-129, 2014.
112. Lanni, E.J., Masyuko, R.N., Driscoll, C.M., Aerts, J.T., Shrout, J.D., Bohn, P.W., and Sweedler, J.V.: MALDI-guided SIMS: multiscale imaging of metabolites in bacterial biofilms. Anal. Chem. 86:9139-9145, 2014.

113. Dunham, S.J.B., Comi, T.J., Ko, K., Li, B., Baig, N.F., Morales-Soto, N., Shrout, J.D., Bohn, P.W., and Sweedler, J.V.: Metal-assisted polyatomic SIMS and laser desorption/ionization for enhanced small molecule imaging of bacterial biofilms. Biointerphases 11:02A325, 2016.
114. Caldwell, R.L. and Caprioli, R.M.: Tissue profiling by mass spectrometry: a review of methodology and applications. Mol. Cell. Proteomics 4:394-401, 2005.
115. Walch, A., Rauser, S., Deininger, S.-O., and Höfler, H.: MALDI imaging mass spectrometry for direct tissue analysis: a new frontier for molecular histology. Histochem. Cell Biol. 130:421-434, 2008.
116. Snyder, D.T., Pulliam, C.J., Ouyang, Z., and Cooks, R.G.: Miniature and fieldable mass spectrometers: recent advances. Anal. Chem. 88:2-29, 2016.
117. Lancaster, C. and Espinoza, E.: Analysis of select *Dalbergia* and trade timber using direct analysis in real time and time-of-flight mass spectrometry for CITES enforcement. Rapid Commun. Mass Spectrom. 26:1147-1156, 2012.
118. Pavarini, D.P., Da Silva, D.B., Carollo, C.A., Portella, A.P.F., Latansio-Aidar, S.R., Cavalin, P.O., Oliveira, V.C., Rosado, B.H.P., Aidar, M.P.M., Bolzani, V.S., Lopes, N.P., and Joly, C.A.: Application of MALDI-MS analysis of rainforest chemodiversity: a keystone for biodiversity conservation and sustainable use. J. Mass Spectrom. 47:1482-1485, 2012.
119. Leefmann, T., Heim, C., Siljeström, S., Blumenberg, M., Sjövall, P., and Thiel, V.: Spectral characterization of ten cyclic lipids using time-of-flight secondary ion mass spectrometry. Rapid Commun. Mass Spectrom. 27:565-581, 2013.
120. Sumner, D.Y., Hawes, I., Mackey, T.J., Jungblut, A.D., and Doran, P.T.: Antarctic microbial mats: a modern analog for Archean lacustrine oxygen oases. Geology 43:887-890, 2015.
121. Vertes, A., Hitchins, V., and Phillips, K.S.: Analytical challenges of microbial biofilms on medical devices. Anal. Chem. 84:3858-3866, 2012.
122. Ifa, D.R., Wu, C., Ouyang, Z., and Cooks, R.G.: Desorption electrospray ionization and other ambient ionization methods: current progress and preview. Analyst 135:669-681, 2010.

123. Mulligan, C.C., Talaty, N., and Cooks, R.G.: Desorption electrospray ionization with a portable mass spectrometer: *in situ* analysis of ambient surfaces. Chem. Commun. 0:1709-1711, 2006.
124. Keil, A., Talaty, N., Janfelt, C., Noll, R.J., Gao, L., Ouyang, Z., and Cooks, R.G.: Ambient mass spectrometry with a handheld mass spectrometer at high pressure. Anal. Chem. 79:7734-7739, 2007.
125. Hendricks, P.I., Dalgleish, J.K., Shelley, J.T., Kirleis, M.A., McNicholas, M.T., Li, L., Chen, T.-C., Chen, C.-H., Duncan, J.S., Boudreau, F., Noll, R.J., Denton, J.P., Roach, T.A., Ouyang, Z., and Cooks, R.G.: Autonomous in situ analysis and real-time chemical detection using a backpack miniature mass spectrometer: concept, instrumentation development, and performance. Anal. Chem. 86:2900-2908, 2014.
126. Salter, T.L.R., Bunch, J., and Gilmore, I.S.: Importance of sample form and surface temperature for analysis by ambient plasma mass spectrometry (PADI). Anal. Chem. 86:9264-9270, 2014.
127. Wiley, J.S., Shelley, J.T., and Cooks, R.G.: Handheld low-temperature plasma probe for portable “point-and-shoot” ambient ionization mass spectrometry. Anal. Chem. 85:6545-6552, 2013.
128. Albert, A., Shelley, J., and Engelhard, C.: Plasma-based ambient desorption/ionization mass spectrometry: state-of-the-art in qualitative and quantitative analysis. Anal. Bioanal. Chem. 406:6111-6127, 2014.
129. Nemes, P., Barton, A.A., Li, Y., and Vertes, A.: Ambient molecular imaging and depth profiling of live tissue by infrared laser ablation electrospray ionization mass spectrometry. Anal. Chem. 80:4575-4582, 2008.
130. Wu, J., Hughes, C.S., Picard, P., Letarte, S., Gaudreault, M., Lévesque, J.-F., Nicoll-Griffith, D.A., and Bateman, K.P.: High-throughput cytochrome P450 inhibition assays using laser diode thermal desorption-atmospheric pressure chemical ionization-tandem mass spectrometry. Anal. Chem. 79:4657-4665, 2007.
131. Yung, Y.P., Veryovkin, I.V., Cui, Y., and Hanley, L. *Atmospheric pressure photoionization with and without laser ablation on a portable ion trap mass spectrometer.* in *63rd ASMS Conf. on Mass Spectrom. & Allied Topics*. 2015. America's Center, St. Louis, Missouri.

132. Robb, D.B., Covey, T.R., and Bruins, A.P.: Atmospheric pressure photoionization: an ionization method for liquid chromatography–mass spectrometry. Anal. Chem. 72:3653-3659, 2000.
133. Blaze M.T., M., Takahashi, L.K., Zhou, J., Ahmed, M., Gasper, G.L., Pleticha, F.D., and Hanley, L.: Brominated tyrosine and polyelectrolyte multilayer analysis by laser desorption VUV postionization and secondary ion mass spectrometry. Anal. Chem. 83:4962-4969, 2011.
134. Santos-Gomes, P.C. and Fernandes-Ferreira, M.: Organ- and season-dependent variation in the essential oil composition of *Salvia officinalis* L. cultivated at two different sites. J. Agric. Food Chem. 49:2908-2916, 2001.
135. Lépine, F., Milot, S., Déziel, E., He, J., and Rahme, L.G.: Electrospray/mass spectrometric identification and analysis of 4-hydroxy-2-alkylquinolines (HAQs) produced by *Pseudomonas aeruginosa*. J. Am. Soc. Mass Spectrom. 15:862-869, 2004.
136. Cui, Y., Frey, R.L., Ferry, J.L., and Ferguson, P.L.: Identification of hydroxyl radical oxidation products of N-hexanoyl-homoserine lactone by reversed-phase high-performance liquid chromatography coupled with electrospray ionization tandem mass spectrometry. Rapid Commun. Mass Spectrom. 23:1212-1220, 2009.
137. De Kievit, T.R.: Quorum sensing in *Pseudomonas aeruginosa* biofilms. Environ. Microbiol. 11:279-288, 2009.
138. Chen, Z. and Vertes, A.: Early plume expansion in atmospheric pressure midinfrared laser ablation of water-rich targets. Phys. Rev. E 77:036316, 2008.
139. Luosujärvi, L., Arvola, V., Haapala, M., Poï• L, J., Saarela, V., Franssila, S., Kotiaho, T., Kostianen, R., and Kauppila, T.J.: Desorption and ionization mechanisms in desorption atmospheric pressure photoionization. Anal. Chem. 80:7460-7466, 2008.
140. Mckay, K., Salter, T., Bowfield, A., Walsh, J., Gilmore, I., and Bradley, J.: Comparison of three plasma sources for ambient desorption/ionization mass spectrometry. J. Am. Soc. Mass Spectrom. 25:1528-1537, 2014.
141. Kirker, K.R. and James, G.A.: *In vitro* studies evaluating the effects of biofilms on wound-healing cells: a review. APMIS 125:344-352, 2017.

142. Nussbaum, S.R., Carter, M.J., Fife, C.E., Davanzo, J., Haught, R., Nusgart, M., and Cartwright, D.: An economic evaluation of the impact, cost, and medicare policy implications of chronic nonhealing wounds. Value Health 21:27-32, 2018.
143. Frykberg, R.G. and Banks, J.: Challenges in the treatment of chronic wounds. Adv. Wound Care 4:560-582, 2015.
144. Serra, R., Grande, R., Butrico, L., Rossi, A., Settimio, U.F., Caroleo, B., Amato, B., Gallelli, L., and De Franciscis, S.: Chronic wound infections: the role of *Pseudomonas aeruginosa* and *Staphylococcus aureus*. Expert Rev. Anti Infect. Ther. 13:605-613, 2015.
145. Omar, A., Wright, J., Schultz, G., Burrell, R., and Nadworny, P.: Microbial biofilms and chronic wounds. Microorganisms 5:1-9, 2017.
146. Ollero, M., Brouillard, F., and Edelman, A.: Cystic fibrosis enters the proteomics scene: new answers to old questions. Proteomics 6:4084-4099, 2006.
147. Tolker-Nielsen, T.: *Pseudomonas aeruginosa* biofilm infections: from molecular biofilm biology to new treatment possibilities. APMIS 122:1-51, 2014.
148. Sriramulu, D.D., Nimtz, M., and Romling, U.: Proteome analysis reveals adaptation of *Pseudomonas aeruginosa* to the cystic fibrosis lung environment. Proteomics 5:3712-3721, 2005.
149. Eberl, L. and Riedel, K.: Mining quorum sensing regulated proteins – role of bacterial cell-to-cell communication in global gene regulation as assessed by proteomics. Proteomics 11:3070-3085, 2011.
150. Lee, C.K., De Anda, J., Baker, A.E., Bennett, R.R., Luo, Y., Lee, E.Y., Keefe, J.A., Helali, J.S., Ma, J., Zhao, K., Golestanian, R., O'toole, G.A., and Wong, G.C.L.: Multigenerational memory and adaptive adhesion in early bacterial biofilm communities. Proc. Natl. Acad. Sci. U. S. A. 2018.
151. Rojo, F.: Carbon catabolite repression in *Pseudomonas* : optimizing metabolic versatility and interactions with the environment. FEMS Microbiol. Rev. 34:658-684, 2010.

152. Carlson, R.P., Beck, A.E., Phalak, P., Fields, M.W., Gedeon, T., Hanley, L., Harcombe, W.R., Henson, M.A., and Heys, J.J.: Competitive resource allocation to metabolic pathways contributes to overflow metabolisms and emergent properties in cross-feeding microbial consortia. Biochem. Soc. Trans. 46:269-284, 2018.
153. Anderson, R.L. and Wood, W.A.: Carbohydrate metabolism in microorganisms. Annu. Rev. Microbiol. 23:539-578, 1969.
154. Chen, Y.D., Varasteh, B.B., and Reaven, G.M.: Plasma lactate concentration in obesity and type 2 diabetes. Diabete Metab. 19:348-54, 1993.
155. Dhall, S., Do, D., Garcia, M., Wijesinghe, D.S., Brandon, A., Kim, J., Sanchez, A., Lyubovitsky, J., Gallagher, S., Nothnagel, E.A., Chalfant, C.E., Patel, R.P., Schiller, N., and Martins-Green, M.: A novel model of chronic wounds: importance of redox imbalance and biofilm-forming bacteria for establishment of chronicity. PLoS One 9:e109848, 2014.
156. Okorie, O.N. and Dellinger, P.: Lactate: biomarker and potential therapeutic target. Crit. Care Clin. 27:299-326, 2011.
157. Stephen, B., Oliver, R.S., Humzah, J., G., S.A., Kath, V., and Peter, V.: The lactate conundrum in wound healing: clinical and experimental findings indicate the requirement for a rapid point-of-care diagnostic. Biotechnol. Prog. 28:917-924, 2012.
158. Jiang, T., Gao, C., Ma, C., and Xu, P.: Microbial lactate utilization: enzymes, pathogenesis, and regulation. Trends Microbiol. 22:589-599, 2014.
159. Smith, H., Tang, C.M., and Exley, R.M.: Effect of host lactate on Gonococci and Meningococci: new concepts on the role of metabolites in pathogenicity. Infect. Immun. 75:4190-4198, 2007.
160. Fuller, J.R., Vitko, N.P., Perkowski, E.F., Scott, E., Khatri, D., Spontak, J.S., Thurlow, L.R., and Richardson, A.R.: Identification of a lactate-quinone oxidoreductase in *Staphylococcus aureus* that is essential for virulence. Front. Cell. Infect. Microbiol. 1:1-15, 2011.
161. Kell, D.B., Brown, M., Davey, H.M., Dunn, W.B., Spasic, I., and Oliver, S.G.: Metabolic footprinting and systems biology: the medium is the message. Nat. Rev. Microbiol. 3:557-565, 2005.

162. Behrends, V., Ebbels, T.M.D., Williams, H.D., and Bundy, J.G.: Time-resolved metabolic footprinting for nonlinear modeling of bacterial substrate utilization. Appl. Environ. Microbiol. 75:2453-2463, 2009.
163. Chumnanpuen, P., Hansen, M.a.E., Smedsgaard, J., and Nielsen, J.: Dynamic metabolic footprinting reveals the key components of metabolic network in yeast *Saccharomyces cerevisiae*. Int. J. Genomics 2014:894296, 2014.
164. Ammons, M.C.B., Tripet, B.P., Carlson, R.P., Kirker, K.R., Gross, M.A., Stanisich, J.J., and Copié, V.: Quantitative NMR metabolite profiling of Methicillin-Resistant and Methicillin-Susceptible *Staphylococcus aureus* discriminates between biofilm and planktonic phenotypes. J. Proteome Res. 13:2973-2985, 2014.
165. Weston, A.D. and Hood, L.: Systems biology, proteomics, and the future of health care: toward predictive, preventative, and personalized medicine. J. Proteome Res. 3:179-196, 2004.
166. Mayne, J., Ning, Z., Zhang, X., Starr, A.E., Chen, R., Deeke, S., Chiang, C.-K., Xu, B., Wen, M., Cheng, K., Seebun, D., Star, A., Moore, J.I., and Figeys, D.: Bottom-up proteomics (2013–2015): keeping up in the era of systems biology. Anal. Chem. 88:95-121, 2016.
167. Broadbent, J., Walsh, T., and Upton, Z.: Proteomics in chronic wound research: potentials in healing and health. Proteomics Clin. Appl. 4:204-214, 2010.
168. Taverna, D., Pollins, A.C., Sindona, G., Caprioli, R.M., and Nanney, L.B.: Imaging mass spectrometry for assessing cutaneous wound healing: analysis of pressure ulcers. J. Proteome Res. 14:986-996, 2015.
169. Eming, S.A., Koch, M., Krieger, A., Brachvogel, B., Kreft, S., Bruckner-Tuderman, L., Krieg, T., Shannon, J.D., and Fox, J.W.: Differential proteomic analysis distinguishes tissue repair biomarker signatures in wound exudates obtained from normal healing and chronic wounds. J. Proteome Res. 9:4758-4766, 2010.
170. Li, Z., Adams, R.M., Chourey, K., Hurst, G.B., Hettich, R.L., and Pan, C.: Systematic comparison of label-free, metabolic labeling, and isobaric chemical labeling for quantitative proteomics on LTQ Orbitrap Velos. J. Proteome Res. 11:1582-1590, 2012.

171. Woods, J., Boegli, L., Kirker, K.R., Agostinho, A.M., Durch, A.M., Delancey Pulcini, E., Stewart, P.S., and James, G.A.: Development and application of a polymicrobial, *in vitro*, wound biofilm model. J. Appl. Microbiol. 112:998-1006, 2012.
172. McGill, S.L. and Carlson, R.P.: ***Exometabolomics of *P. aeru****. to be submitted 2018.
173. Mann, M. *Filter Aided Sample Preparation (FASP) Method*. 2013 February 15, 2017]; Available from: <http://www.biochem.mpg.de/226356/FASP>.
174. Tyanova, S., Temu, T., and Cox, J.: The MaxQuant computational platform for mass spectrometry-based shotgun proteomics. Nat. Protoc. 11:2301-2319, 2016.
175. Tyanova, S., Temu, T., Sinitcyn, P., Carlson, A., Hein, M.Y., Geiger, T., Mann, M., and Cox, J.: The Perseus computational platform for comprehensive analysis of (prote)omics data. Nat. Methods 13:731-740, 2016.
176. Szklarczyk, D., Franceschini, A., Wyder, S., Forslund, K., Heller, D., Huerta-Cepas, J., Simonovic, M., Roth, A., Santos, A., Tsafou, K.P., Kuhn, M., Bork, P., Jensen, L.J., and Von mering, C.: STRING v10: protein–protein interaction networks, integrated over the tree of life. Nucleic Acids Res. 43:D447-D452, 2015.
177. Winsor, G.L., Griffiths, E.J., Lo, R., Dhillon, B.K., Shay, J.A., and Brinkman, F.S.L.: Enhanced annotations and features for comparing thousands of *Pseudomonas* genomes in the Pseudomonas genome database. Nucleic Acids Res. 44:D646–D653, 2016.
178. Kanehisa, M., Sato, Y., Kawashima, M., Furumichi, M., and Tanabe, M.: KEGG as a reference resource for gene and protein annotation. Nucleic Acids Res. 44:D457-D462, 2016.
179. Pietrocola, F., Galluzzi, L., Bravo-San pedro, José m., Madeo, F., and Kroemer, G.: Acetyl coenzyme A: a central metabolite and second messenger. Cell Metab. 21:805-821, 2015.
180. Chubukov, V., Gerosa, L., Kochanowski, K., and Sauer, U.: Coordination of microbial metabolism. Nat. Rev. Microbiol. 12:327-340, 2014.
181. Conway, T.: The Entner-Doudoroff pathway: history, physiology and molecular biology. FEMS Microbiol. Rev. 9:1-27, 1992.

182. Cho, I. and Blaser, M.J.: The human microbiome: at the interface of health and disease. Nat. Rev. Genet. 13:260-270, 2012.
183. Myszka, K. and Czaczyk, K.: Bacterial biofilms on food contact surfaces - a review. Pol. J. Food Nutr. Sci. 61:173-180, 2011.
184. Barbieri, D., Boselli, M., Cavrini, F., Colombo, V., Gherardi, M., Landini, M.P., Laurita, R., Liguori, A., and Stancampiano, A.: Investigation of the antimicrobial activity at safe levels for eukaryotic cells of a low power atmospheric pressure inductively coupled plasma source. Biointerphases 10:029519, 2015.
185. Ferrell, J.R., Bogovich, E.R., Lee, N.R., Gray, R.L., and Pappas, D.D.: Studies of air, water, and ethanol vapor atmospheric pressure plasmas for antimicrobial applications. Biointerphases 10:021001, 2015.
186. Zuroff, T.R., Bernstein, H., Lloyd-Randolfi, J., Jimenez-Taracido, L., Stewart, P.S., and Carlson, R.P.: Robustness analysis of culturing perturbations on *Escherichia coli* colony biofilm beta-lactam and aminoglycoside antibiotic tolerance BMC Microbiol. 10:185, 2010.
187. Phalak, P., Chen, J., Carlson, R.P., and Henson, M.A.: Metabolic modeling of a chronic wound biofilm consortium predicts spatial partitioning of bacterial species. BMC Syst. Biol. 10:90, 2016.
188. Hasin, Y., Seldin, M., and Lusi, A.: Multi-omics approaches to disease. Genome Biol. 18:83, 2017.
189. Sonnleitner, E. and Bläsi, U.: Regulation of Hfq by the RNA CrcZ in *Pseudomonas aeruginosa* carbon catabolite repression. PLoS Genet. 10:e1004440, 2014.
190. Longo, F., Motta, S., Mauri, P., Landini, P., and Rossi, E.: Interplay of the modified nucleotide phosphoadenosine 5'-phosphosulfate (PAPS) with global regulatory proteins in *Escherichia coli*: modulation of cyclic AMP (cAMP)-dependent gene expression and interaction with the HupA regulatory protein. Chem.-Biol. Interact. 259:39-47, 2016.
191. Browne, P., Barret, M., O'gara, F., and Morrissey, J.P.: Computational prediction of the Crc regulon identifies genus-wide and species-specific targets of catabolite repression control in *Pseudomonas* bacteria. BMC Microbiol. 10:300, 2010.

192. Williams, H.D., Zlosnik, J.E.A., and Ryall, B.: Oxygen, cyanide and energy generation in the cystic fibrosis pathogen *Pseudomonas aeruginosa*. Adv. Microb. Physiol. 52:1-71, 2007.
193. Bielecki, P., Puchalka, J., Wos-Oxley, M.L., Loessner, H., Glik, J., Kawecki, M., Nowak, M., Tümmler, B., Weiss, S., and Dos Santos, V.a.P.M.: *In-Vivo* expression profiling of *Pseudomonas aeruginosa* infections reveals niche-specific and strain-independent transcriptional programs. PLoS One 6:e24235, 2011.
194. Vasil, M.L. and Darwin, A.J.: Regulation of Bacterial Virulence. American Society of Microbiology, 2013.
195. Pederick, V.G., Eijkelkamp, B.A., Begg, S.L., Ween, M.P., Mcallister, L.J., Paton, J.C., and Mcdevitt, C.A.: ZnuA and zinc homeostasis in *Pseudomonas aeruginosa*. Sci. Rep. 5:13139, 2015.
196. Johnson, L., Mulcahy, H., Kanevets, U., Shi, Y., and Lewenza, S.: Surface-localized spermidine protects the *Pseudomonas aeruginosa* outer membrane from antibiotic treatment and oxidative stress. J. Bacteriol. 194:813-826, 2012.
197. Temple, L.M., Sage, A.E., Schweizer, H.P., and Phibbs, P.V.: Carbohydrate catabolism in *Pseudomonas aeruginosa*. In: Pseudomonas, eds. T.C. Montie, 35-72. Boston, MA, Springer US, 1998.
198. O'toole, G.A., Gibbs, K.A., Hager, P.W., Phibbs Jr., P.V., and Kolter, R.: The global carbon metabolism regulator Crc is a component of a signal transduction pathway required for biofilm development by *Pseudomonas aeruginosa*. J. Bacteriol. 182:425-431, 2000.
199. Zhang, L., Chiang, W.-C., Gao, Q., Givskov, M., Tolker-Nielsen, T., Yang, L., and Zhang, G.: The catabolite repression control protein Crc plays a role in the development of antimicrobial-tolerant subpopulations in *Pseudomonas aeruginosa* biofilms. Microbiology 158:3014-3019, 2012.
200. Zhang, L., Gao, Q., Chen, W., Qin, H., Hengzhuang, W., Chen, Y., Yang, L., and Zhang, G.: Regulation of pqs quorum sensing via catabolite repression control in *Pseudomonas aeruginosa*. Microbiology 159:1931-1936, 2013.
201. Wolfe, A.J.: The acetate switch. Microbiol. Mol. Biol. Rev. 69:12-50, 2005.

202. Zhang, Y., Fonslow, B.R., Shan, B., Baek, M.-C., and Yates, J.R.: Protein analysis by shotgun/bottom-up proteomics. Chem. Rev. 113:2343-2394, 2013.
203. Si, T., Li, B., Zhang, K., Xu, Y., Zhao, H., and Sweedler, J.V.: Characterization of *Bacillus subtilis* colony biofilms via mass spectrometry and fluorescence imaging. J. Proteome Res. 15:1955-1962, 2016.

APPENDIX

Copyright

Chapter 4

Standard ACS AuthorsChoice/Editors' Choice Usage Agreement

<https://pubs.acs.org/doi/abs/10.1021/acs.analchem.7b01745>

VITA

YENI PAMELA YUNG

EDUCATION

University of Illinois at Chicago, Chicago, IL

- *PhD, Analytical Chemistry*, GPA: 3.8/4.0, Expected Aug 2018
- *MS, Analytical Chemistry*, GPA: 3.8/4.0, 2016
- *BA, Chemistry with Minor in Mathematics*, GPA: 3.8/4.0, Magna Cum Laude, 2009

Oakton Community College, Skokie, IL

- *AS, Science or Math*, GPA: 3.9/4.0, High Honors, 2007

RESEARCH EXPERIENCE

Graduate Analytical Researcher

AUG 2012 – PRESENT

Advisor: Luke Hanley, University of Illinois at Chicago, Chicago, IL

Developed, executed, and tested mass spectrometric methods and instrumentations for metabolic analyses of chronic wound planktonic and biofilm cultures.

- Designed, installed, and qualified portable atmospheric pressure ionization sources for matrix-free metabolite detection in biofilms with minimal sample prep, a complementary method to MALDI
- Statistical and bioanalytical quantitative analyses of large-scale LC-MS proteomic data utilizing bioinformatic platforms identifying ~500 bacterial proteins and differentiating metabolic differences in response to the environment

WORK EXPERIENCE

Graduate Analytical Researcher

OCT 2015 – MAY 2017

RRC-MMPF, University of Illinois at Chicago, Chicago, IL

Provided the support base, at the university Research Resources Center, for industrial and academic clients who benefit from utilizing MS for their research, publications, and grant proposals.

- Operated and performed routine and non-routine maintenance on commercial mass spectrometers and GC-, and LC- interfaces without outside support saving facility thousands of dollars and time
- Conducted quantitative, qualitative, and exact mass analyses on client submitted samples (i.e. organic/inorganic synthetics, VOCs, residual solvents, and crude oil samples) and disseminated reports of data interpretations
- Extended MS consultation services and trained 10 new users on MS safety use and operations

Quality Control Analytical Chemist

NOV 2010 – JUN 2012

Morton Grove Pharmaceutical, Morton Grove, IL

Inspected, sampled, and tested raw materials, stability, in-process, and finished products of nasal spray and oral suspensions for quality ensuring all physical and chemical specifications are met prior to market release.

- Collaborated with Validation on failure mode and effects analysis (FMEA) and operational/performance qualifications (OQ/PQ) in implementing a new reverse osmosis (RO) water system to increase manufacturing throughput
- Oversaw and managed instrument logbooks for calibration, maintenance, and usage, as well as, reviewed analyst notebooks for data and accuracy
- Supervised and trained 5 new hires on methodology and instrumentation

Research & Development Lab Technician

APR 2010 – NOV 2010

Blistex Inc., Oak Brook, IL

Performed qualitative physical analyses on stability and new product developments.

- Assisted formulation chemists in apparatus setup for bench- and pilot-scale production for new product implementation
- Disposed of chemical waste according to OSHA guideline 29 CFR 1926.252
- GLP/GMP compliant

TEACHING EXPERIENCE

General Chemistry Teaching Assistant

AUG 2012 – MAY 2014

University of Illinois at Chicago, Chicago, IL

Conducted weekly discussion and laboratory sessions for 42 undergraduate students.

- Mandated and supervised lab safety for PPE, safe handling of lab equipment and chemicals, and proper disposal of waste in accordance to the departmental chemical hygiene procedures
- Assessed student lab reports providing timely feedback to help improve their scientific writing
- Devised and prepared weekly agendas reviewing basic concepts and problem-solving strategies to engage students in learning and prepare students for examinations

PUBLICATIONS

1. “Delineating *Pseudomonas aeruginosa* Metabolism in Planktonic and Biofilm Cultures Through Multi-Omics”, **Y. P. Yung**, S. L. McGill, S. M. Cologna, H. Chen, R. P. Carlson, L. Hanley. (in preparation)
2. “Application of Laser Ablation MS”, **Y. P. Yung** and L. Hanley. (in preparation)
3. “Solid sampling with a diode laser for portable ambient mass spectrometry”, **Y. P. Yung**, R. Wickramasinghe, A. Vaikkinen, T.J. Kauppila, I.V. Veryovkin, and L. Hanley. *Analytical Chemistry* 89 (14), 7297-7301 (2017).
4. “Identification and characterization of PPAR α ligands in the hippocampus”, A. Roy, M. Kundu, M. Jana, R.K. Mishra, **Y. Yung**, C.H. Luan, F.J. Gonzalez, and K. Pahan. *Nature Chemical Biology* 12 (12), 1075-1083 (2016).

PRESENTATIONS (Note: The presenter is underlined.)

Oral Presentation

1. “*Pseudomonas aeruginosa* Proteomics for Models of Multispecies Biofilms”, **Y.P. Yung**, S.L. McGill, S.M. Cologna, H. Chen, R. Carlson, and L. Hanley, Pittcon, Chicago, IL 5-9 March, 2017.

Poster Presentation

1. “Metabolic Differences between Monoculture and Co-culture *Pseudomonas aeruginosa* and *Staphylococcus aureus* Compared by Label Free Quantitation Proteome Analyses”, **Y.P. Yung**, S.L. McGill, S.M. Cologna, H. Chen, R.P. Carlson, and L. Hanley, 66th ASMS Conference on Mass Spectrometry and Allied Topics, San Diego, CA June 3-7, 2018.

2. “Protein Expressional Changes of *Pseudomonas aeruginosa* in Lactate-Supplemented Media”, **Y.P. Yung**, S.L. McGill, S.M. Cologna, H. Chen, R.P. Carlson, and L. Hanley, 65th ASMS Conference on Mass Spectrometry and Allied Topics, Indianapolis, IN, June 4-8, 2017.
3. “*Pseudomonas aeruginosa* Proteomics for Models of Multispecies Biofilms”, **Y.P. Yung**, S.L. McGill, S.M. Cologna, H. Chen, R. Carlson, and L. Hanley, Sanibel Conference on Peptidomics, Clearwater, FL 19-22 January, 2017.
4. “Laser ablation atmospheric pressure photoionization on a portable ion trap mass spectrometer”, **Y.P. Yung**, I.V. Veryovkin, Y. Cui, and L. Hanley, 63rd ASMS Conference on Mass Spectrometry and Allied Topics, St. Louis, MO, May 31-June 4, 2015.
5. “High lateral resolution mass spectrometry imaging using femtosecond laser desorption VUV postionization”, **G.E. Barry**, Y. Cui, M.W. Majeski, D.R. Cavazos, **Y.P. Yung**, I.V. Veryovkin, and L. Hanley, 63rd ASMS Conference on Mass Spectrometry and Allied Topics, St. Louis, MO, May 31-June 4, 2015.
6. “Atmospheric pressure photoionization with and without laser ablation on a portable ion trap”, I.V. Veryovkin, **Y.P. Yung**, Y. Cui and **L. Hanley**, Sanibel Conference on Forensic & Portable Mass Spectrometry, Clearwater Beach, FL, 22-25 January 2015.
7. “Mass spectrometry with using femtosecond lasers and postionization to characterize biomaterials interfaces”, **Y. Cui**, **Y.P. Yung**, and L. Hanley, 61st International AVS Symposium and Exhibition, Baltimore, MD, November 2014.

AFFILIATION

ASMS

AWARDS

- President’s Scholars – Spring 2006, Summer 2006, Fall 2006, Summer 2007
- Dean’s List – Spring 2008, Fall 2008